Rheology and Microstructure of Shear Thickening Suspensions

A Thesis

Submitted in Partial Fulfillment of the Requirement for the Degree of

Doctor of Philosophy

By

T. AJEETH PRABHU

Department of Chemical Engineering
Indian Institute of Technology Guwahati
Guwahati-781039, Assam, India

January 2022

Dedicated

To

My Parents, My Wife, and My Mentor

Department of Chemical Engineering
Indian Institute of Technology
Guwahati
Guwahati, Assam 781039

STATEMENT

I hereby declare that the content embodied in this thesis entitled **"Rheology and Microstructure of Shear Thickening Suspensions"** is the result of investigations and experiments carried out by me at the Flow Visualization Lab, Department of Chemical Engineering, Indian Institute of Technology Guwahati, India, under the supervision of **Prof. Anugrah Singh**.

In keeping with the general practice of reporting scientific observations, due acknowledgments have been made wherever the work described is based on the findings of other investigators.

January, 2022 AJEETH PRABHU TEKKATI

Department of Chemical Engineering

Indian Institute of Technology

Guwahati

Guwahati, Assam 781039

CERTIFICATE

It is certified that the work contained in this thesis entitled **"Rheology and Microstructure of Shear Thickening Suspensions"** done by **Mr. Ajeeth Prabhu Tekkati** (Roll No. 166107030) has been carried out under my supervision, and this work has not been submitted elsewhere for a degree.

Guwahati
January, 2022

Dr. Anugrah Singh
Professor
Department of Chemical Engineering
Indian Institute of Technology Guwahati
Guwahati – 781039
Assam, India

Acknowledgments

This thesis becomes a reality with the kind support and help of many individuals. With great pleasure, I express my deep sense of thanks and gratitude to all of them who have made my stay and doctoral studies at IIT Guwahati memorable.

I express my sincere thanks to my supervisor ***Prof. Anugrah Singh*** *for the continuous support throughout my research journey. He provided me with an excellent lab facility to work with freedom and an atmosphere for thinking and execution, which grew my interest in the topic. Also, his positive attitude and encouragement helped me perform and complete the research objectives. His support in doing the experiments, analyzing the data, and preparing the manuscripts is invaluable. The weekly, monthly group meetings and mock presentations help me make things more accessible at the last minute. I heartily appreciate his patience and perseverance, which helped propel me through difficult situations. It has been a remarkable working experience with him.*

I am grateful to the Terminal Ballistic Research Laboratory, Defence Research and Development Organization, Government of India (Project no. ARMREB/CDSW/2016/175) for their financial support to carry out this research work.

I want to extend my sincere gratitude to my doctoral committee chairman ***Dr. Raghvendra Gupta****, Department of Chemical Engineering, for his valuable suggestions, evaluation, and proper direction during my annual progress seminar*

and synopsis. I shall always be obliged to other doctoral committee members, ***Dr. S Omkar Deshmukh****, Department of Chemical Engineering, and* ***Prof. Manmohan Pandey****, Department of Mechanical Engineering, who inspite of their busy schedules, have always made themselves available for valuable discussions and versatile support.*

I want to express my sincere thanks to my professors ***Dr. Rajesh Kumar Upadhyay*** *and* ***Dr. Anki Reddy Katha,*** *Department of Chemical Engineering, for their valuable suggestions, which significantly benefitted the progress of my research work.*

I also thank the Head of the Department of Chemical Engineering for the administrative support. Furthermore, I would like to thank other faculty members, research scholars, and non-teaching staff of the Department of Chemical Engineering, IIT Guwahati, for their kind cooperation in all aspects. I want to thank the in-charges of Analytical Lab, Chemical Engineering Dept for providing interfacial rheometer experimental setup, Central Instrumental Facility (CIF), and Center for Nanotechnology, IIT Guwahati, for providing FESEM facility.

I thank the management and department of chemical engineering at Gayatri Vidhya Parishad College of Engineering (Autonomous), Vishakhapatnam, for giving me this opportunity to conduct my research work as a QIP research scholar at IIT Guwahati.

I especially thank Mr. Bharath Velaga for extending his help in characterizing the particles and sharing pleasant memories during my stay and travel in and around IIT Guwahati. We have shared a fulfilling friendship that has

nurtured integral parts of my doctorate studying experience. I also thank Mr. Nilay Kumar (JRF) and Mr. Sachin Shrestha (Intern) for their assistance in conducting experiments.

I thank my labmates Dr. Bhaskar, Dr. Sudarshan, Dr. Mallikarjun, Mr. Vikas, Mr. Rupak, Mr. Indrajeet, Mr. Bineeth, Mr. Shadab, Mr. Jyoti Krishna, Mr. Nasaba, Ms. Salma, Mr. Vishnu, Ms. Bharathi, for their support during my work in my lab.

I am deeply grateful to convey my sincere gratitude to my parents and family members for their sustained help and encouragement in all my personal and academic ventures. I feel proud and blessed to have my mother, Mrs. Veena Prabhu, and my father, Mr. T.K.N. Prabhu. Special thanks to my wife Ananya, who always strengthened my morale by standing beside me in all situations and supporting me while doing my experiments.

I wish to thank many other people whose names are not mentioned here, but this does not mean that I have forgotten their help. Above all, I am thankful to God Almighty for giving me a wonderful and healthy life.

Ajeeth Prabhu Tekkati

ABSTRACT

Colloidal suspensions of particles in viscous fluids exhibit a wide range of rheological behavior such as shear thinning and shear thickening. Shear thickening is a phenomenon in which the viscosity of suspension increases with an increase in shear rate and is commonly known as dilatant fluids. Considering the ability of shear thickening fluids to increase its viscosity with an increase in the applied stress, it enables them to be used in several applications, such as damping devices and body armours. Though shear thickening fluids comprise simple raw materials, achieving a discontinuous shear thickening at lower weight fractions is highly challenging. In the current study, we present a systematic rheological study on the fumed silica suspensions to understand the effect of fluid and particle parameters on the critical shear rate and shear thickening ratio. It was observed that the removal of air bubbles and water contamination is crucial to prepare good shear thickening fluids. A careful sample preparation method was adopted to properly disperse the fumed silica particles in polyethylene glycol solution, and we achieved discontinuous shear thickening at low particle concentration. It was observed that the critical shear rate in shear thickening suspension is strongly influenced by both carrier fluid and particle concentration. However, the shear thickening ratio is mainly influenced by the particle parameters and the contact forces between the particles. Increasing the amount of smaller particles in the suspension significantly decreases the maximum viscosity and shifts the onset of shear thickening to higher values of critical shear

rates with a much smaller shear thickening ratio. Further, a possible mechanism has been proposed based on the influence of carrier fluid and particle size distribution to explain the rheological behavior of shear thickening suspension. Our results clearly show the hydroclusters formation as the primary reason for the discontinuous shear thickening and their subsequent break up at high shear rates to cause second shear thinning. Extending the investigations to understand the influence of the addition of nanofillers on the rheological behavior of shear thickening suspensions, a systematic rheological study was carried out for fumed silica-PEG STFs by adding nanofillers such as Graphene Oxide, Multi-Walled Carbon Nanotubes, and mica particles. The addition of Graphene oxide (GO) particles exhibited higher relative viscosities and a decrease in the onset of shear thickening. In contrast, the addition of Multi-Walled Carbon Nanotubes (MWCNT) and Mica particles showed a decrease in the shear thickening ratio and an increase in critical shear rate. Finally, we report experimental studies on rheology and microstructure in discontinuous shear thickening of fumed silica suspensions. The formation of particle clusters was observed after the critical shear rate, and their size increases during the shear thickening. At higher shear rates, these clusters were found to break down due to strong shear forces, and a continuous decrease in viscosity was observed. The suspension viscosity and the first normal stress difference (N_1) variation with the shear rate showed similar dependence. The sign of the first normal stress difference was negative during shear thickening, which is consistent with the hydrodynamic model of cluster formation. A linear variation of N_1 with shear rate during the shear thickening further indicates its predominantly hydrodynamic origin and supports the recent Stokesian dynamics simulation studies

on discontinuous shear thickening based on the hydrodynamic model of nonsmooth colloids. On the other hand, a non-linear decrease in the first normal stress difference with the shear rate in the second shear-thinning region is primarily due to the breaking of large clusters into smaller ones, and with a possibility of frictional contacts within these hydroclusters. The oscillatory shear measurements were also performed, and the samples displayed strain thickening similar to shear thickening. Finally, the similarity between the steady and dynamic shear rheology at high strain amplitudes was observed using the modified Cox-Merz rule.

Abbreviations

FESEM	Field Emission Scanning Electron Microscopy
XRD	X-Ray Diffraction
FTIR	Fourier Transform Infrared
JCPDS	Joint Committee on Powder Diffraction Standards
FS	Fumed Silica
GO	Graphene Oxide
MWCNT	Multi-Walled Carbon-Nano Tube
PEG	Polyethylene Glycol
STF's	Shear Thickening Fluids
STR	Shear Thickening Ratio
STP	Shear Thickening Period
CSR	Critical Shear Rate
CST	Continuous Shear Thickening
DST	Discontinuous Shear Thickening
LAOS	Large Amplitude Oscillatory Shear
SAOS	Small Amplitude Oscillatory Shear
SANS	Small Angle Neutron Scattering
LMA	Levenberg-Marquardt Algorithm

List of Symbols

$\dot{\gamma}$	Shear rate
$\dot{\gamma}_c$	Critical shear rate
$\dot{\gamma}_{max}$	Maximum shear rate
τ	Shear stress
τ_{max}	Maximum shear stress
η	Viscosity
η_0	Zero-shear viscosity
η_c	Critical viscosity
η_{max}	Maximum viscosity
η_f	Solvent viscosity
η_r	Relative viscosity
Φ	Volume fraction
Φ_c	Critical volume fraction
Φ_m	Maximum packing fraction
γ	Surface tension of the solvent
Υ_1	First normal stress difference coefficient
G'	Storage modulus
G''	Loss modulus
γ_0	Strain amplitude
ω	Angular frequency
η^*	Complex viscosity
$\dot{\gamma}^{dyn}$	Maximum dynamic shear rate

$\bar{\tau}_d$	Average dynamic shear stress
χ^2	Chi-square
N_1	First normal stress difference
F_z	Normal force
Re_p	Particle Reynolds number
a	Particle radius
h	Interparticle distance
F_h	Hydrodynamic force
wt%	Weight fraction

Contents

List of Figures

List of Tables

CHAPTER 1 INTRODUCTION

1.1 Background and Motivation

Concentrated suspension of solid particles dispersed in a viscous liquid shows non-Newtonian behavior even if the carrier fluid is Newtonian. The rheology and dynamics of these suspensions exhibit a wide range of behavior such as shear thinning and shear thickening. Shear thickening is a phenomenon in which the viscosity of suspension increases with an increase in shear rate and is commonly known as dilatant fluids (Barnes, 1989). Depending on the particle concentration, shear thickening suspensions are broadly classified into two forms. At lower particle concentration, the viscosity increases continuously with an increase in shear rate, referred to as continuous shear thickening. On the other hand, at higher particle concentration, a sudden jump of viscosity (several orders of magnitude) can be observed with an increase in shear rate. A sharp jump in viscosity is effectively a fluid to solid-like transition referred to as dis-continuous shear thickening (Brown and Jaeger, 2012). Shear thickening suspensions are ubiquitous in industrial applications such as cosmetics, pharmaceuticals, the food industry, the transportation of slurries, plastic processing, and oil and gas industry, etc. However, considering its unique reversibility aspect, these suspensions are investigated in developing body armors, bulletproof vests, liquid coupling, medical devices, sporting equipment, damping devices, and smart materials (Lee and Wagner, 2003; Fischer et al., 2006). The first application to utilize the shear thickening fluids in liquid armour systems was attempted by Gates Jr (1968).

In a simple shear flow, the particles are driven by several forces such as Brownian forces, hydrodynamic forces, electrostatic forces, and steric forces.

However, the particular mechanism under which these forces play an essential role in thickening the suspension is still elusive. Therefore, in order to understand the phenomena of shear thickening, it is required to obtain the microstructure under flow. Hoffman (1972, 1974) first investigated simultaneous flow and microstructure in a shear plane by conducting small-angle light scattering experiments. It was observed that at low shear rates, the particles in the suspension had formed ordered layers parallel to the velocity direction. Hoffman also observed that the structure changes from the order to disorder transition at the onset of shear thickening. Later, Brady and Bossis (1985) proposed a hydro-cluster theory which states that at a higher shear rate, the hydrodynamic forces overcome the inter-particle repulsive forces causing the particles to come into close contact. As a result, these particles form clusters resulting in large aggregates and an increase in viscosity which can cause the whole suspension to jam. Recent studies have related this shear thickening transition to frictional particle interactions and dilation (Brown and Jaeger, 2014; Fall et al., 2009). Stokesian dynamics simulations carried out by Mari et al. (2014) found that frictional contact force between the particles is responsible for the jamming condition in dense suspension. Cheng et al. (2011) carried out experiments by combining fast confocal microscopy with shear measurements while considering microscopic single-particle dynamics to investigate the microstructure of the suspension in different flow regimes. These experimental results supported that shear thickening of suspension arises due to particle clustering induced by hydrodynamic interaction between the particles.

However, to synthesize the desired shear thickening fluid (STF), it is essential to understand the role of particle and fluid parameters on the rheology. To achieve this, a systematic approach of studying the rheology and microstructure of shear thickening fluids has to be done. Many investigations were carried by steady shear measurements to understand the behavior of the shear thickening suspensions. However, due to the complex flow behavior of the non-Newtonian fluids, the steady shear measurements are not sufficient to understand the flow behavior. Hence, the dynamic shear rheology becomes necessary to understand their rheological properties (Raghavan and Khan, 1997). Investigation on the dynamic responses of suspensions was carried out to understand the relation between stress-controlled critical shear rate and frequency-dependent critical strain (Lee and Wagner, 2003; Fischer et al., 2006; Galindo-Rosales et al., 2009). A combination of rheological measurements and flow visualization techniques was required to understand the shear thickening phenomena at a fundamental level which can be helpful in the selection of fluid and particles, their shape, and sizes that could be used to make the shear thickening fluids of better rheological properties.

1.2 Objectives of the research work

The objective of the present research work focuses on synthesizing shear thickening fluids that enable the removal of air bubbles and any water contamination. Also, a systematic rheological study on shear thickening suspensions was investigated to understand the effect of different parameters. Furthermore, as discussed earlier, to understand the mechanism of shear thickening suspensions, experiments were carried out to determine the microstructure of the suspensions by

direct visualization techniques like Rheo-microscopy and also by Particle Image Velocimetry (PIV). In summary, the objectives of the research work can be given below:

1. Synthesis of shear thickening fluids and investigating the effect of various parameters on the rheological properties.
2. Studies on the effect of particle size distribution on the rheology of shear thickening suspensions.
3. Studies on the effect of the addition of fillers on shear thickening.
4. Visualization of microstructure in shear thickening suspensions along with rheological measurements using a Rheo-microscopy setup.

1.3 Organization of the Thesis

In the present thesis, the objectives mentioned earlier have been organized in the following four chapters before a summary, and the future scope of the research has been discussed.

Chapter 1 presents the general overview of the shear thickening suspension and the outline of the proposed theories to understand the mechanism of the shear thickening suspension. The objectives and aims of this thesis have been given along with its organization.

Chapter 2 briefly describes the literature on the background of rheology, the concept of shear thickening behavior, different types of shear thickening, shear thickening mechanisms, the general composition of suspensions, rheological properties, and factors influencing shear thickening behavior have been reviewed.

This chapter also discusses the different theories proposed in the literature on the mechanism of shear thickening behavior. Also, a detailed description of recent advances in imaging the microstructure of the concentrated suspensions under flow is included in this chapter. Furthermore, experimental studies in the literature to measure the normal stress behavior of the suspensions are also discussed and highlighted.

Chapter 3 describes the materials used in the experimental studies and their sources. Also, a detailed procedure for preparing the shear thickening suspensions by mechanical and sonochemical homogenization methods is provided. The steady-state and dynamic rheological measurements and particle characterization were done and analyzed.

Chapter 4 presents a systematic rheological study on the fumed silica suspensions to understand the effect of different parameters on the critical shear rate and shear thickening ratio. Also, the influence of particle size distribution on the rheology of shear thickening suspensions has been studied.

Chapter 5 investigates the effect of the addition of fillers on the rheological behavior of shear thickening fluids (STF). This involved preparing shear thickening suspensions with the addition of fillers to the fumed silica particles for a given weight fraction and a carrier fluid. The Shear thickening ratio and critical shear rate variation with various additives were also studied.

Chapter 6 describes the experimental studies on rheology and microstructure in discontinuous shear thickening suspensions. The macroscopic

behavior of hydrocluster formation at a critical shear rate and their subsequent breakup at a higher shear rate were captured using Rheo-Microscopy studies. We also determine the mechanism of shear thickening behavior by studying the first normal stress difference (N_1) of fumed silica suspensions in steady shear rheology. Further, the oscillatory shear measurements of the suspensions were also evaluated to determine the linear viscoelastic behavior.

Chapter 7 summarizes the salient findings of the present investigation and provides new ideas for future research.

CHAPTER 2 Literature Review

2.1 Rheology

The term Rheology was first invented by Professor Bingham and defined as the study of deformation and flow of matter. Knowledge of this subject is essential for scientists employed in many industries, including plastics, printing inks, detergents, oils, etc. In 1687, Issac Newton gave attention to liquids in his book "Principia" and said that "The resistance which arises from the lack of slipperiness of the parts of the liquid, other things being equal, is proportional to the velocity with which the parts of the liquid are separated from one another." This lack of slipperiness is called viscosity and is synonymous with "internal friction" and is a measure of "resistance to flow." Researchers and industrialists who work in rheology are forced to learn the sub-areas, including rheometry, constitutive equations, measurement of flow behavior in complex geometries, and calculation of behavior in complex flows. Flow regimes of fluids can generally be classified into two groups as Newtonian and non-Newtonian fluid behaviors (Barnes, 1989).

2.2 Shear Thickening Fluids

Shear thickening fluids (STF) are commonly known as dilatant fluids, which exhibit non-Newtonian rheological behavior. The viscosity of shear thickening suspensions increases with the increase in shear rate (Barnes, 1989; Lee and Wagner, 2006; Wagner and Brady, 2009). The main advantage of STF is its unique aspect of reversibility. In industrial applications, these fluids are observed to be a problem due to overloading in mixer motors, mixer blade damage, and jamming in small openings (Barnes, 1989). However, considering the ability of shear thickening fluids to increase its viscosity with an increase in the applied stress, it enables them

to be used in several applications such as damping devices, body armours, smart materials, and liquid couplings (Lee and Wagner, 2003; Fischer et al., 2006; Zhang et al., 2010). The first application to utilize the STFs in liquid armour systems was attempted by Gates (1968).

2.3 Types of Shear Thickening Systems

Ding et al., in 2013, explained that shear thickening systems could be of two types. One is particle-based shear thickening systems, and the other is non-particle shear thickening.

2.3.1 Particle-Based Shear Thickening Systems

Shear thickening fluids, in general, are composed of colloidal particles such as silicon dioxide or other oxides, calcium carbonate, cornstarch, polystyrene, polymethylmethacrylate, naturally and synthetically occurring minerals with an average particle size of 1 nm to 1 μm. These colloidal particles are dispersed in carrier fluids such as water, ethylene glycol, polyethylene glycol, poly (propylene glycol), and glycerine (Barnes, 1989; Wagner and Wetzel, 2006; Maranzano and Wagner, 2002; Brown and Jaeger, 2009; Cheng et al., 2011; Warren et al., 2015; Moriana et al., 2016). Ethylene glycol and polyethylene glycol are the most widely used carrier fluids due to their combination of stability, high boiling point, polarity, and non-flammable properties (Chen et al., 2005; Moriana et al., 2016).

2.3.2 Non-Particle Based Shear Thickening Systems

Non-particle-based shear thickening systems, including segmental mobility of polymers about their glass transition and physically cross-linked polymer

networks. When any amorphous polymer is at glass transition, it will shear thicken when the shear rate is increased (Montgomery and Macknight, 2005). The cross-linked polymer networks will shear thicken when the energy of the physical bond is the same as that of the thermal energy. At low shear rates, the particles show physical bonding with the liquid and are considered solid-like behavior at high shear rates. Polyvinyl alcohol containing boric acid and polydimethylsiloxane containing boric acid are two examples that are well known.

2.4 Characterization of Different Types of Shear Thickening

The Shear thickening fluids are broadly classified into two forms. One is Continuous shear thickening, and the other is Discontinuous shear thickening

2.4.1 Continuous Shear thickening

The degree to which the viscosity increases with shear rate depends on the volume fraction of solid particles also referred to as the packing fraction Φ. Shear thickening is generally not observed in dilute suspensions but gradually appears at an intermediate packing fraction around 0.3-0.4. At these particle concentrations, the viscosity increases are relatively mild and often referred to as continuous shear thickening. As the packing fraction increases, the rate of increase in viscosity with shear rate becomes larger, and the shear thickening region starts at a critical shear rate independent of packing fractions (Brown and Jaeger, 2012).

2.4.2 Discontinuous Shear Thickening

Many shear thickening fluids evolve from continuous to discontinuous shear thickening with increasing packing fraction up to the point that the viscosity and shear stress appear to jump discontinuously by orders of magnitude beyond a critical shear rate. This apparent discontinuous jump in the viscosity with shear rate is called Discontinuous Shear Thickening (DST) and is shown in **Figure 2.1**. (Brown and Jaeger, 2012; Maranzano and Wagner, 2001a).

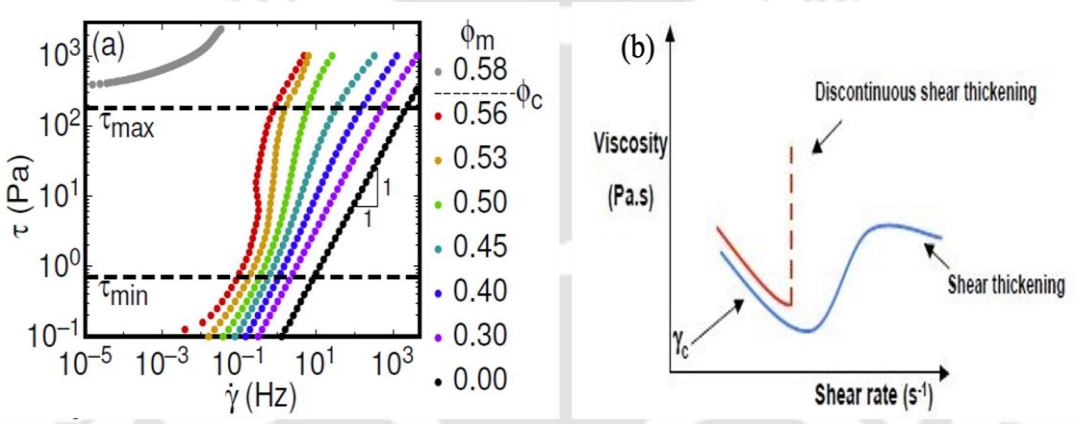

Figure 2.1 (a) Shear stress vs. shear rate in which the region defines shear thickening with a slope greater than 1. (b) Different types of Shear thickening (Brown and Jaeger, 2012)

2.5 Mechanism of Shear Thickening Fluids

Several researchers have proposed theories to understand the phenomenon of shear thickening behavior, including the formation of particle clusters by hydrodynamic lubrication forces and the order-disorder transition.

2.5.1 Order-disorder Transition

The order-disorder transition mechanism was first identified and developed by Hoffman (Hoffman, 1972, 1974). He proposed that below a critical shear rate,

particles in suspension are in a layered order, but beyond a critical shear rate, hydrodynamic forces acting on the particles become stronger, and the layered orientation is disrupted; as a result of this process, layered particles disorder and the transition from order to disorder causes a drastic increase in suspension viscosity. Later Boersma et al. (1990) also proposed this mechanism by explaining that repulsive inter-particle forces keep the particles separated at a shear rate below the shear thickening transition. Smooth strings or layers of particles produce an ordered structure with relatively low viscosity, but as the shear rate increases, the hydrodynamic forces begin to overcome the repulsive inter-particle force, which leads to a destruction of the order in the dispersion and the generation of hydroclusters (Boersma et al., 1990). Egres and Wagner showed that discontinuous shear thickening could occur without an order-disorder transition (Egres and Wagner, 2006).

2.5.2 Hydrocluster Theory

Brady and Bossis (1985) proposed a hydro-cluster theory which states that at a higher shear rate, the hydrodynamic forces overcome the inter-particle repulsive forces causing the particles to come into close contact. These particles form clusters resulting in large aggregates and an increase in viscosity which can cause the whole suspension to jam, as shown in **Figure 2.2**(a). Wagner and Brady (2009) studied more thoroughly on hydroclustering and proposed that viscosity curves are in quantitative agreement with measurements for continuous shear thickening in terms of both the critical shear rate and the magnitude of the increase

in viscosity. Recent work by Cheng et al. (2011) has supported the hydro-clustering hypothesis through confocal microscopy measurements, shown in **Figure 2.2** (b).

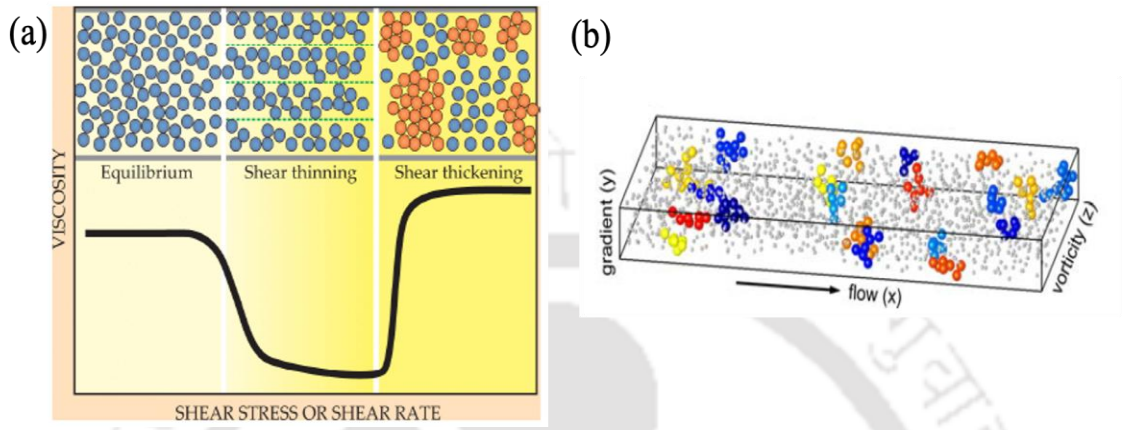

Figure 2.2 (a) Change in the microstructure of a colloidal dispersion (Wagner and Brady, 2009) (b) Instantaneous real-space configuration of hydroclusters. Different colors indicate different clusters. Particles outside the large clusters are drawn with a smaller size for clarity (Cheng et al., 2011).

2.6 Parameters Controlling Shear Thickening Behavior

Various parameters can influence the rheological behavior of shear thickening fluids, such as particle volume fraction, particle aspect ratio, particle size, particle size distribution, particle-particle interactions, a liquid medium, and multiphase, like the addition of fillers.

2.6.1 Effect of Particle Volume Fraction

One of the most significant parameters that influence the rheology of STFs is the volume fraction or weight fraction. Previous studies have reported that the critical shear rate decreases with increased particle weight fraction due to hydrodynamic forces overcoming the repulsive forces between the particles.

Hydrodynamic forces become greater in increased particle concentration suspensions due to the reduced distance between particles, and therefore, less shear rate is required to overcome repulsive forces (Maranzano and Wagner, 2002; Kalman et al., 2007; Chen et al., 2015; Gurgen and Kushan, 2016). Barnes (1989) stated that shear thickening generally onsets at a particle volume fraction of 0.5 and schematically represented the viscosity versus shear rate for shear thickening systems, with phase volume as a parameter (**Figure 2.3**(a)).

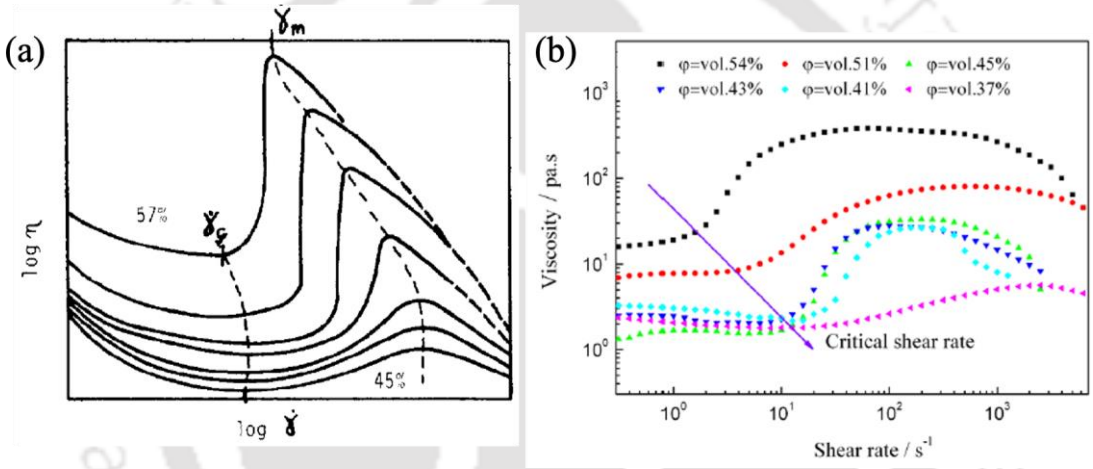

Figure 2.3 Figure (a) Schematic representation of viscosity versus shear rate for shear thickening systems, with approximate phase volume as a parameter (Barnes, 1989). (b) Steady rheological behavior of PCC suspensions with different at T = 25^{0}C (Chen et al., 2015)

2.6.2 Effect of Particle Aspect Ratio

The effect of particle shapes on the rheological properties of shear thickening fluids was found in early studies. The rod-shaped particles are the most effective particles among various particle shapes to improve shear thickening. Brown et al. (2010) stated that particles with high aspect ratios are more prone to increase the

viscosity of STFs due to particle interlocking and rotational motion in the flow field, as shown in **Figure 2.4**.

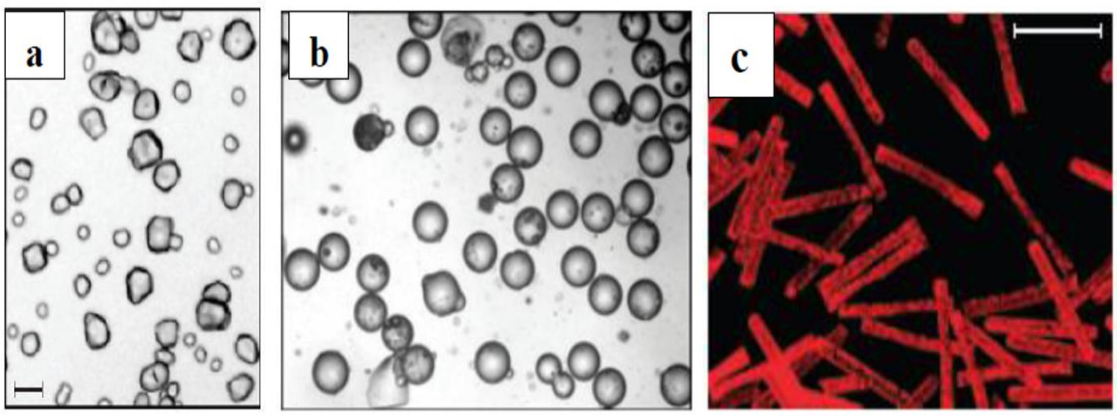

Figure 2.4 Particles dispersed in shear thickening fluids: a) cornstarch particles: b) soda-lime glass spheres with hydrophobic silane coating: c) rod-shaped ferromagnetic particles (Brown et al., 2010)

2.6.3 Effect of Particle Size

Particle size is another crucial factor in the rheological behavior of STFs. The size of the particles used in shear thickening fluids ranges from 1 nm to 1 μm. Previous experimental studies found that the critical shear rate increases as the particle size reduces. The role of the Brownian forces can be considered in the assessment of this trend since they dominate nanoparticle suspensions and delay the thickening for higher shear rates due to increased repulsive stresses between particles (Barnes, 1989; Maranzano and Wagner, 2001).

2.6.4 Effects of The Particle Size Distribution

The shear thickening ratio can be influenced by the particle size ratio and particle size distribution (Barnes, 1989; Greenwood et al., 1997; Maranzano and

Wagner, 2001). Collins et al. (1979) suggested that broadening of the particle size distribution leads to a decrease in the suspension viscosity and a shift in the critical shear rate to lower values. Later, for a bimodal suspension of sterically stabilized PMMA particles, D'Haene et al. (1994) proposed a procedure to calculate the limiting viscosities from the characteristics of monodispersed systems. The bimodal suspensions have shown lower viscosity but a higher critical shear rate compared to the monodispersed suspension (Maranzano and Wagner, 2001). Recently, Guy et al. (2020) tested the Wyart–Cates model for non-Brownian shear thickening using bidisperse suspensions. Their results showed that the WC model applies only in the monodisperse limit and fails when substantial bidispersity is introduced. They attributed the failure of the model due to its inability to distinguish large–large, large–small, and small–small frictional contacts.

2.6.5 Effects of Particle-Particle Interactions

Interactions between the particles play an essential role in the rheological characteristics of suspensions. Particles in the shear thickening system may remain neutral or repel one another due to entropic or steric interactions. At low shear rates, the deflocculated suspensions exhibit low viscosity but their viscosity increases by shear thickening at higher shear rates. By contrast, flocculated suspensions have high viscosity at low shear rates, and shear thinning behavior is seen as the shear rate increases (Barnes, 1989).

2.6.6 Effects of Carrier Fluid

Carrier fluid is vital for the rheological behavior of shear thickening suspensions. It is found that higher molecular weight fluid-based STFs exhibit

higher viscosity, explained by longer molecular chains that hinder the relative movement of adjacent layers of fluid relative to each other. Also, lower critical shear rates are observed by increasing the molecular weight of carrier fluids. Shear thickening is achieved with lower amounts of solid particles using higher molecular weight fluids in suspensions. Moriana et al. (2016) investigated fumed silica-based STFs using PEG and PPG liquids and reported that thickening behavior is found to occur at lower shear rates in PPG suspensions, as shown in **Figure 2.5**(a). Qin et al. (2017) investigated the effect of liquid medium for suspensions of polystyrene spheres of 55 wt% in PEG carrier fluids. Regardless of the shear thickening mechanism, this trend is also observed in pure carrier fluids, as shown in **Figure 2.5**(b).

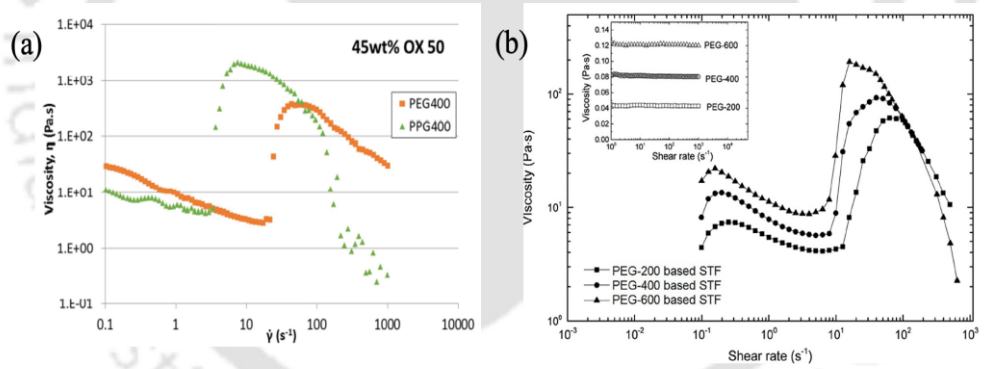

Figure 2.5 (a) Viscosity measured as a function of shear rate under steady shear conditions for STF containing 45 wt.% OX50 using different carrier fluids (Moriana et al., 2016). (b) Effects of liquid medium for suspensions of polystyrene spheres (55 wt%) in PEG carrier fluids (Qin et al., 2017)

2.6.7 Effect of Addition of Fillers

Although several researchers have studied the various parameters, the addition of nanofillers is another significant parameter that influences the

rheological behavior of shear thickening suspensions. Shear thickening suspensions with different nanofillers are chosen to impart specific properties to the resulting suspension, significantly benefiting the composite material. These nanofillers are typically graphene, carbon nanotubes, ceramic, and metal particles. The inclusion of these nanofillers provides tensile strength to the shear thickening fluid, and load transfer can be efficiently carried throughout the material. Nanofillers generally have an apparent diameter ranging from 1 nm to 80 μm and are dispersed in shear thickening suspensions with compositions varying from 0.01 wt % to 10 wt %.

Xu et al. (2010) investigated the shear thickening suspensions based on additives with different concentrations and molecular chain lengths. They have considered three different additives with different molecular chain lengths of PEG4000, PEG6000, and PEG10000. A significant effect in shear thickening was observed with increasing the concentration and the molecular chain length of additives. Gurgen et al. (2016) studied the influence of micron-sized ceramic and carbide particles as additives in silica-based shear thickening suspensions. Their experimental results demonstrated that additive particles in the shear thickening suspensions disrupt the thickening behavior and suggested that the intensity of the disruption depends on additive particle size and additive concentration.

Recently, Singh et al. (2019) carried out experiments on fumed silica-based shear thickening suspensions dispersed in polyethylene glycol with nano-clay as an additive. Experimental studies were performed to improve the impact resistance of p-aramid fabrics by adding silica-halloysite to the existing shear thickening fluid (Laha and Majumdar, 2016). Their experimental results showed a more intense

shear thickening with increasing the amount of silica-halloysite in the suspensions, as shown in **Figure 2.6**. Furthermore, the impact energy absorption by p-aramid fabrics increased drastically by adding these halloysites to the suspensions. Ge et al. (2017) have compared the rheological properties of shear thickening fluids reinforced with SiC nanowires with pure shear thickening fluid. Interestingly, they observed almost a 30% increase in the initial and maximum viscosity of the suspensions with SiC nanowires.

In recent experimental studies, extensive research was carried out on the addition of carbon nanofillers as additives. These carbon nanofillers are widely used in polymer composites as they have played a significant role in enhancing the rheological properties of the suspensions and the mechanical properties of the materials. Majumdar et al. (2011) demonstrated a discontinuous shear thickening transition in a flocculated suspension of MWNT at low weight fractions dispersed in a low viscosity Newtonian fluid. Their experimental results showed that the viscosity jumps drastically by four to six orders of magnitude with an increase in shear stress. Later, Sha et al. (2013) investigated the influence of the addition of carbon nanofillers on the shear thickening behavior. The shear thickening effect was significantly enhanced by the addition of graphene nanoplates (GNs) and carbon nanotubes (CNTs). The results also showed that the shear thickening behavior with CNTs was more effective than GNs.

Hasanzadeh and Mottaghitalab (2016) carried out experiments on the rheological behavior of fumed silica suspensions using multi-walled carbon nanotubes (MWNTs). The results showed that the addition of MWNTs strongly

influences the rheological properties of concentrated silica suspension. However, the critical viscosity of the suspension decreased, and the onset of shear thickening appeared at a higher shear rate with the inclusion of MWNTs. In contrast to Hasanzadeh and Mottaghitalab, Wei et al. (2020) demonstrated that MWCNT/SiO_2-STFs have significant shear thickening behavior. They observed that when the weight fraction of MWNTs is 0.8%, the shear thickening performance was more efficient and showed a viscosity increase by 191%, and the critical shear rate decreased by 60.19%. Huang et al. (2015) experimentally studied the rheological behavior of concentrated silica-based shear thickening suspensions using graphene oxide as an additive. The obtained results showed a significant change in critical shear rate, the viscosity of the suspension, storage modulus, and loss modulus of suspensions, as shown in **Figure 2.6**

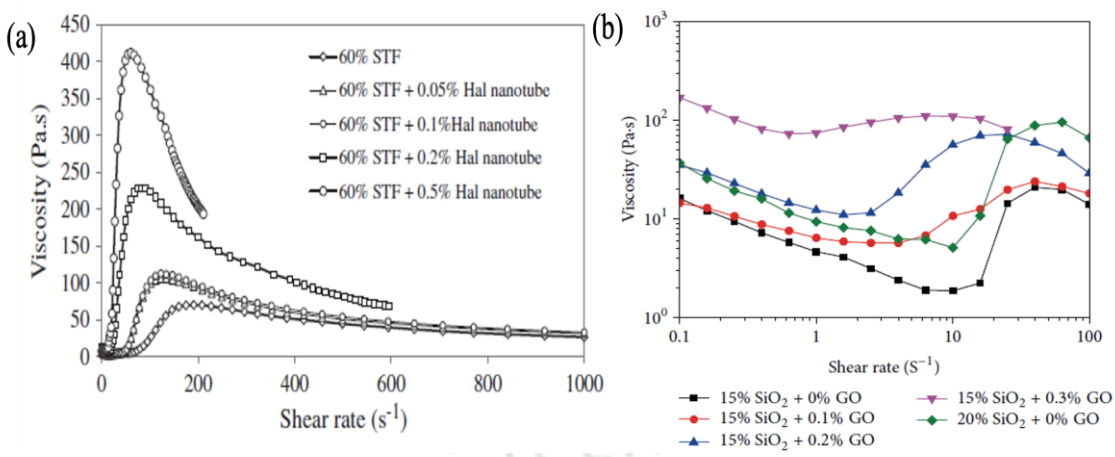

Figure 2.6 (a) Rheological behavior of STF with 60% silica and different loading of Hal nanotubes (Laha et al., 2016), (b) shear rate vs. viscosity of silica/PEG-based STF with various loading amounts of GO and silica (Huang et al., 2015)

.

2.7 Microstructure Visualization

In a simple shear flow, the particles are driven by several forces such as Brownian forces, hydrodynamic forces, electrostatic forces, and steric forces. However, a clear understanding of the mechanism under which these forces play an essential role for the suspension to shear thicken is still elusive. To understand the phenomena of shear thickening behavior, it is also required to obtain the microstructure under flow. Microstructural investigation of the suspensions in the radial and tangential shear planes using neutron scattering experiments has been carried out using rheo-SANS to understand the hydrodynamic contributions in the formation of clusters during shear thickening (Brady and Bossis, 1985; Maranzano and Wagner, 2002).

In the last decade, the advancement of technology has provided the simultaneous visualization of microstructure and rheological measurements in dense suspensions. One of the methods is to use confocal microscopy for imaging the microstructure of suspension during shear. Recent experimental studies using a counter-rotating cone and plate and a parallel plate shear cell coupled with confocal microscopy have provided a three-dimensional image of concentrated suspension during flow (Lee and Wagner, 2006; Derks et al., 2004; Cohen et al., 2004; Besseling et al., 2007; Besseling et al., 2009). Cheng et al. (2011) carried out experiments by combining fast confocal microscopy with shear stress measurements while considering microscopic single-particle dynamics to investigate the structure of the suspension in different flow regimes (**Figure 2.7**). Their data showed continuous shear thickening. The volume fraction of their samples were well below those needed

for jamming or glassy behavior. It is expected that in such a system, the hydrodynamic interactions dominate over the frictional contact between the particles. This lead them to conclude that continuous shear thickening arises from particle clustering induced by hydrodynamic lubrication forces. Recently, Lin et al. (2015) directly measured the hydrodynamic and contact force contributions to shear thickening using shear reversal experiments on micron-sized silica and latex particles. Their results showed that continuous shear thickening does not originate from hydrodynamic interactions but from the formation of particle contacts.

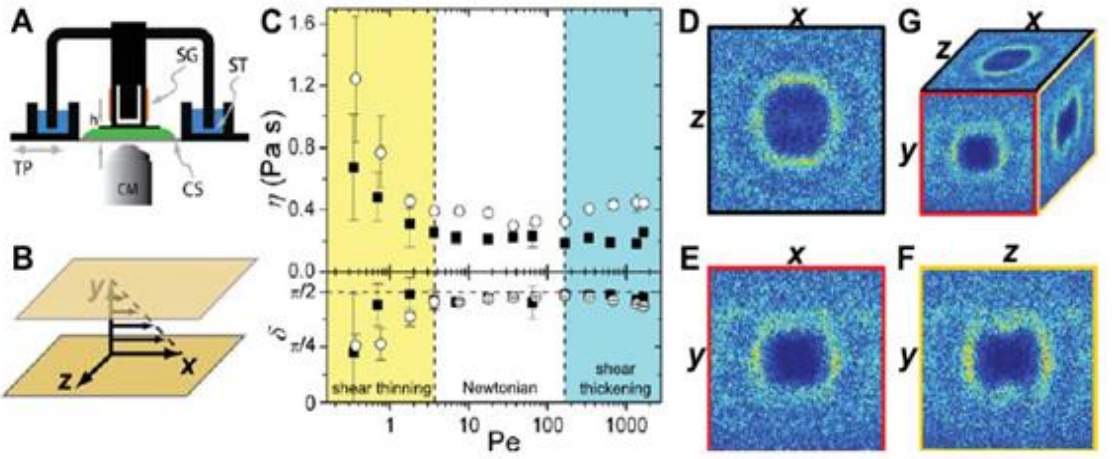

Figure 2.7 (A) Setup. CM, confocal microscope; SG, strain gauge; CS, colloidal suspension; ST, solvent trap. (B) coordinates. (C) Colloidal suspension rheology versus Pe for Φ= 0.34 (square) and Φ = 0.47 (circle). Upper and lower panel show η and δ, respectively. Vertical dashed lines mark boundaries between rheological regimes. (D to G) $g(\vec{r})$ for Φ = 0.34 sample at Pe = 0.036. (D to F) show cuts of $g(\vec{r})$ in the z-x, x-y, and z-y planes, and (G) indicates their orientation. Each plane is identified with a different bounding box color (Cheng et al., 2011)

Recent numerical simulations considering short-range lubrication and frictional contact forces attributed the formation of system-spanning force chains of the particles for strong shear thickening (Seto et al., 2013; Mari et al., 2014). Stokesian dynamics simulations carried out by Mari et al. (2014) reported that frictional contact force between the particles is responsible for the jamming condition in dense suspension. Wyart and Cates (2014) established that S-shaped flow curves arise generically within the scenario of stress-induced contact proliferation and predicted two distinct types of discontinuous shear thickening in the absence of inertia in dense Brownian suspensions. They predicted discontinuous shear thickening to arise when finite-range repulsions defer contact formation until a characteristic stress level is exceeded.

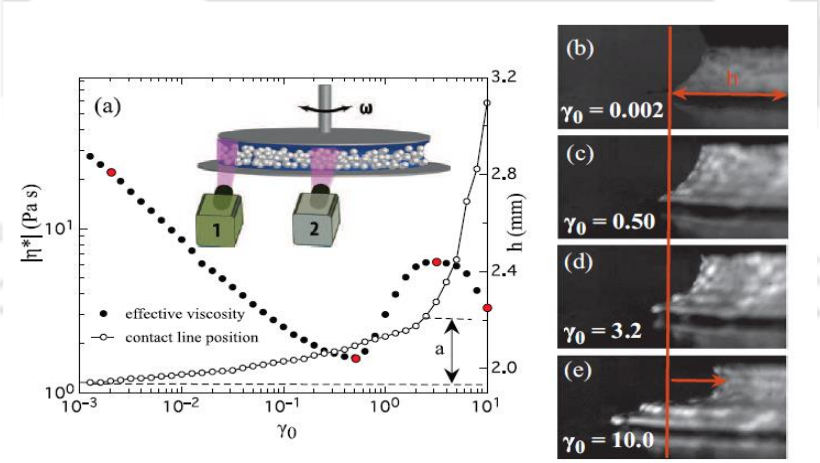

Figure 2.8 Movement of the suspension-air interface. (a) Viscosity $|\eta^*|$ and radial distance, h, to the outer edge of the suspension as a function of the applied strain amplitude γ_0. Inset: a sketch of the setup. Cameras 1 and 2 are used for imaging the interface and the velocity profile. (b)–(e) Images of the suspension boundary at specific γ_0 values, which are also displayed as red dots in (a). The vertical red line indicates the initial contact line position between suspension and substrate (Qin et al., 2014)

Qin et al. (2014) have experimentally investigated the shear thickening in dense granular suspension. They have analyzed the shear profile by directly imaging the suspension-air interface and extracted the viscosity contributions induced by hydrodynamics, dilation, and sedimentation, as shown in **Figure 2.8**. Metzner and Whitlock (1958) demonstrated that dilation in the suspension of titanium dioxide particles started with the onset of shear thickening for a range of particle volume fractions. However, they observed dilation but no shear thickening in the case of glass bead suspensions. This indicates that dilation is not always equivalent to shear thickening. Maharjan et al. (2021) investigated dilation-induced surface deformations in DST suspension by directly visualizing the surface of the suspension in a rheometer. A roughened surface of the suspension is observed, indicating the dilation effects.

Experimental studies on shear thickening have mostly reported the fundamental behavior of the suspension and the influence of different parameters on the onset of shear thickening. In a simple shear flow, the rheological properties of the suspensions are characterized by shear viscosity, first and second normal stress differences. Significant efforts have been made to determine the effect of particle loading, size, distribution, and carrier fluid on the rise in the viscosity of shear thickening suspensions (D'Haene and Mewis, 1994; Greenwood et al., 1997; Maranzano and Wagner, 2001; Kalman et al., 2007; Warren et al., 2015; Gurgen and Kushan, 2016; Moriana et al., 2016; Qin et al.,2017). However, the behavior of normal stress differences and their relation to shear thickening (in particular, the DST) are not yet completely understood. The normal stress difference measurements in a concentrated suspension are essential as they provide evidence

of non-Newtonian behavior (Phung et al., 1996; Foss and Brady, 2000; Singh and Nott, 2003).

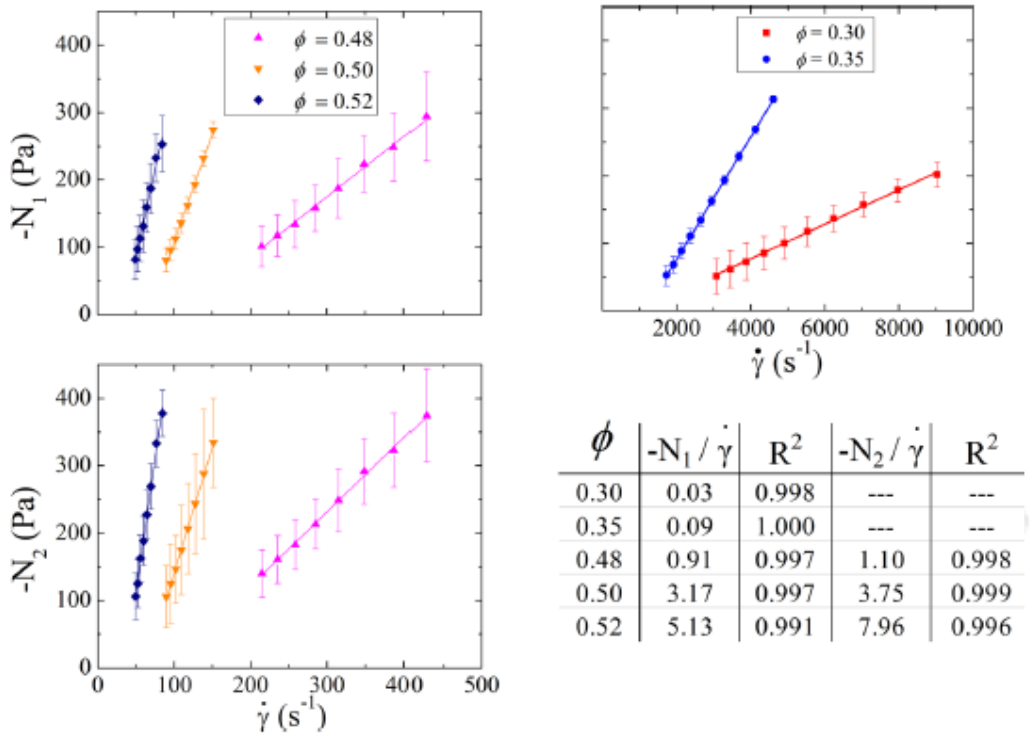

ϕ	$-N_1/\dot{\gamma}$	R^2	$-N_2/\dot{\gamma}$	R^2
0.30	0.03	0.998	---	---
0.35	0.09	1.000	---	---
0.48	0.91	0.997	1.10	0.998
0.50	3.17	0.997	3.75	0.999
0.52	5.13	0.991	7.96	0.996

Figure 2.9 First (top) and second (bottom left) normal stress differences in the shear-thickened state as a function of the shear rate plotted on linear axes. The linear regression analysis for each volume fraction is shown in the bottom right (Cwalina and Wagner, 2014)

The clustering or change in particle arrangement cannot be taken as evidence of the purely hydrodynamic nature of these clusters. The sign of the first normal stress difference is considered to be more clear evidence of the hydrodynamic or frictional nature of clusters (Cwalina and Wagner, 2014). Cwalina and Wagner (2014) experimentally studied the shear stress and the first and second normal stress differences in the shear-thickened state as a function of the particle volume

fraction. Their experimental results showed negative normal stress differences that varied linearly with the shear rate in the shear thickening state, shown in **Figure 2.9**.

Recent experiments and simulation studies reported a transition of the first normal stress difference from negative to positive value due to increased frictional contact forces over the hydrodynamic lubrication forces at high volume fractions (Hébraud, 2009; Lootens et al., 2005; Couturier et al., 2011; Gurnon and Wagner, 2015; Royer et al., 2016; Singh et al., 2018). Cao et al. (2021) studied shear jamming in a polymer-based granular suspension. They reported the transition of discontinuous shear thickening to shear jamming, accompanied by a negative to positive N_1 at higher particle concentration (**Figure 2.10**).

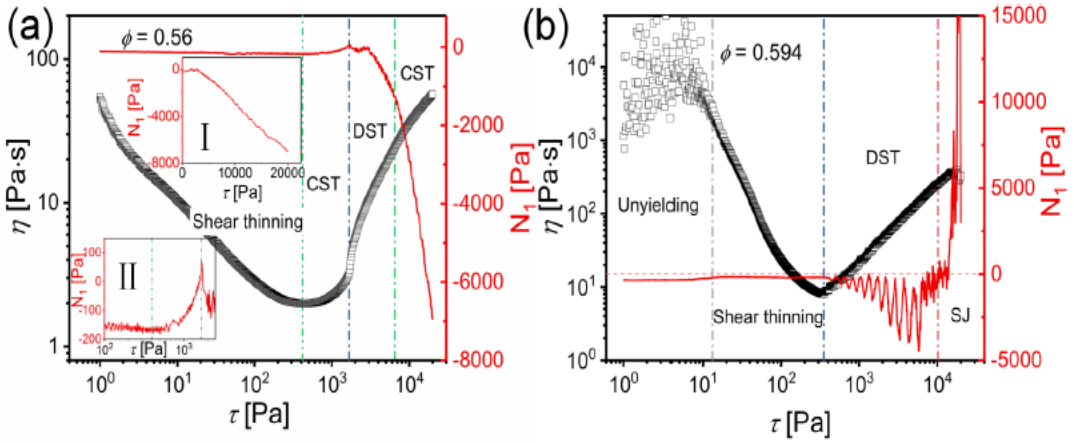

Figure 2.10 The apparent viscosity η and first normal stress difference N_1 vs. the shear stress τ for (a) $\Phi = 0.56$ and (b) $\Phi = 0.594$. Inset I: N_1 vs. τ in the linear coordinate system indicates that $-N_1$ is proportional to τ. Inset II: an enlarged view of N_1 during the CST to DST transition. The positive contribution to N_1 in the CST area originates from the Brownian motion (Cao et al., 2021)

Seto and Giusteri (2018) investigated the origin of normal stress differences using inertialess particle dynamics simulations. Their simulation data show that upon increasing the volume fraction in the high Péclet-number limit, there is a transition from a regime in which the negative values of N_1 are essentially determined by hydrodynamic interactions to a regime having synergies between hydrodynamic and contact interactions that produce even more evident negative values. Lee et al. (2020) have compared the experimental rheology data of colloidal dispersions with model predictions where the dominant effect is contact friction. Interestingly, in a recent simulation study, Wang et al. (2020) demonstrated that a hydrodynamic model without any contact friction can explain the discontinuous shear thickening in dense suspensions for particles with rough surfaces. Their simulations predicted a negative first normal stress difference at moderate to high Peclet number.

In some studies, dynamic shear rheology has also been used to understand their rheological properties (Raghavan and Khan, 1997; Galindo-Rosales et al., 2009; Laun et al., 1991). Investigations on the dynamic responses of suspensions were carried out to understand the relation between stress-controlled critical shear rate and frequency-dependent critical strain (Lee and Wagner, 2003; Fischer et al., 2006; Galindo-Rosales et al., 2009). Laun et al. (1991) initially studied the dynamic shear thickening of a polymer latex dispersion and reported the critical strain amplitude at a fixed angular frequency. Later, Raghavan and Khan (1997) qualitatively explained the hydrodynamic clustering mechanism by correlating the strain thickening and shear thickening using a modified Cox-Merz rule. They also reported the shear thickening response of nonflocculated fumed silica particles

dispersed in polar and nonpolar solvents (Raghavan et al., 1998; Raghavan et al., 2000)

Recently, Swarna et al. (2018) studied the dynamic shear response of silica nanoparticle suspensions in polyethylene glycol and demonstrated the impact of silica surface modification on the linear and nonlinear viscoelasticities. The recent rheological studies on shear thickening suspensions have probed the role of hydrodynamic and frictional forces in explaining the phenomena of discontinuous shear thickening. There are some examples of discontinuous shear thickening in different suspensions with negative normal stress differences, which support hydrodynamic models, and some with positive normal stress differences, which support frictional models.

CHAPTER 3 Materials and Methodology

3.1 Introduction

This chapter will discuss the materials and methodology for the preparation of shear thickening suspension by mechanical and Sonochemical methods. Steady and dynamic rheological measurements of the prepared samples were analyzed using a rheometer. The particle characterization was done by conducting Field Emission Scanning Electron Microscopy (FESEM), Powder X-Ray Diffraction, and FTIR.

3.2 Materials

The materials used for the preparation of shear thickening fluids are explained below.

- **Fumed Silica**

Two nano-sized fumed silica particles of sizes 7 and 200 nm were used as dispersed phase (solid) and purchased from Sigma-Aldrich. Due to its thixotropic behavior and thickening property, fumed silica is the most favored material as a rheological modifier. It has a high specific surface area and branching structure, which displays its remarkable rheological properties. Fumed silica particles are readily available and naturally branched aggregates that enable close contact between the particles at a critical shear rate. It is amorphous nonporous silica synthesized by high temperature (flame) hydrolysis of $SiCl_4$ in O_2 (N_2)/H_2 flame. It is hydrophilic due to the hydroxyl or silanol group (-OH) on the surface. The microdroplets of amorphous silica fuse into a branch and form a chain-like agglomerate.

- **Fillers**

Graphene oxide (3-6 layers, 0.8-2nm Diameter, 5-10µm Length), Multi-Walled Carbon Nanotube (5-20nm Diameter, 10-µm Length) were used as fillers and were purchased from TECHINSTRO company. Mica particle (15-µm length) is also used as filler.

- **Polyethylene glycol**

Polyethylene glycol is a water-soluble, synthetic polar polymer that absorbs the surface of silica particles. This absorption leads to an increase in the hydrodynamic boundary of particles and the overall viscosity of the system. These fluids are Newtonian with low viscosity, are non-toxic, and have good stability. Polyethylene glycol (PEG), having different molecular weights were selected as a Newtonian carrier fluid (Sigma Aldrich). The average molecular weights selected for PEGs were 200, 300, and 400 g/mole. The physical properties of these fluids are given in **Table 3.1**.

Table 3.1 Physical properties of Polyethylene glycol (PEG)

PEG	Molecular Weight (g/mole)	Density (g/cm^3)	Viscosity at 20°C (mPa.s)	Refractive Index	Melting Point (°C)
PEG 200	200	1.124	60	1.4580 to 1.4610	-65
PEG 300	300	1.125	95	1.4620 to 1.4650	-11
PEG 400	400	1.128	120	1.4650 to 1.4680	4-8

- **Ethanol**

Ethanol is an organic chemical solvent used to mix silica particles, and polyethylene glycol was purchased from Merck. Because of its molecular structure, it allows for the dissolving of both hydrophobic and hydrophilic compounds. Ethanol (Merck) is a polar molecule due to its hydroxyl (OH) group, with the high electronegativity of oxygen, allowing hydrogen bonding to occur with other molecules. The ethyl alcohol is used to help the impregnation procedure of STFs by reducing the surface tension of solutions and provides well-impregnated fabrics.

- **Blender**

The blender (Universal motor, RO-122, HP 1/20) was used to mechanically mix the fumed silica particles and polyethylene glycol in an excess amount of ethanol until all the silica particles were dispersed uniformly. It works through the centrifugal force generated by its impeller. When the liquid in question moves in a circular motion and at high speed, the so-called "Venturi" effect is generated, forcing the silica particles to mix quickly in polyethylene glycol.

- **Ultrasonic Homogenizer**

The ultrasonic homogenizer was used to sonicate the sample for proper mixing of the suspension. Sonication applies sound energy to agitate the particles in a sample for various purposes. Ultrasonic frequencies (>20 kHz) are usually used, leading to the process also being known as ultra-sonication. In this process, an ultrasonic bath (Lab companion UC-02) is used, which has a frequency of 40 kHz. Sonication is much better than mechanical agitation.

- **SPINOT Magnetic Stirrer Hot Plate**

The magnetic stirrer hot plate (Tarsons) is often used to substitute for a hot air oven to evaporate the excess ethanol solvent. The hot plate is maintained at 80-100^{0}C to evaporate the solvent as the ethanol boiling point is very low.

- **Agate Mortar and Pestle**

A mortar pestle is used to grind the dried material to obtain shear thickening fluid made of natural agate with highly polished grinding surfaces. These mortar pestles are excellent for preparing laboratory samples and high-purity powders. The agate material is a special silicate with a main composition of SiO_2. It is resistant to detergent, and thermal endurance is limited to up to 350^{0}C.

- **Vacuum Desiccator**

The resulting sample produced during the grinding process contains tiny air bubbles which are needed to be removed. These samples are kept in a vacuum desiccator (Tarsons) for 24 hr. allowing the bubbles to rise. The final samples were transparent and devoid of any water contamination.

3.3 Preparation of Shear Thickening Suspension

Achieving shear thickening at lower-weight fractions is highly desired in many practical applications. In this study, we could achieve a high shear thickening ratio by following the proper procedure for preparing the suspension that enables removing air bubbles and any water contamination. The presence of even tiny bubbles is detrimental to the preparation of shear thickening suspension. The shear thickening suspension was prepared by two methods. One was prepared using the

mechanical agitation method and the other by the sonochemical homogenization method. The complete methodology of these methods is explained below.

3.3.1 Mechanical Agitation Method

Shear thickening suspensions of lower concentrations (10-20wt%) were prepared by adding the required amount of fumed silica nanoparticles in polyethylene glycol. A blender was used to mix until the silica particles were evenly dispersed in the carrier fluid. The resultant sample contains tiny bubbles that are to be removed. Therefore, the sample is kept in a vacuum desiccator for 24 hours, allowing the bubbles to rise and get a transparent fluid. However, shear thickening suspensions of higher concentrations ($> 20\%$) were difficult to synthesis in one step. Hence preparation of the shear thickening suspension was synthesized in two steps. Initially, 10% shear thickening suspensions were fabricated, and later silica powders were added in intervals and blended sufficiently. After adding fumed silica in a carrier fluid, the sample became solid with more agitation, making it challenging to mix. Therefore, a 30 min rest in between the stirring gives the sample to become liquid again. The above step is repeated until the required concentration of fumed silica is dispersed in the carrier fluid. Later, the sample is kept in a vacuum desiccator for 24 hours to remove the bubbles. Usually, the time taken for the fabrication of shear thickening suspension by the mechanical agitation method is more than 48 hours for higher concentrations which were time-consuming. An illustration of sample preparation is given in **Figure 3.1**.

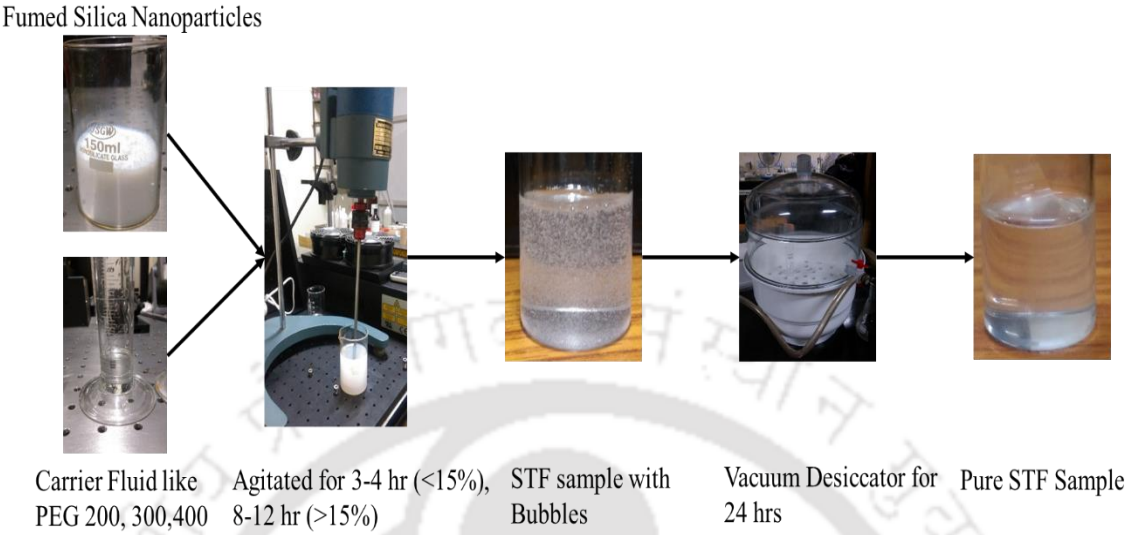

Figure 3.1 Illustration of sample preparation by mechanical agitation method

3.3.2 Sonochemical Homogenization Method

To achieve discontinuous shear thickening at low to moderate particle concentration, we have prepared the shear thickening suspensions with fumed silica particles dispersed in polyethylene glycol by sonication method. This preparation methodology is efficient, fast and gives final suspension devoid of any water contamination. Shear thickening suspensions were prepared by adding fumed silica nanoparticles and PEG in an excess amount of ethanol. The mixture was kept in a sonication bath and maintained at room temperature for 4-5 hr to achieve stable and well-dispersed solutions. Later, the sample was heated above 85°C to evaporate the excess amount of solvent. The resultant samples were grinded in an agate mortar and pestle to get shear thickening fluid. However, tiny air bubbles were formed during the grinding of samples, which needed to be removed. Therefore, these samples were kept in a vacuum desiccator for 24 hr allowing the bubbles to

rise. The final samples were transparent and devoid of any water contamination. The schematic of the sample preparation method by sonochemical homogenization is given in **Figure 3.2**.

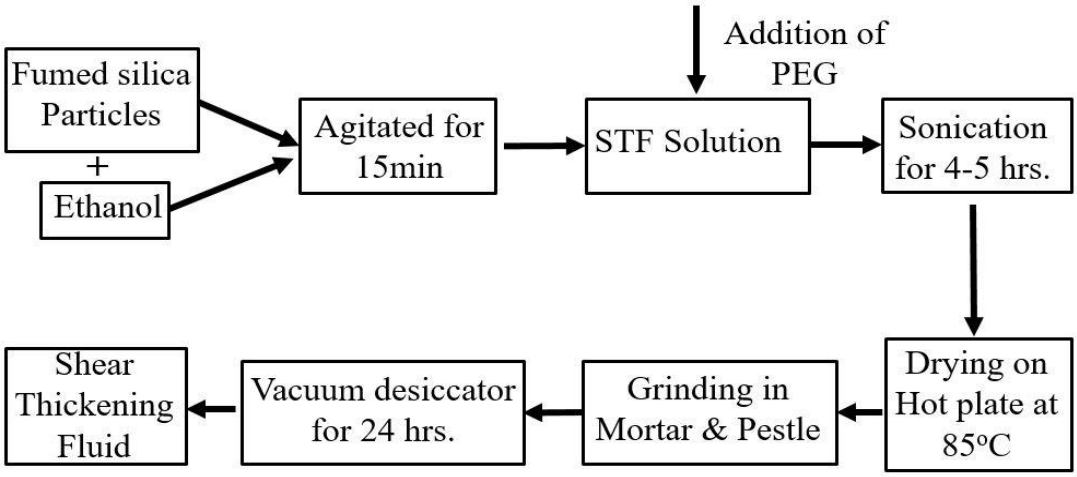

Figure 3.2 Schematic of sample preparation method by sonochemical method

In this study, to prepare a 20wt% sample fumed silica of 3 grams was dispersed in 80-90ml of ethyl alcohol to obtain a stable solution. The sample was agitated for 15 min at 750 rpm with the help of a blender. Later, 10.7 ml of PEG is added and mixed for 15 min at 750 rpm. After mixing, the sample was lept in sonication for 3-4 h in an ultrasonication bath at a frequency of 40KHz. The obtained sample was poured into Petri dishes, and the excess ethanol was evaporated at 85 ^{0}C. Petri dishes were used to reduce evaporation time by increasing the surface area. After drying, obtained materials were grinded with the help of an agate mortar and pestle. The obtained fluids were kept in a vacuum desiccator to remove the air bubble, which could adversely influence the rheological analyses. An illustration of sample preparation is given in **Figure 3.3**.

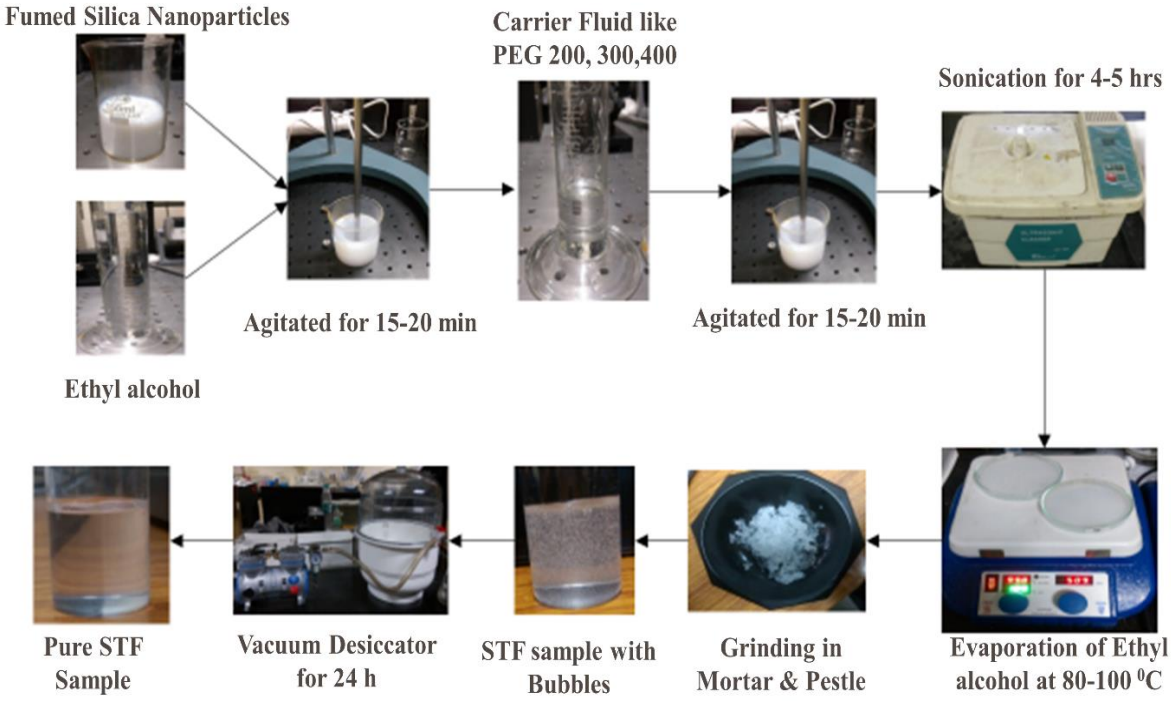

Figure 3.3 Illustration of sample preparation by the sonochemical homogenization method

Figure 3.4 shows the comparison of viscosity versus shear rate behavior for the samples of 15 wt%, 200 nm fumed silica particles in PEG 300 prepared using the mechanical agitation method and the Sonochemical homogenization method. We can observe that though the low shear viscosity and critical shear rates for both the samples are similar, the maximum viscosity is higher for the sample prepared using the Sonochemical method. We also noticed that the sample prepared using the mechanical method showed continuous shear thickening behavior compared to the one prepared with the Sonochemical homogenization method.

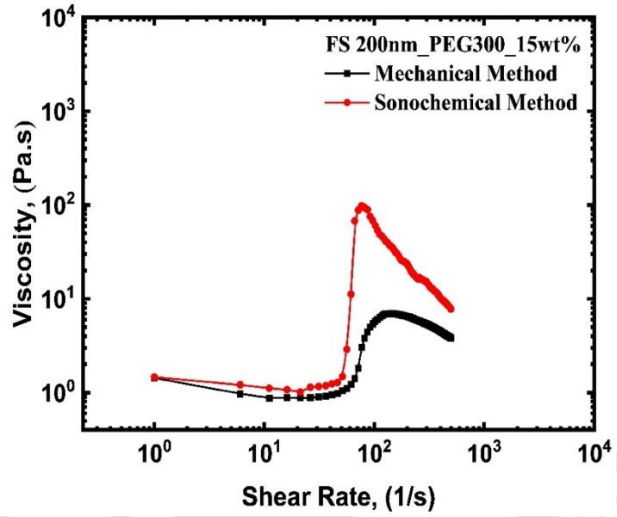

Figure 3.4 Comparison of viscosity versus shear rate behavior for the samples (15 wt%, 200 nm fumed silica particles in PEG 300) prepared using the mechanical agitation method and the Sonochemical homogenization method.

3.4 Rheological Characterization

All rheological measurements for the samples were performed using a Rheometer (MCR 301, Anton Paar) with a 2° cone and plate geometry diameter of 25mm. A temperature control device (Viscotherm VT2) was used to maintain the temperature of the sample at 25°C throughout the test. Rheological measurement of concentrated suspensions can be complicated due to wall slip. To prevent wall slip, serrated cone-plate geometry was used in all but rheomicroscopy experiments where the bottom plate was replaced by a transparent glass plate. Shear thickening samples were placed on the bottom plate, and the upper plate was lowered to a gap of 0.107mm. A pictorial representation of the rheometer is shown in **Figure 3.5**. Rheological shear measurements were done two ways: one by steady shear analysis and the other by dynamic shear measurements.

Figure 3.5 Pictorial representation of Anton Paar MCR 301 rheometer

3.4.1 Steady Shear Measurements

Steady shear rheological measurements are performed to observe the equilibrium microstructure and bulk viscosity of materials. Under steady shearing, the shear thickening sample was rotated by varying the shear rate from 1 to 500 s^{-1} at a constant room temperature of 25 ˚C. A total of 100 measuring points were plotted in the time duration of 6 secs, with each measuring point plotted after 5 sec. The shear rate vs. viscosity graphs were generated to compare various parameters. Experiments were repeated to check the reproducibility and consistency of the samples.

3.4.2 Dynamic Shear Measurements

Dynamic shear measurements of the sample were performed by vibrating between the plates. In dynamic shear measurements, a sinusoidal oscillation of stress or strain is applied to the sample. Two oscillatory measurements were also performed: strain amplitude sweeps at a constant frequency and angular frequency

sweeps at a constant strain. Strain sweeps were measured by varying the strain from 1 to 1000% at a constant frequency of 10, 50, 100 rad/s, and frequency sweeps were carried out in the range of 0.1 to 100 rad/s, at a constant strain of 100, 500, 1000%. Complex modulus can be separated into real and imaginary parts: storage modulus (G') and loss modulus (G''). Storage modulus defines the stored energy by the sample material, whereas loss modulus defines the dissipated energy by the material.

3.5 Characterization of Silica Particles

3.5.1 Microstructural Evaluation by Field Emission Scanning Electron Microscopy (FESEM)

Morphology of the fumed silica particles and the prepared suspension was evaluated using a Zeiss make sigma model Field Emission Scanning Electron Microscopy (FESEM). Fumed silica particles were dispersed in water in a small amount and sonicated for 15 min for better dispersion of the particles in the water. A drop of the solution was dried on an ITO plate to characterize the fumed silica particles. Before the analysis, the gold sputtering technique was applied to prevent electron charge accumulation.

3.5.2 Powder X-ray Diffraction

Wide-angle x-ray diffraction (XRD) patterns of the 7nm and 200nm fumed silica and nanofillers were determined by Powder X-Ray Diffraction (Model: SmartLab, Make: Rigaku, Japan). Data were collected in the range of 5–90° with an increment of 0.02 at 20°/min scan speed and 5 kW X-Ray power. The CuKα1

of the 1.5416 Å wavelength source was used with a nickel filter. The phases of the synthesized materials were compared with their simulated pattern obtained from Joint Committee on Powder Diffraction Standards (JCPDS) database.

3.5.3 Fourier Transform Infrared Spectroscopy

FTIR spectra were obtained using an IR Affinity Fourier Transform Infrared spectrometer (Make: Shimadzu, Japan) to identify the functional groups of the silica nanoparticles and fillers. The FTIR spectra were collected in a wavelength range of 400 –4000 cm^{-1} with 30 scans and a resolution of 4 cm^{-1}.

CHAPTER 4 Effect of Fluid and Particle Parameters on Shear Thickening

4.1 Introduction

This chapter presents a systematic rheological study on the shear thickening suspensions prepared from fumed silica particles at low particle concentrations. Fumed silica particles are easily available and are naturally branched aggregates which enable close contact between the particles at a critical shear rate. In many practical applications, achieving shear thickening at lower-weight fractions is highly desired. This was possible by following a proper procedure for preparing the suspension that enables the removal of air bubbles and any water contamination, as described in the earlier chapter. We believe that such air pockets may be exposed to low-pressure fields at high shear rates, causing them to expand and prevent particle to particle contact. This scenario may lead to continuous shear thickening and poor shear thickening behavior. This could be one of the reasons why the majority of the previous experiments have reported continuous shear-thinning followed by shear thickening even at moderate particle concentration. Our investigations at low to moderate particle concentrations showed Newtonian behavior below the critical shear rate. We have prepared the shear thickening suspensions with fumed silica particles dispersed in PEG by the sonication method. Suspensions were prepared by considering a different combination of weight fractions of fumed silica particles and polyethylene glycol (PEG) of different molecular weights. Further, the rheological properties of these samples were investigated to understand the effect of various parameters on shear thickening. A possible mechanism for the role of carrier fluid and particle size distribution on the shear thickening behavior of fumed silica suspension has been proposed. The obtained results exhibited the fundamental behavior of shear thickening and

enabled us to analyze the influence of different parameters on the quality of shear thickening.

4.2 Results and Discussion

4.2.1 X-Ray Diffraction

The XRD patterns of 7nm and 200nm fumed silica nanoparticles used in this study are shown in **Figure 4.1**, which can be used to deduce the phase composition of the samples. It was observed that both silica particles exhibited similar XRD patterns with a broad peak in the range of 20° to 30°, which indicates that the samples used are in an amorphous state.

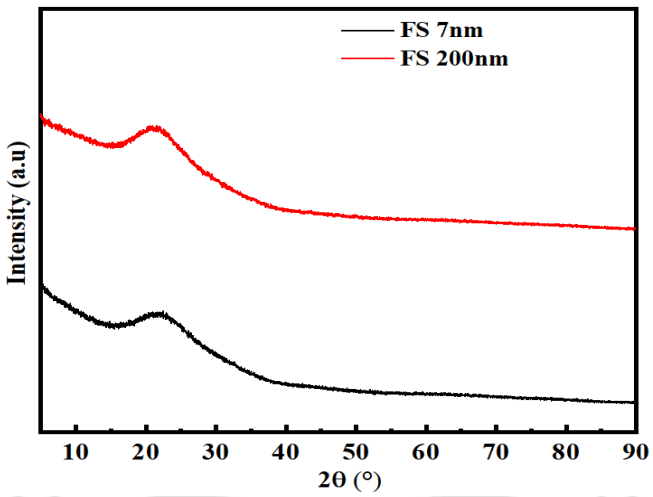

Figure 4.1 XRD patterns of 7 nm, 200 fumed silica particles

4.2.2 FTIR

The FTIR spectra of 7nm and 200nm fumed silica nanoparticles are shown in figure 4.2. It was found that both silica nanoparticles showed a distinct

absorption peak at 3430 $cm^{-1,}$ which corresponds to the presence of silanol groups (Si-OH) on the surface of silica particles.

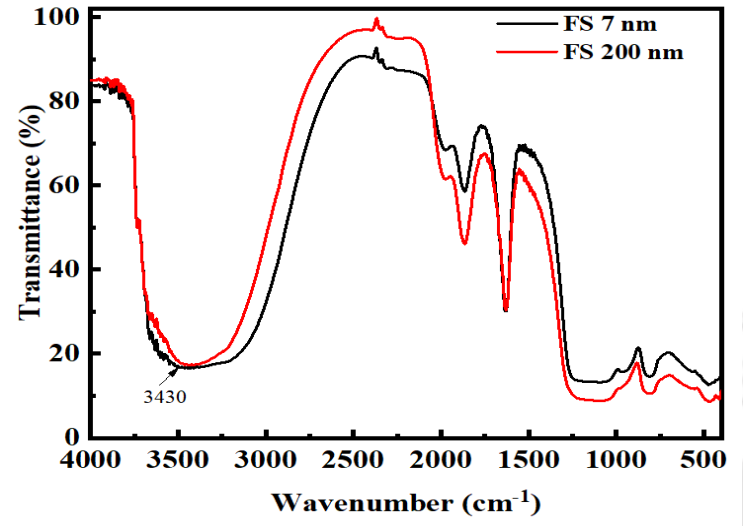

Figure 4.2 FTIR spectra of 7nm and 200nm fumed silica particles

4.2.3 Microstructural Characterization

The FESEM images of fumed silica and STF samples are shown in **Figure 4.3**. Images of silica nanoparticles dispersed in water can be seen in **Figure 4.3**(a) and (b). Both the fumed silica particles (7 and 200 nm) tend to form aggregates that are difficult to disperse completely. The average aggregate size varied depending upon the individual primary particle size. We have calculated the mean and standard deviation of primary and cluster particle size by considering 20 different clusters in the FESEM images. An image of dilute dispersion of fumed silica (7 nm) in water is shown in **Figure 4.3**(a). The primary particle size of this sample showed a mean value of 7.3 nm and a standard deviation of 1.1 nm. The average length of their aggregates was found to be 18.5 nm with a standard

deviation of 3.7 nm. The image of dilute dispersion of 200-nm fumed silica particles in water is shown in **Figure 4.3**(b). For this sample, the mean and standard deviation of the primary particle was 21.36 nm and 3.14 nm, respectively. The average length of aggregates was measured to be 203.8 nm with a standard deviation of 23.8 nm. **Figure 4.3**(c) shows the image of 200-nm silica particle suspension in PEG-200. It is clear from **Figure 4.3**(c) that the carrier fluid has completely coated the particles.

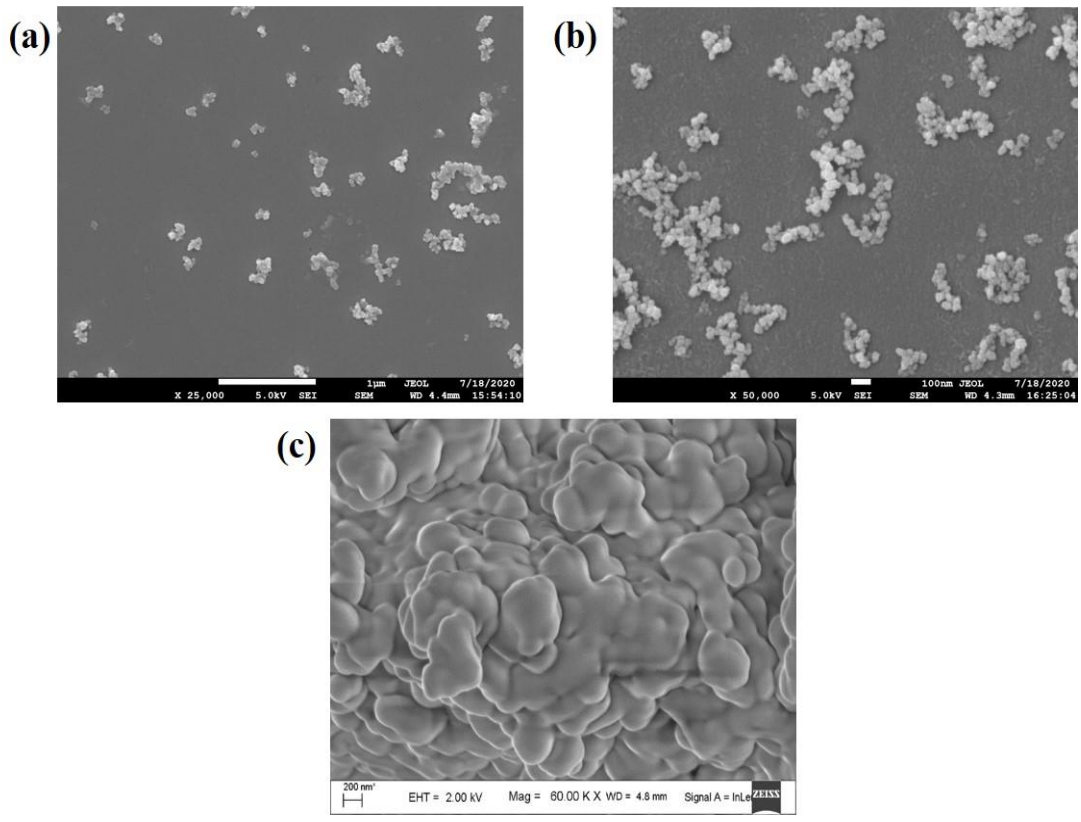

Figure 4.3 FESEM images of (a) fumed silica, 7 nm; (b) fumed silica, 200 nm; (c) STF prepared from 200 nm fumed silica particles in PEG 200

4.2.4 Influence of Particle Concentration

The influence of different parameters on the rheological properties of shear thickening fluids is studied by considering monodispersed suspensions. The rheological properties of the monodispersed STF samples were prepared by changing the weight fractions of 200 nm fumed silica in PEG and were tested at room temperature. **Figure 4.4** shows the viscosity as a function of the shear rate for different weight fractions of silica particles. **Figure 4.4** (a), (b), and (c), respectively, show the plots for 200 nm fumed silica particle suspensions in PEG 200, PEG 300, and PEG 400. The particle concentrations studied in these experiments were 15, 20, 25, and 30 wt%. All the samples showed a similar trend of discontinuous shear thickening behaviour.

It can be clearly observed that at very low shear rates, the 15 and 20 wt% samples showed nearly Newtonian behavior; 25 wt% and 30 wt% samples exhibited a shear-thinning behavior. The shear rate beyond which the shear thickening begins is said to be the critical shear rate ($\dot{\gamma}_c$). Further increase in the shear rate causes the viscosity to increase dramatically, reaching a maximum viscosity value of η_{max}. The ratio of the maximum viscosity of the suspension to the viscosity of the suspension at the critical shear rate is defined as the shear thickening ratio (STR), which signifies the ability of the suspension to thicken. After the point of maximum viscosity value (η_{max}), a steep decrease in viscosity can be seen with the increase in shear rate leading to a second shear-thinning behavior. It is to be noted that in very dense shear thickening suspensions, the boundary failure and edge fracture can also lead to viscosity decrease. Dhar et al. (2020) have reported boundary failures in shear thickening suspensions for particle volume fraction, $\phi \geq 0.55$. Since our

experiments were at low particle concentration, it is unlikely that the whole sample undergoes boundary failure. However, microscopic failures at random locations of the sample cannot be ruled out. Unfortunately, through experimental techniques, we cannot distinguish between the microscopic failures of jammed suspension and the breakage of hydroclusters in opaque systems. Full 3D simulations can be used to study these events and to find out the mechanism behind the second viscosity decrease in shear thickening suspensions.

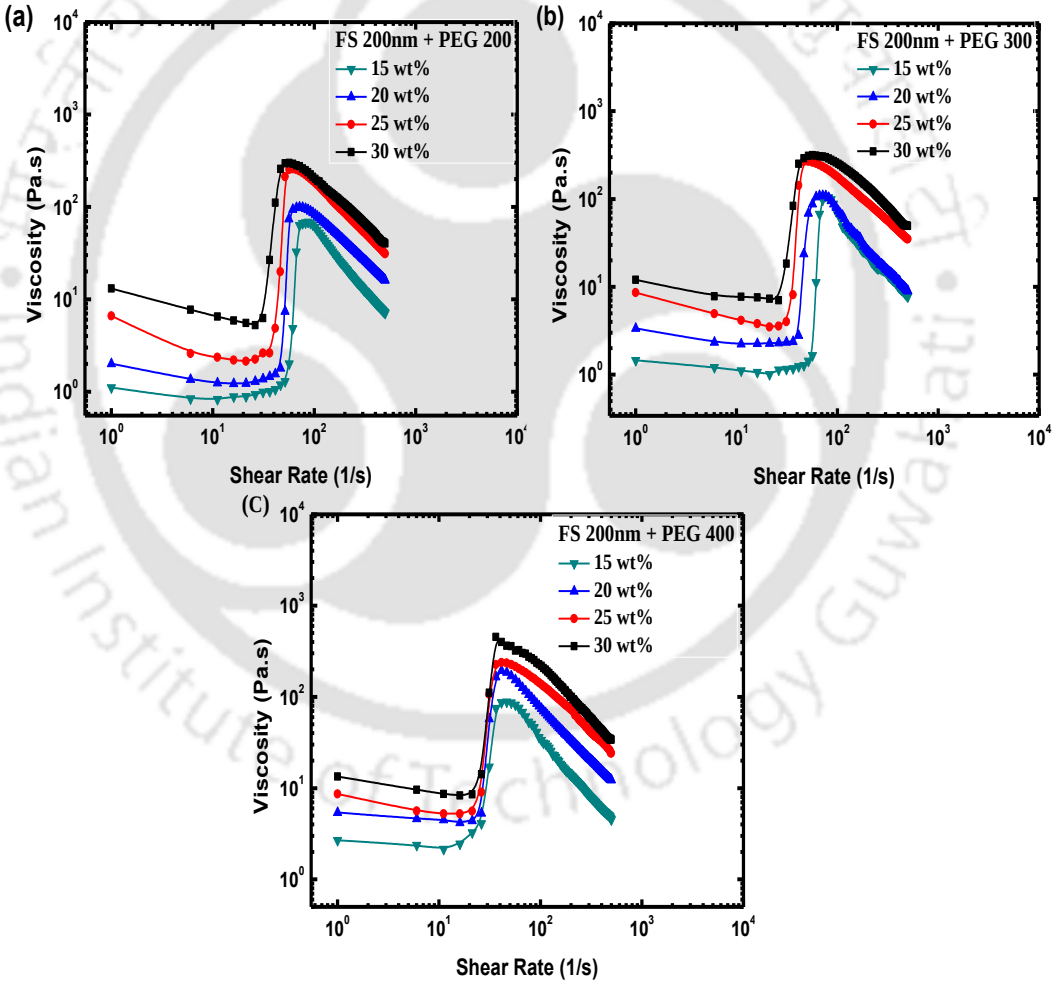

Figure 4.4 Suspension viscosity as a function of shear rate for different weight fractions of particles: (a) Fumed silica, 200nm in PEG 200 (b) Fumed silica, 200nm in PEG 300 (c) Fumed silica, 200 nm in PEG 400

It can also be observed from the viscosity versus shear rate plots that the critical shear rate decreases with the increasing weight fraction of fumed silica, and maximum viscosity increases. This decrease in the critical shear rate with particle concentration can be explained by the fact that the hydrodynamic force is inversely proportional to the interparticle distance, which enforces the particles to approach each other. When these particles approach each other at the critical shear rate, the hydrodynamic forces overcome the lubrication force and any interparticle repulsive forces causing the particles to form hydroclusters. Interparticle distance between the particles reduces as the particle concentration increases. Therefore, a lower critical shear rate is required to form hydroclusters at higher particle concentrations. Hydroclusters are disrupted when the sum of separating forces are more significant than the hydrodynamic forces, which brings the particles closer to form aggregates that can be visualized in CHAPTER 6. An estimate of hydrodynamic force $F_h \sim f(\eta_o a^3 \dot{\gamma} h^{-1})$ has been derived for particles by solving the Stokes equation (Boersma et al., 1990; Warren et al., 2015). Here, η_o is the zero-shear viscosity of the carrier fluid, a is the particle radius, $\dot{\gamma}$ is the shear rate, and h is the interparticle distance. Some previous works on colloidal suspensions have suggested that shear thickening is driven primarily by the formation of frictional contacts, with hydrodynamic forces playing a supporting role at lower concentrations (Royer et al., 2016). Particle level numerical simulations have suggested that the shear thickening transition in granular suspension is due to the system-spanning frictional contacts (Seto et al., 2013; Mari et al., 2014).

Upon increasing the weight fraction of silica particles, three effects on the viscosity curves are observed. First, an increase in the effective suspension viscosity

at lower shear rates can be seen with an increase in particle concentration. Second, a decrease in the critical shear rate is observed with the increase in the weight fraction of particles. Lastly, the maximum viscosity (η_{max}) increases with particle concentration. Another interesting observation we can make is that at higher concentrations (25 wt.% and 30 wt.%), the η_{max} values for PEG 200, 300, and 400 are nearly the same, even though the viscosity of pure PEG increases with molecular weight. This indicates that η_{max} is mainly influenced by particle-particle interactions, and at higher concentrations, these particles come into frictional contact with each other. When frictional forces come into play, the nature of fluid does not seem to affect the suspension viscosity.

Similarly, **Figure 4.5** shows the viscosity as a function of shear rate for different weight fractions for 7nm fumed silica particles. **Figure 4.5** (a), (b), and (c), respectively, show the plots for 7nm fumed silica particle suspensions in PEG 200, PEG 300, and PEG 400. The particle concentrations studied in these experiments were 15, 20, 25, and 30 wt%. The figure illustrates that increasing the concentration from 15 % weight fraction to 30% increases the maximum viscosity. It can also be seen from **Figure 4.5**(a), (b), and (c) that the sample containing 15wt% exhibits a continuous shear thickening behaviour when compared with other wt% in PEG 200,300, and 400. This behavior can be explained by the role of Brownian forces as they dominate nanoparticle suspensions and delay the thickening for higher critical shear rates.

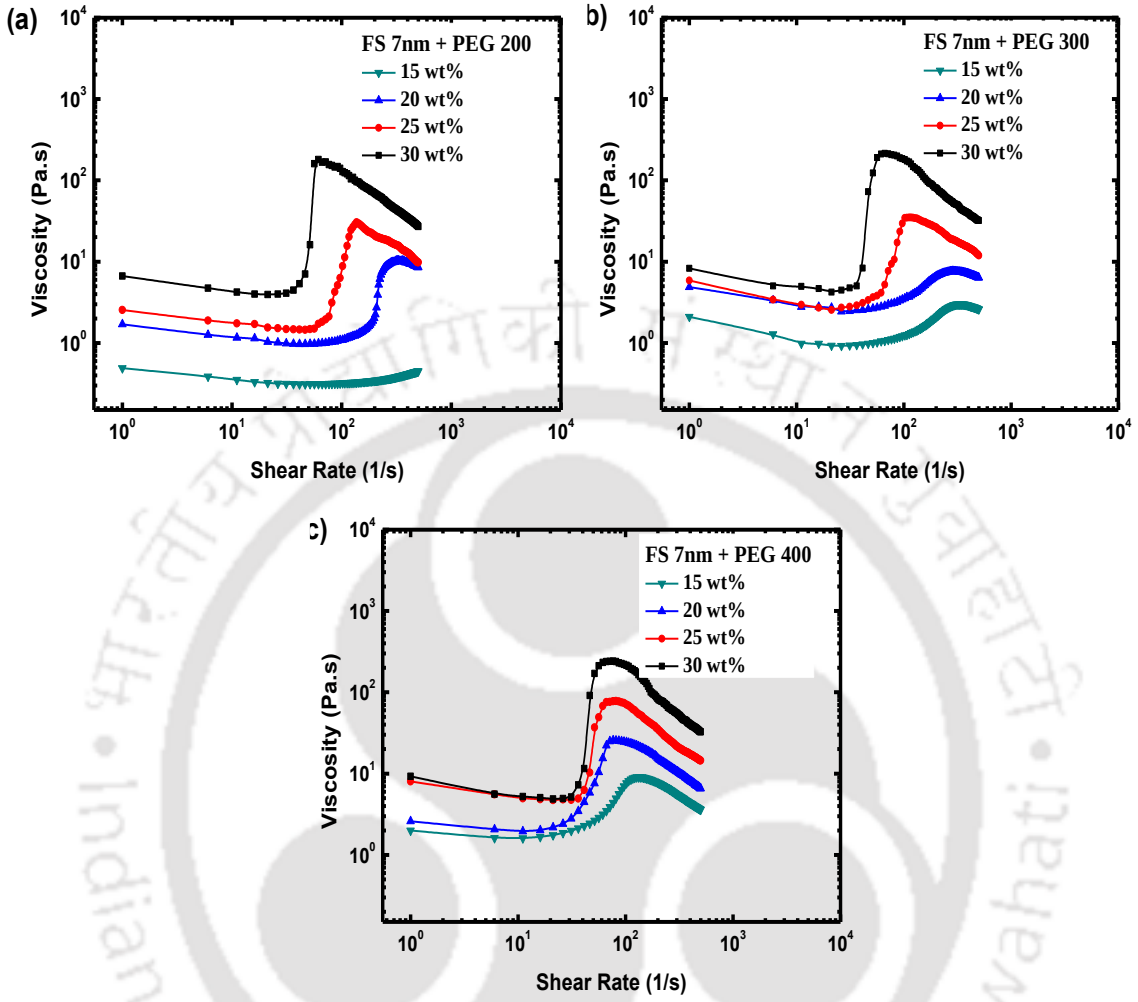

Figure 4.5 Suspension viscosity as a function of shear rate for different weight fractions of particles: (a) Fumed silica, 7nm in PEG 200 (b) Fumed silica, 7nm in PEG 300 (c) Fumed silica, 7nm in PEG 400.

4.2.5 Influence of Carrier Fluid

To further investigate the influence of carrier fluid on the onset of shear thickening, suspensions were prepared in three different fluids. Fumed silica of 200 nm particle size was dispersed in PEG 200, PEG 300, and PEG 400. **Figure 4.6** shows viscosity as a function of steady shear rate for fumed silica suspensions.

Figure 4.6 (a) and (b) show the viscosity variation of suspension in PEG 200, PEG 300, and PEG 400 for 25 wt% and 30 wt% samples, respectively. The initial shear thinning (before the critical shear rate) was much weaker for the 25 wt% sample in comparison to the 30 wt% sample. Shear thickening started after the critical shear rate. After reaching maximum suspension viscosity, a steep decrease in viscosity with shear rate is observed. It can also be observed that fumed silica particles suspended in PEG 400 display a lower critical shear rate compared to the suspension in PEG 200 and PEG 300.

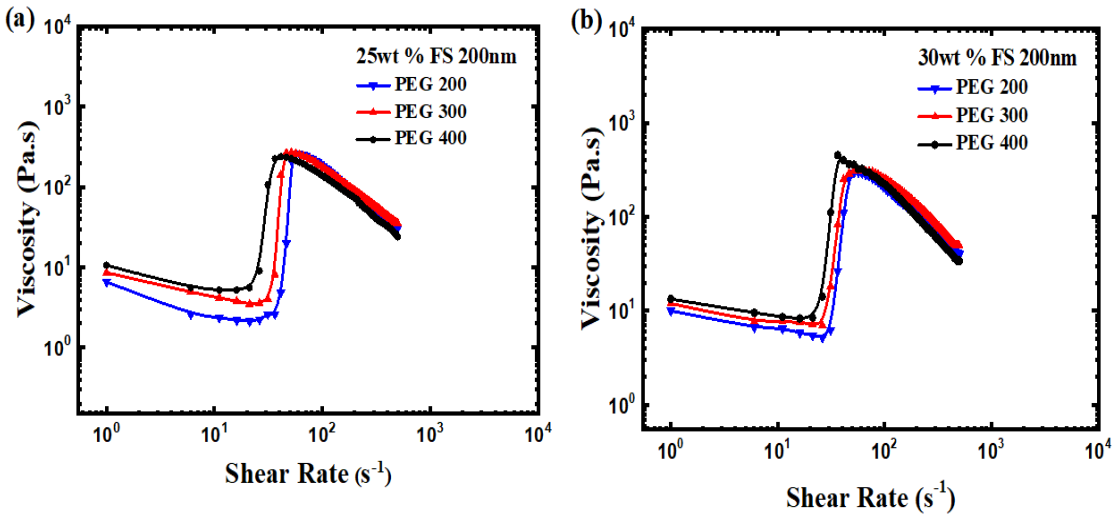

Figure 4.6 Suspension viscosity as a function of shear rate for different molecular weights of PEG (a) 25wt% of 200 nm fumed silica; (b) 30wt% of 200 nm fumed silica

These results demonstrate that increasing the molecular weight of carrier fluid decreases the critical shear rate but increases the maximum viscosity. It should be noted from the physical properties (**Table 3.1**) that the viscosity of PEG itself increases with an increase in molecular weight. A possible theory has been put forward by Raghavan et al. (2000) that hydrogen bonding occurs between silanol

groups of fumed silica particles and the polymer chains of carrier fluid. The higher the molecular weight of PEG, the longer the polymer chain is, causing the formation of larger aggregates with more silica particles. Thus, the formation of hydroclusters starts at a lower critical shear rate. Raghavan et al. (2000) initially proposed that a solvation layer is developed on silica surfaces due to hydrogen bonding between surface hydroxyl groups and polymer chains of the carrier fluid. Surface morphology in **Figure 4.3** showed that fumed silica particles had branched structures containing aggregates of spherical particles. If hydrogen bonds are formed between the open ends of the hydroxyl group of silica particles and the polymer chains of carrier fluid, this will lead to the formation of more branched structures. This can attribute to smaller interparticle distancing and requires a lesser critical shear rate to form shear thickening. Therefore, the formation of hydroclusters in PEG 400 based STFs requires a reduced critical shear rate than PEG 200 and PEG 300.

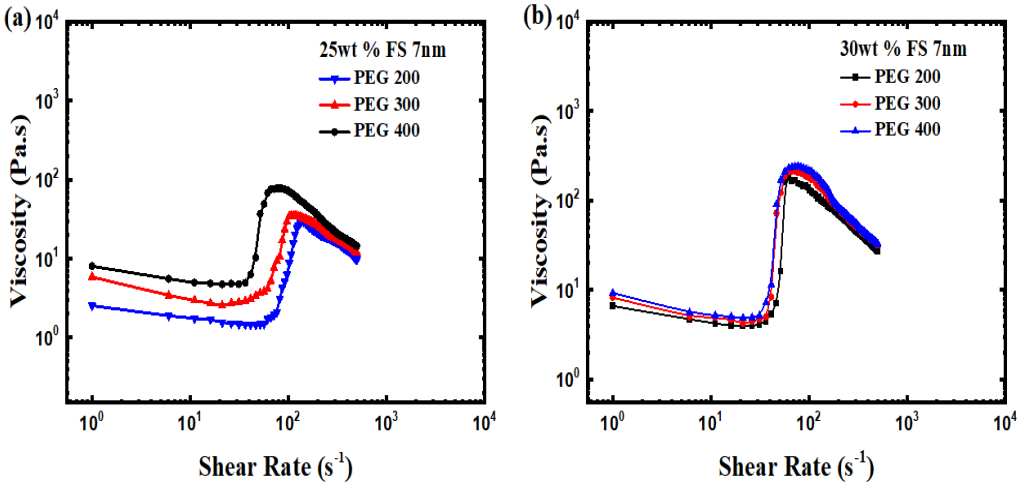

Figure 4.7 Suspension viscosity as a function of shear rate for different molecular weights of PEG (a) 25wt% of 7 nm fumed silica; (b) 30wt% of 7 nm fumed silica

Similarly, fumed silica of 7nm particle size was dispersed in PEG 200, PEG 300, and PEG 400 to investigate the influence of carrier fluid for smaller particle sizes. **Figure 4.7** shows viscosity as a function of steady shear rate for 7nm fumed silica suspensions. **Figure 4.7**(a) and (b) show the viscosity variation of suspension in PEG 200, PEG 300, and PEG 400 for 25 wt% and 30 wt% samples, respectively. It can be observed that fumed silica particles at 25 wt% in PEG 200 and PEG 300 showed a trend of continuous shear thickening behavior compared to PEG 400. However, the samples at 30 wt% showed a trend of discontinuous shear thickening behavior similar to 200 nm particle size. This can be attributed to the role of the Brownian forces that can be considered in the assessment of this trend since they dominate nanoparticle suspensions and delay the thickening for higher shear rates due to increased repulsive stresses between particles. Comparing the samples with 200nm particle size, a higher critical shear rate and minimum viscosity are observed.

Critical shear rate and shear thickening ratio are the two significant parameters studied to understand the rheological behavior of shear thickening suspensions. The shear thickening ratio is defined as the ratio of maximum viscosity to the viscosity at the critical shear rate. From the graphs shown in **Figure 4.4** and **Figure 4.6**, the critical shear rate values, maximum viscosity, and viscosity at the critical shear rates were calculated. **Figure 4.8** shows a graphical representation of the critical parameters of shear thickening suspensions and their dependence on the weight fraction of the particles. **Figure 4.8** (a) and (b) show the shear thickening ratio and the critical shear rate plotted against the weight fractions of 200 nm fumed silica particles for three different carrier fluids. It can be seen that the shear thickening ratio (STR) increases with the decrease in the molecular weight of the

carrier fluid. The larger the shear thickening ratio higher is the resistance of the suspension against shear. An increase in the shear thickening ratio can also be observed by increasing the particle concentration in a given carrier fluid. Moreover, the STR value (between 20-30 wt%) is found to increase almost linearly with the particle concentration.

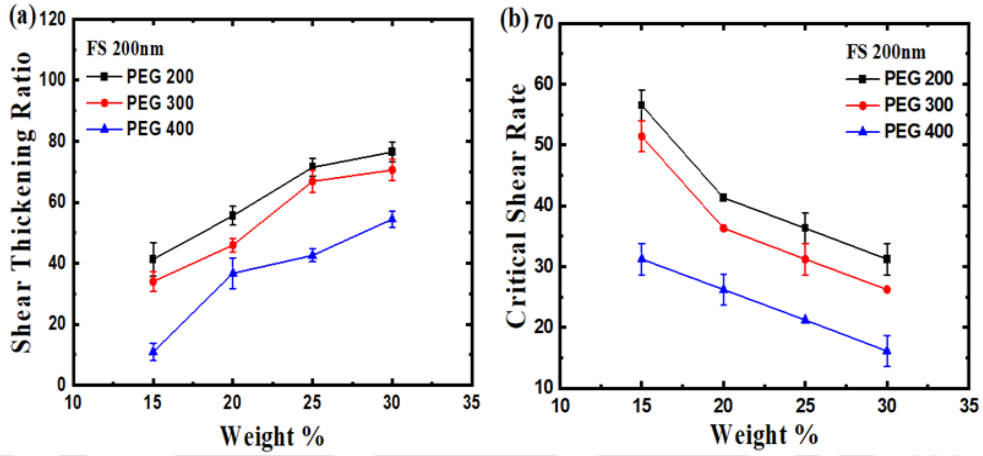

Figure 4.8 Graphical representation of the critical parameters for 200nm fumed silica suspension: (a) shear thickening ratio, (b) critical shear rate plotted as a function of particle concentration for three different carrier fluids

As said earlier, reducing the distances between the particles result in a large shear thickening ratio at lower critical shear rates($\dot{\gamma}_c$). **Figure 4.8**(b) compares the values of the critical shear rate for different carrier fluids. The critical shear rate for 30 wt% silica suspension in PEG 400 was much lower compared to PEG 200 and PEG 300. The decrease in the critical shear rate with particle concentration (between 20-30 wt%) is also approximately linear. The critical shear rate required for the onset of shear thickening for 15 wt% silica suspension in PEG 400 is similar to 30 wt% in PEG 200 and 25 wt% in PEG 300. These results show that shear

thickening can be achieved with a lower concentration of silica particles dispersed in a higher molecular weight carrier fluid. From these analysis, we also infer that a high shear thickening ratio can be obtained with a low molecular weight carrier fluid. This is primarily due to the fact that low molecular weight PEG has lower viscosity with reduced hydrodynamic resistance to prevent particles from close contact. Also, by increasing the weight fraction of silica particles, lower values of the critical shear rate can be achieved.

4.2.6 Influence of Particle Size

The rheology of suspensions strongly depends upon the size of dispersed particles. Experiments were carried out to investigate the influence of particle size on the onset of shear thickening behavior. **Figure 4.9** shows the viscosity as a function of the shear rate for different fumed silica particles dispersed in PEG 300. The particle concentrations studied in these experiments were 15, 20, 25, and 30 wt%. It can be observed that fumed silica particles of 7nm showed a trend of continuous shear thickening behavior at a lower particle concentration of 15 and 20wt%. However, a discontinuous shear thickening behavior is observed with increasing the concentration from 15wt% to 30wt%. It can also be seen that the critical shear rate is inversely proportional to the size of the particles, i.e., the larger the particle size lesser is the critical shear rate. This decrease in critical shear rate can be attributed to the fact that it is easier for particles of larger sizes to come in contact when the shear rate is increased. Our experimental results are similar to previous investigations (Barnes, 1989; Hoffman, 1972; Maranzano et al., 2001). Previous experimental studies found that the critical shear rate increases as the

particle size reduces. The role of the Brownian forces can be considered in the assessment of this trend since they dominate nanoparticle suspensions and delay the thickening for higher shear rates due to increased repulsive stresses between particles.

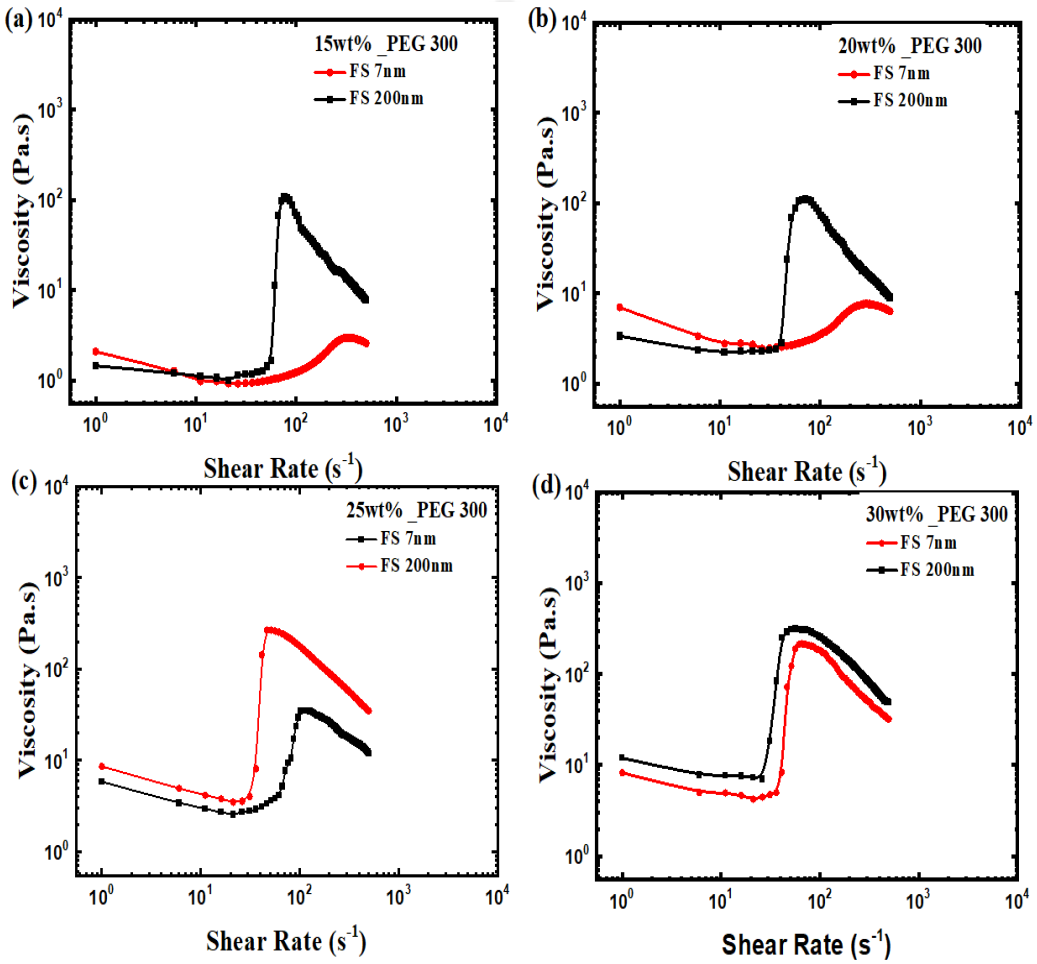

Figure 4.9 Suspension viscosity as a function of shear rate for different fumed silica particle sizes suspended in PEG 300: (a) 15wt%; (b) 20wt%; (c) 25wt%; (d) 30wt%

4.2.7 Influence of Particle Size Distribution

Experiments with monodispersed suspensions showed that the onset of shear thickening can be influenced by both carrier fluid and particle concentration. It is observed that a much higher value of shear thickening ratio can be obtained by dispersing the particles in a lower molecular weight carrier fluid (PEG 200). In order to study the influence of particle size distribution on the rheology of shear thickening suspensions, the samples were prepared by mixing 200 nm and 7 nm fumed silica particles in PEG 200. Suspensions comprised of a mixture of fumed silica particles of 200 nm and 7 nm in the ratio of 75:25, 50:50, and 25:75 were dispersed in PEG 200 while keeping the overall weight % of the particles constant. **Figure 4.10** (a), (b), and (c) show the viscosity as a function of shear rate for shear thickening suspension comprising a mixture of 200nm and 7nm fumed silica particles in PEG 200 at a constant particle concentration of 15, 20, and 25 wt%, respectively.

It can be observed from **Figure 4.10**(a) that the suspension of 7 nm fumed silica at lower concentrations showed a continuous shear thickening behavior. With increasing the concentration of 200nm silica particles, the critical shear rate decreased, and a discontinuous shear thickening behavior was observed. Previous experimental studies showed that, with an increase in particle size, the onset of shear thickening is attained at lower values of critical shear rate (Barnes, 1989; Maranzano and Wagner, 2001; Lee et al., 2009; Moriana et al., 2016). The suspension of 100% 7nm fumed silica particles has a comparatively lower η_{max} and a higher critical shear rate. **Figure 4.10**(b) and (c) show the viscosity graphs for suspensions at 20 wt% of particles in PEG 200. Similar to the previous case, it can

be noticed that with increasing the concentration of large-sized particles, the maximum viscosity (η_{max}) increases, and the critical shear rate decreases. However, we notice that the relative concentration of larger particles required to achieve the discontinuous shear thickening behavior decreased compared to the 15 wt% suspensions.

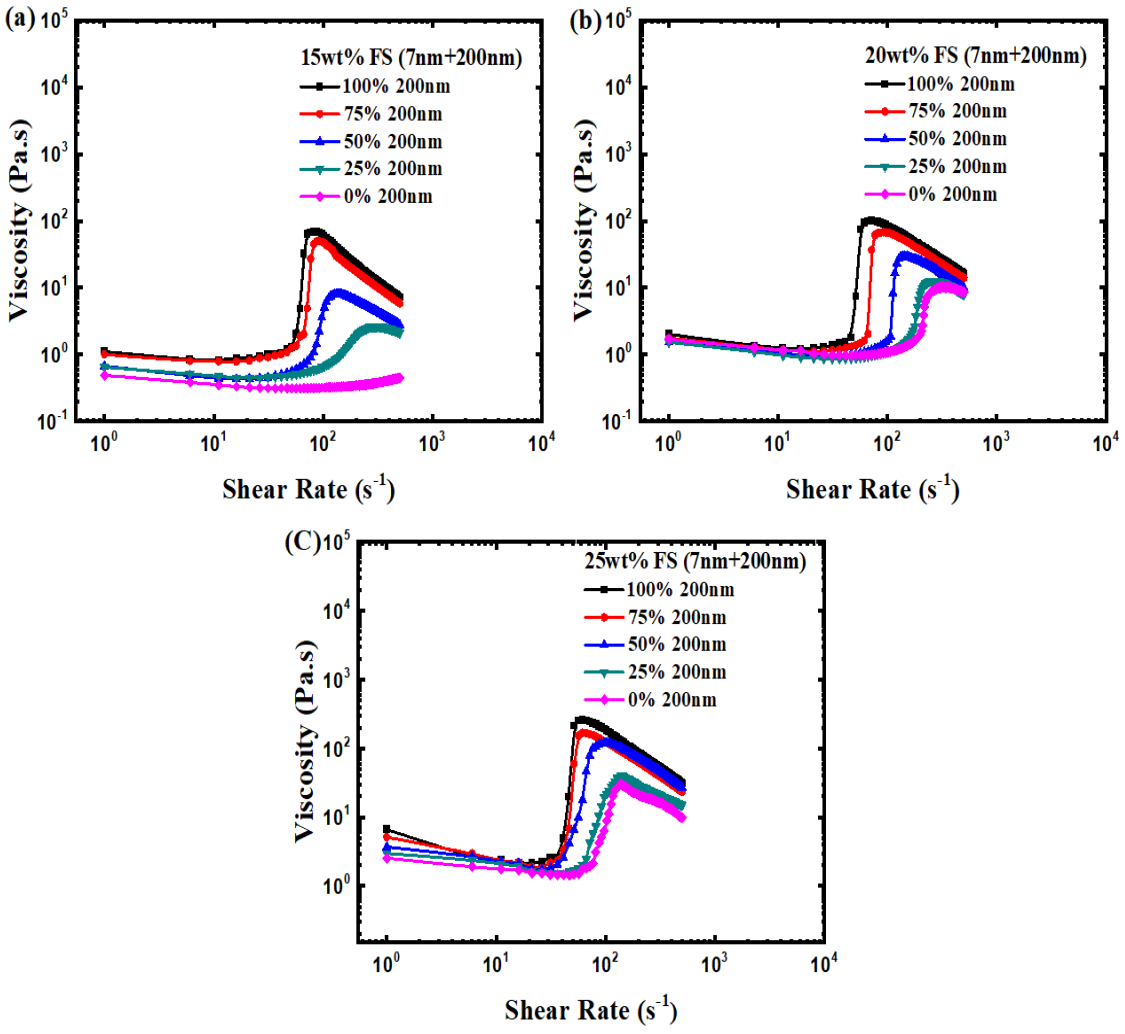

Figure 4.10 Steady shear viscosity curves of suspension comprised of 200nm and 7nm fumed silica in PEG 200 at various proportions. The overall concentration of particles was kept constant: (a) 15wt%, (b) 20wt%

Brown and Jaeger (2012) studied the variation of maximum shear stress (τ_{max}) on the ratio of surface tension of the solvent scaled by the particle radius for a wide variety of suspensions and observed a linear relationship. However, they observed a significant variation in the values of τ_{max} within a band whose width varied by order of magnitude. The factors they attributed to this large variation were particle shape, particle roughness, and particle interaction. If we analyse our experimental data (for 20 wt%), the product of maximum viscosity and shear rate for 200 nm particles is ~ 5000 Pa, and for 7 nm particles, it is ~ 4500 Pa. If we consider the ratio of surface tension of the carrier fluid to the particle radius, the trend is different from the predictions of Brown and Jaeger (2012). However, it is interesting to note that the values of maximum shear stress (τ_{max}) and their variation is well within the band specified by Brown and Jaeger (2012). The reason for the quantitative and qualitative difference could be attributed to the fact that for fumed silica particles, the average roughness for larger particles could be more compared to the smaller particles. We would also like to mention that Brown and Jaeger (2012) have presented data of maximum stress for colloidal silica suspension and not for the fumed silica suspension. We believe that the geometric factor of the particles also plays an important role in deciding the maximum stress achieved during the shear thickening process.

The broadening of particle size distribution can lead to a decrease in the overall viscosity and poor shear thickening behavior, as observed by Collins et al. (1979). Our results confirm that increasing the amount of smaller particles in a suspension of bigger particles decreases the maximum viscosity and shifts the onset of shear thickening to higher values of critical shear rates. **Figure 4.11** illustrates

the critical parameters of shear thickening measured as a function of weight percentages of particles in the PEG 200 solution. It can be seen from **Figure 4.11**(a) that the shear thickening ratios are low for a mixture containing 50% or more of smaller size silica particles. A larger shear thickening ratio is achieved for fumed silica particles consisting of 200 nm. For all the samples, the increase in STR with wt% was observed to be nearly linear. A decrease in STR values is observed with the addition of 7 nm silica particles. On the other hand, from **Figure 4.11**(b), it can be observed that the critical share rate decreases linearly with an increase in the particle concentration. With increasing the percentage of 7 nm particles in the 200 nm fumed silica suspension, it can be observed that the critical shear rate shifts to higher values.

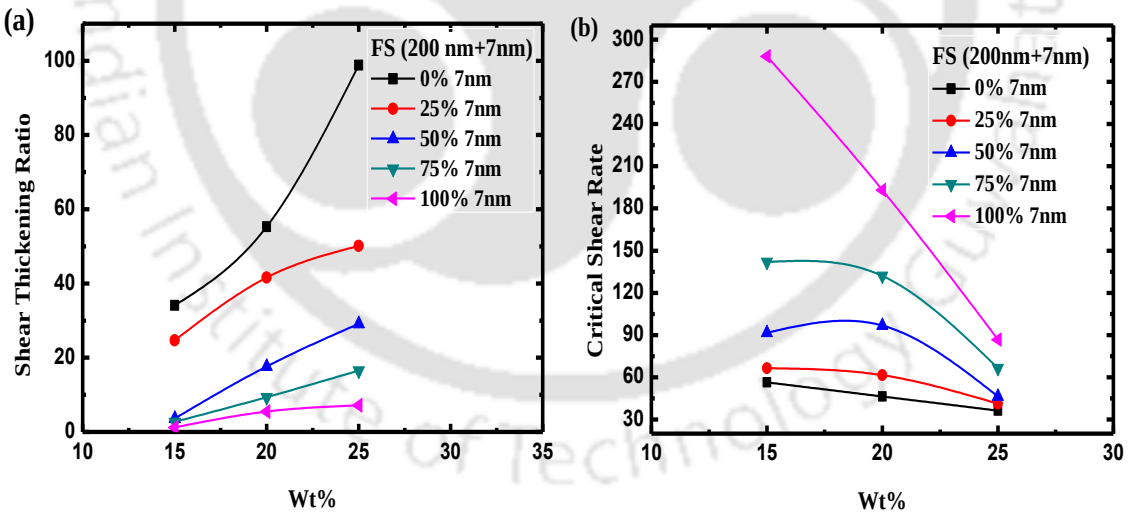

Figure 4.11 Graphical representation of critical parameters plotted as a function of weight fraction of shear thickening suspensions consisting of a mixture of fumed silica particles of 200nm and 7nm in PEG 200

We would like to mention that the above trends displayed a nearly linear increase in the shear thickening ratio and a linear decrease in the critical shear rate with an increase in the concentration of particles for all the mixtures. However, when we analysed our results to estimate the effect of smaller particles on the overall properties of the mixture, it was observed that the collective behavior is very different from what one would predict by a simple mixing rule. A graphical representation of these critical parameters obtained from the linear mixture model and its comparison with the actual measurements is depicted in **Figure 4.12**. The data with filled symbols represent the measured values, and the open symbols are the predictions from the mixing rule. For example, it can be seen from the figure that for the 1:1 ratio of fumed silica (200 nm:7 nm) at 15 wt%, the true critical shear rate observed is 91.7, whereas the mixing rule predicts a value of 172.25. Also, a lesser shear thickening ratio (3.63) is observed while the predicted value is 17.65. These results indicate that for a suspension mixture comprised of bigger and smaller fumed silica particles, the smaller particles reduce the frictional contact between the larger ones. It is to be noted that due to the contribution from the interparticle interactions between the smaller and larger particles, the linear mixing rule for the critical shear rate and shear thickening ratio may not hold true. Therefore, based on the analysis of our data, we can only speculate this as one of the possible reasons behind the higher critical shear rate and lower shear thickening ratio for bimodal suspensions.

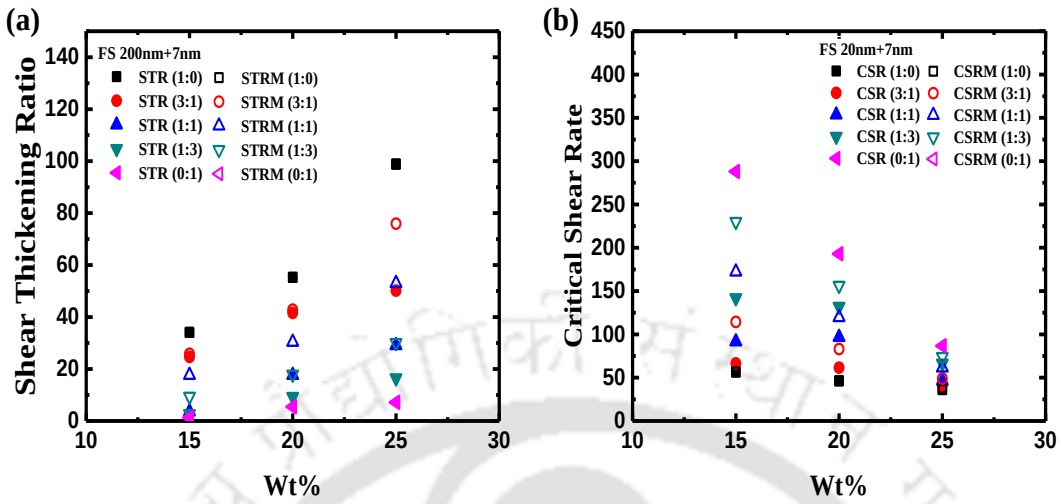

Figure 4.12 Comparison of critical shear thickening parameters obtained from experiments and prediction from mixing model: (a) Shear thickening ratio and (b) Critical shear rate. Fumed silica particles of 200nm and 7nm mixed at different ratios in PEG 200 were used to prepare the suspension. Solid symbols are the experimentally measured shear thickening ratio (STR) and critical shear rate (CSR) and the open symbols represent the corresponding values obtained from the mixture model.

From the above observations, a simple mechanism can be proposed to understand the influence of size distribution on the rheology of shear thickening suspensions (**Figure 4.13**). Before the onset of shear thickening in a monodispersed suspension, the particles are separated by an equilibrium distance. For moderate and large concentrations and at low shear rates, as the particles approach each other by the hydrodynamic forces, the strong repulsive forces between the particles keep the particles moving in a layered microstructure, causing the viscosities of the suspension to decrease. As the shear rate increases, the hydrodynamic forces overcome the repulsive forces, forcing the particles to approach very close to each other. When these particles approach each other, the carrier fluid is displaced

between the gap of the particles resulting in frictional contacts. These frictional contact forces play a vital role in the formation of clusters and causing the suspension to shear thicken. For a suspension comprised of bigger and smaller particles, the fine particles fill the void spaces between the bigger particles. As the shear rate increases, the smaller particles act as a lubricant for the larger particles and reduces the frictional contact between them. Therefore, a reduction in the maximum viscosity (η_{max}) and delay in the onset of shear thickening is observed. Greenwood et al. (1997) reported that the viscosity of the suspension is strongly dependent on the particle size ratio. Thus the effective way to obtain a maximum viscosity is by narrowing the particle size distribution in the shear thickening fluid.

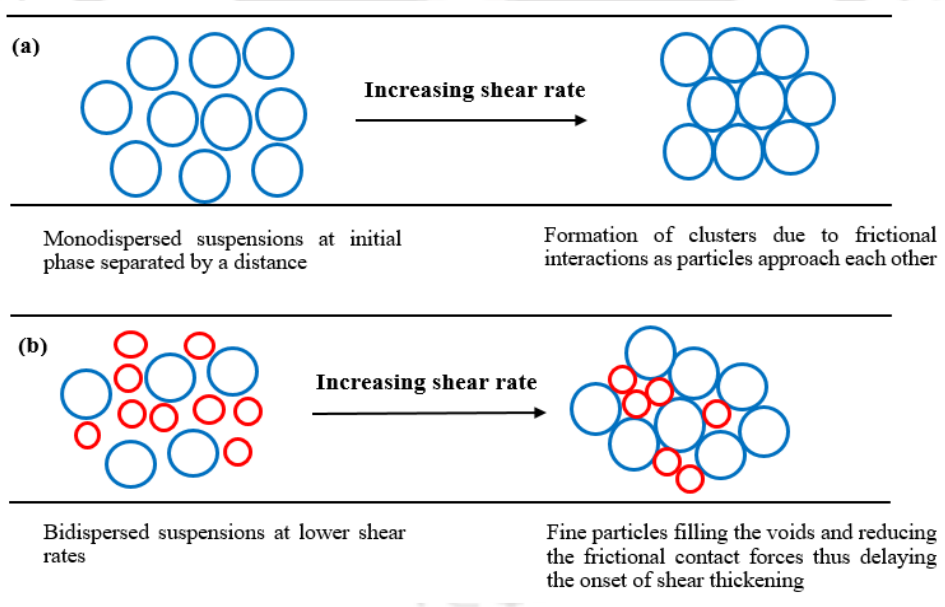

Figure 4.13 Schematic illustrations of the influence of size distribution on the rheological behavior of shear thickening suspension

Though, the hydrodynamic interactions are solely responsible for the hydrocluster formation, this may not always lead to frictional contacts. Mari et al.

(2014) have carried out Stokesian dynamics simulations considering only the pair-wise short-range hydrodynamic lubrication forces and used a contact force model to describe the frictional contacts between the particles. The use of only lubrication force was justified by providing an argument that for dense suspension, the dominant hydrodynamic interactions come from the fluid flow in narrow gaps between nearby particles. They have used a threshold normal force to activate friction and reported continuous shear thickening for particle volume fraction (ϕ) below the critical value (ϕ_c), and discontinuous shear thickening for $\phi > \phi_c$. In a simulation study (not reported here) using the complete hydrodynamic interactions (both long-range many body as well as two body lubrication forces) with the same frictional contact model that was used by Mari et al. (2014), we observed that long-range many body hydrodynamic interactions reduces the frictional particle contacts and delays the onset of shear thickening. Our experimental data reported in this work supports the theory that one would get weak or continuous shear thickening without frictional interactions. Discontinuous shear thickening is observed both in colloidal suspensions as well as granular suspensions. The mechanism for shear thickening in granular suspension is due to the system-spanning frictional contacts. Recent experimental studies on colloidal suspensions have also suggested that shear thickening is driven primarily by the formation of frictional contacts, with hydrodynamic forces playing a supporting role at lower concentrations (Royer et al., 2016). Our analysis further indicates that larger frictional forces between the particles lead to higher shear thickening ratio.

4.3 Conclusions

The influence of carrier fluid and particle size distribution on the rheological behavior of shear thickening suspensions was investigated. Shear thickening suspensions were prepared by an efficient sonochemical method. It was observed that if the suspension is prepared by the mechanical agitation method, the bubbles are difficult to remove. The presence of these bubbles is detrimental to the expected behavior from shear thickening fluids. Experimental results from the prepared shear thickening fluids resulted in a good understanding of the parameters that influence the rheology. All the samples showed a similar trend of discontinuous shear thickening behavior. The onset of shear thickening can be influenced by particle loading, and it is observed that the critical shear rate decreases with an increase in particle concentration. It is also found that the carrier fluid plays a vital role in the onset of shear thickening, and results show that an increase in the molecular weight of carrier fluid decreases the critical shear rate. The experiments have also demonstrated that high shear thickening ratio can be achieved with a lower molecular weight carrier fluid, whereas lower critical shear rates are observed by increasing the particle concentration. On the other hand, by increasing the smaller particles in a bimodal suspension comprised of two different sized particles, we observed a decrease in the maximum suspension viscosity and a shift in the onset of shear thickening to higher values of critical shear rates. These results showed that polydisperse suspension might result in poor shear thickening behavior. Frictional contacts between the particles are believed to play a crucial role in determining the shear thickening ratio.

CHAPTER 5 Effect of Nanofillers on The Shear Thickening

5.1 Introduction

This chapter investigates the effect of the addition of fillers on the rheological behavior of shear thickening fluids (STF). This involved preparing shear thickening suspensions with the addition of fillers to the fumed silica particles for a given weight fraction and a carrier fluid. Adding these fillers provides tensile strength to the STF and allows more efficient load transfer throughout the material, and also deformability and flowability of the STF can be largely maintained. Nanofillers, in general, have an apparent diameter ranging from 0.001 µm to about 150 µm (more preferable 1µm to about 80 µm) and are dispersed in shear thickening suspensions with compositions ranging from about 0.01 wt % to about 50Wt%. (more preferable 0.1 Wt % and 10 Wt %). A specific amount of GO, MWCNT, and mica nanofillers were dispersed in the shear thickening suspensions with fumed silica particles dispersed in PEG. Also, the critical parameters such as shear thickening ratio, critical shear rate, and shear thickening period were analyzed by varying the addition of various additives concentrations.

5.2 Results and Discussions

5.2.1 X-Ray Diffraction

The XRD patterns of GO, MWCNT, and mica nanofillers used in this study are shown in **Figure 5.1**, which can be used to deduce the phase composition of the samples. It was observed that the fillers in this study, i.e., GO, MWCNT, and mica exhibited sharp crystalline peaks. These are the characteristic peaks of the GO, MWCNT, and mica that exactly match the JCDPS.

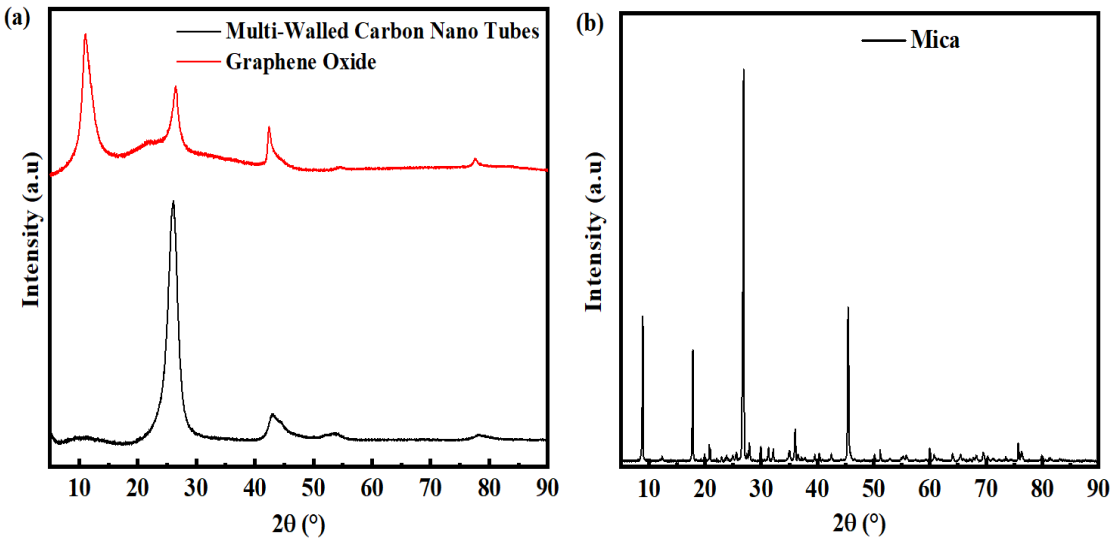

Figure 5.1 XRD patterns of (a) Graphene Oxide and Multi-Walled Carbon Nano Tube fillers and (b) Mica particles

5.2.2 Microstructural Characterization

The surface morphology of the fumed silica nanoparticles and the fillers Graphene Oxide (GO), Multi-walled carbon nanotubes (MWCNT), and Mica particles are shown in **Figure 5.2**. It was observed from **Figure 5.2**(a) that the average primary particle size of fumed silica nanoparticles was found to be 14nm, and the average length of their aggregates was found to be 200 nm. As shown in **Figure 5.2**(b), it was clear that Graphene Oxide has 3-6 layers and a thickness of 1-2 nm. The Multi-walled carbon nanotubes in **Figure 5.2**(c) were observed to be tubular concentric channels with diameter and length to be around 20 nm and 10 micrometers, respectively. **Figure 5.2**(d) shows the microstructure of mica particles, and it was observed that mica particles exhibited 3-8 sheets.

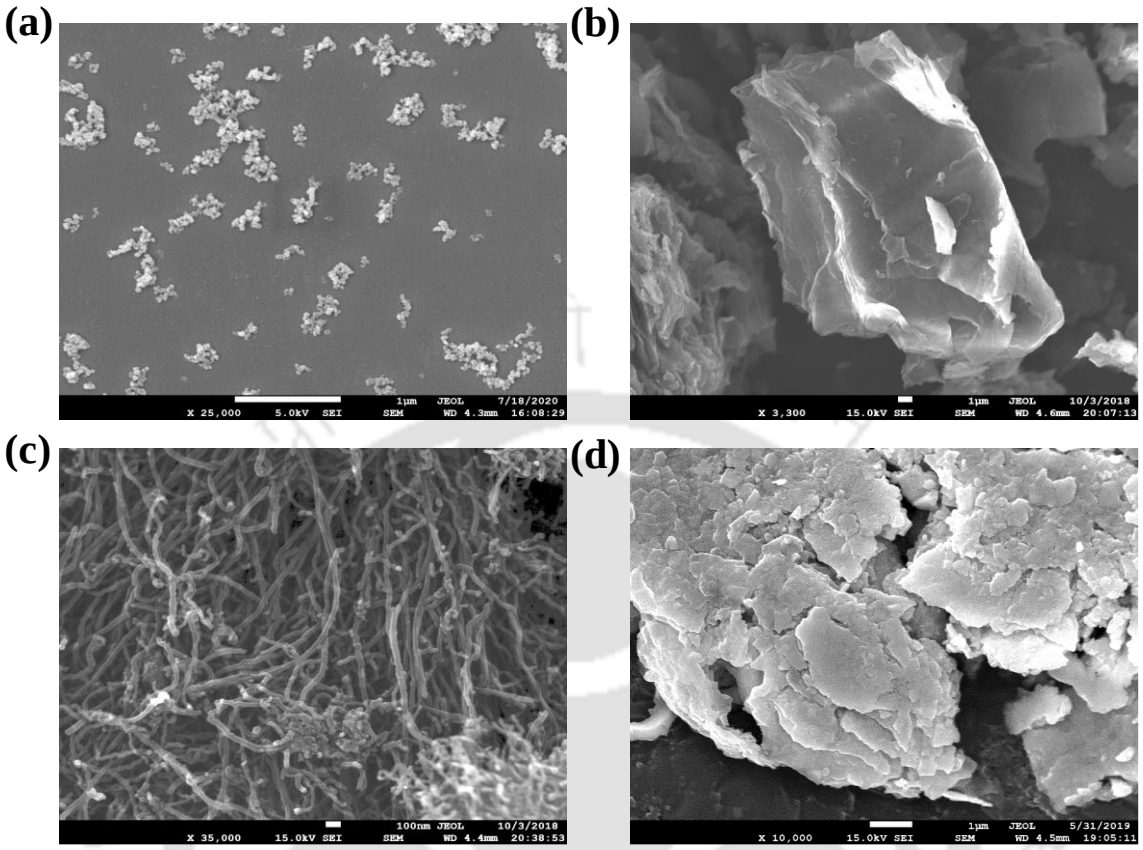

Figure 5.2 Surface morphology images of (a) fumed silica nanoparticles (b) Graphene Oxide (c) Multi-walled carbon nanotubes (d) Mica particles

5.2.3 Influence of addition of Graphene Oxide on shear thickening behavior

The steady-state rheological measurements of the samples were performed at room temperature to study the influence of the addition of GO on the rheological behaviour of fumed silica-based shear thickening suspensions. The suspensions were prepared by varying the concentration of GO (0.2%, 0.4%, 0.6% and 0.8%) to 20wt% fumed silica suspensions. **Figure 5.3** shows the variation of viscosity with the shear rate for 20wt% of fumed silica nanoparticles dispersed in PEG 300 with various GO concentrations. It is evident from **Figure 5.3** that the suspensions

exhibited behavior similar to discontinuous shear thickening with three distinct regions. Initially, the suspension exhibits a shear-thinning behavior at lower shear rates, followed by a sudden increase in viscosity to a maximum viscosity value of η_{max} over a critical shear rate and, finally, shear-thinning behavior with an increase in shear rate.

Compared to 20wt% fumed silica suspensions, the addition of GO nanofillers showed a similar trend of viscosity curve as a function of shear rate. The figure shows that though the maximum viscosity of the suspension of addition of 0.2% GO and 20wt% fumed silica suspensions are similar, a slight increase in critical shear rate is observed with the addition of 0.2% GO. A decrease in the onset of shear thickening was observed upon increasing the GO concentration from 0.2% to 0.8%. It can also be seen that the maximum viscosity of the suspensions increases with increasing GO concentration. For the 20wt% fumed silica suspensions, shear thickening behaviour over a critical shear is attributed to the domination of hydrodynamic forces over the repulsive forces, which enforces the particles to approach each other to form clusters. The remarkable change in the rheological behavior with the addition of GO fillers is due to the interaction between the fumed silica particles and the GO fillers. Surface morphology in **Figure 5.2**(b) showed that GO fillers are sheet-like particles with a large aspect ratio. Thus, GO particles have a more significant hydrodynamic effect which causes a predominant congestion effect which enforces the formation of hydroclusters at lower shear rates with increasing the GO concentration. Our experimental results are consistent with previous studies where a decrease in critical shear rate is observed. Also, the

viscosity of the suspension increases with the addition of GO concentration (Sha et al., 2013; Huang et al., 2015).

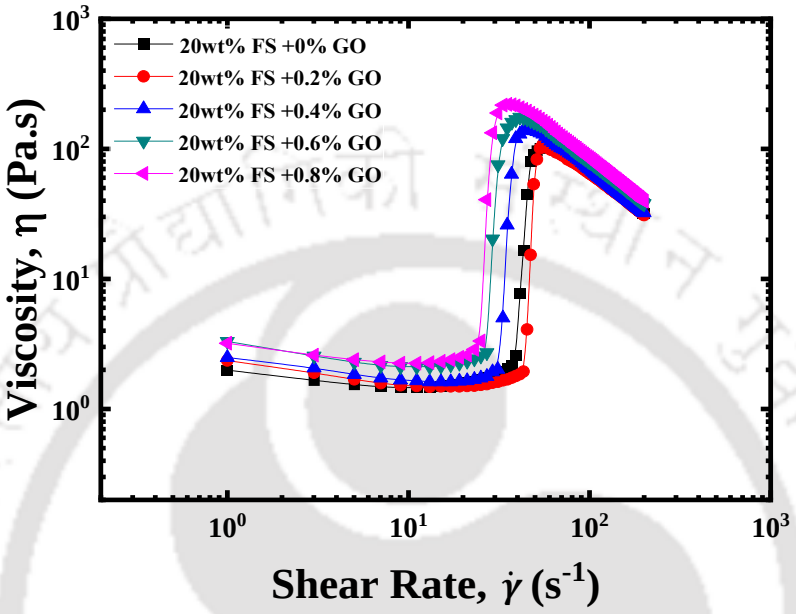

Figure 5.3 Steady-state viscosity variation with the shear rate for 20wt% of fumed silica nanoparticles dispersed in PEG 300 with various GO concentrations

5.2.4 Influence of addition of MWCNT on shear thickening behavior

The influence of the addition of MWCNT on the rheological behaviour of fumed silica-based shear thickening suspensions was studied at room temperature under steady shear. The samples were prepared by varying the concentration of MWCNT (0.2%, 0.4%, 0.6% and 0.8%) to 20wt% fumed silica suspensions. **Figure 5.4** shows the viscosity as a function of shear rate for varying the MWCNT concentration in 20wt% fumed silica suspensions dispersed in PEG 300. It can be observed that all the samples showed three distinct regions similar to that of discontinuous shear thickening behaviour.

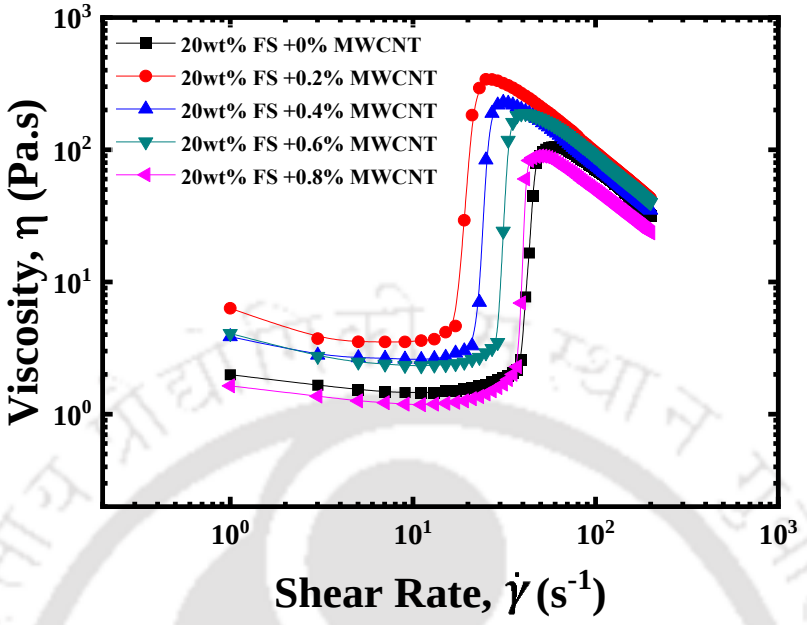

Figure 5.4 Steady-state viscosity variation with the shear rate for 20wt% of fumed silica nanoparticles dispersed in PEG 300 with various MWCNT concentration

It can be seen from **Figure 5.4** that there is a significant effect on the maximum viscosity of the suspension with the addition of MWCNT concentration. However, with increasing the concentration of MWCNT nanofillers from 0.2% to 0.8%, we observed a decrease in maximum viscosity and a shift in the onset of shear thickening to higher values of critical shear rate. It was also observed that the onset of shear thickening and the maximum viscosity of the suspension containing 0.8% GO and 20wt% fumed silica suspensions are similar. Similar to the previous case, it can be seen that with the addition of a small quantity of nanofillers, the critical shear rate decreases, and the maximum viscosity (η_{max}) increases. However, compared to GO nanofillers, the addition of MWCNTs caused an increase in the critical shear rate and a decrease in the viscosity. This increase in critical shear rate

with increasing the concentration of MWCNTs is attributed to the interactions between the fumed silica particles, MWCNT, and the carrier fluid. From the theory proposed by Raghavan et al. (2000), it is well known that silanol groups of fumed silica particles form hydrogen bonds with the hydroxyl groups of the carrier fluid. With the addition of MWCNTs in the suspension, the hydroxyl/carboxyl groups on the surface of MWCNTs can form hydrogen bonds with fumed silica nanoparticles and Polyethylene glycol. Thus, the onset of shear thickening is observed at a lower shear rate. However, increasing the concentration of MWCNTs increases the number of hydrogen bonds in silica-MWCNT-PEG suspension (Hasanzadeh et al., 2016). Due to the similar microstructure of MWCNT and PEG, more hydrogen bonds are formed between MWCNT and PEG, leading to a strong lubrication force between them. Therefore, a higher shear force is required to overcome the strong lubrication force between MWCNTs and PEG, which delays the onset of shear thickening and increases the critical shear rate.

5.2.5 Influence of addition of Mica particles on shear thickening behavior

In order to study the influence of Mica particles as nanofillers on the rheology of fumed silica suspensions, the suspensions were prepared by varying the mica particle concentration in 20wt% fumed silica suspensions in PEG 300. **Figure 5.5** presents the steady-state viscosity variations with the shear rate for different concentrations of mica particles (0.2%, 0.4%, 0.6% 0.8%) in 20wt% fumed silica suspensions in PEG 300. Similar to **Figure 5.3** and **5.4**, the addition of mica particles also showed a trend consistent with discontinuous shear thickening.

Compared to pure fumed silica suspensions, a slight variation was observed in the maximum viscosity and critical shear rate with the addition of mica particles. Moreover, with increasing the concentration of mica particles, an increase in initial viscosity in the shear-thinning region was observed. However, increasing the concentration of mica particles from 0.2% to 0.8% increases the onset of shear thickening and decreases the maximum viscosity. Moreover, it could be observed that the maximum viscosity of the suspensions decreases with increasing mica concentration.

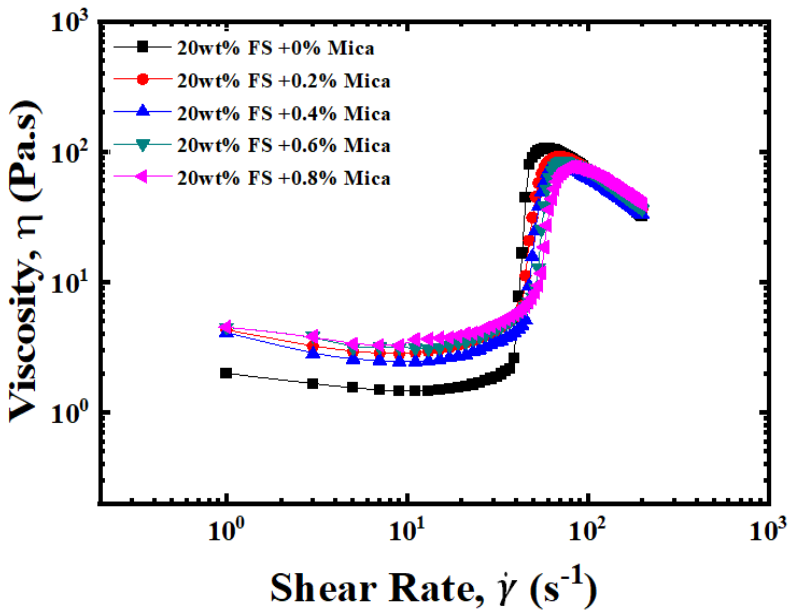

Figure 5.5 Steady-state viscosity variation with the shear rate for 20wt% of fumed silica nanoparticles dispersed in PEG 300 with various Mica concentration

Figure 5.6 shows the comparison of suspension viscosity as a function of the shear rate of 25wt% fumed silica particles dispersed in PEG 300 with the addition of 0.4wt% of various nanofillers in 20wt% fumed silica suspensions. Steady-state rheological measurements indicated that by adding 0.4% GO and MWCNT to

20wt% silica suspensions, the maximum viscosity and critical shear rate of the suspension could be enhanced to be close to that of the suspension containing 25wt% pure shear thickening suspension. This experimental result suggests that at least 5 wt% of silica suspensions can be replaced by a minimal quantity of GO and MWCNT nanofillers to achieve similar rheological properties. Thus, a reduction in the overall weight of the shear thickening suspensions can be achieved, which can be favorable for many applications.

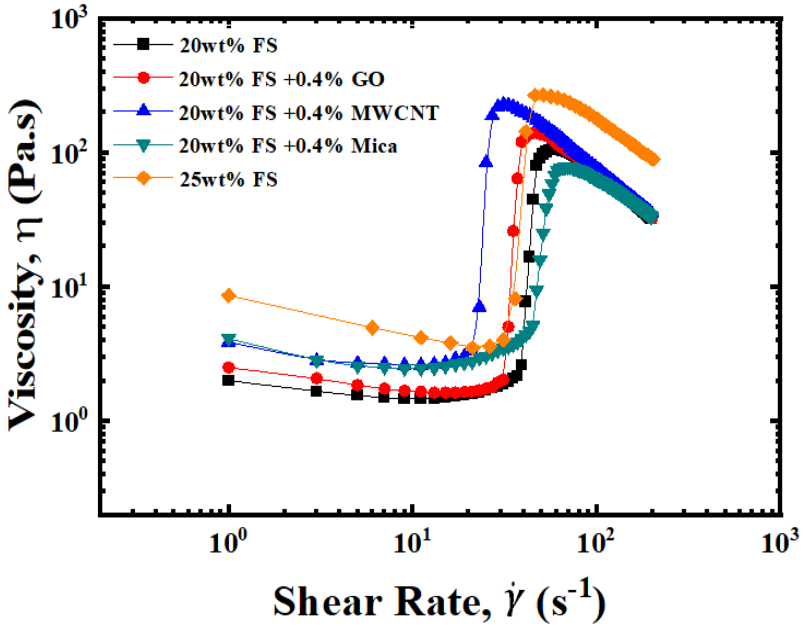

Figure 5.6 Suspension viscosity as a function of shear rate of fumed silica nanoparticles dispersed in PEG 300 with 0.4% concentration of various nanofillers

5.2.6 Critical Parameters

Critical shear rate, shear thickening ratio, and shear thickening period are the three critical parameters studied to understand the characteristics of shear thickening suspensions. The point at which the onset of shear thickening begins is said to be a critical shear rate ($\dot{\gamma}_c$), and the corresponding viscosity is said to be

critical viscosity (η_c). The critical shear rate values were calculated from **Figures** 5.4 and 5.5. **Figure** 5.7 shows the critical shear rate of shear thickening suspensions with different nanofillers and their influence on the weight fraction of the addition of nanofillers. It can be observed that the critical shear rate for 0.2% MWCNT in 20wt% silica suspensions was much lower compared to the addition of 0.2% GO and Mica particles. On the other hand, by increasing the concentration of nanofillers in the suspensions, we observed a lower critical shear rate for GO than MWCNT and Mica particles. Moreover, a linear decrease in the critical shear rate for GO and a linear increase in the critical shear rate for MWCNT and Mica particles was observed with increased nanofiller concentration.

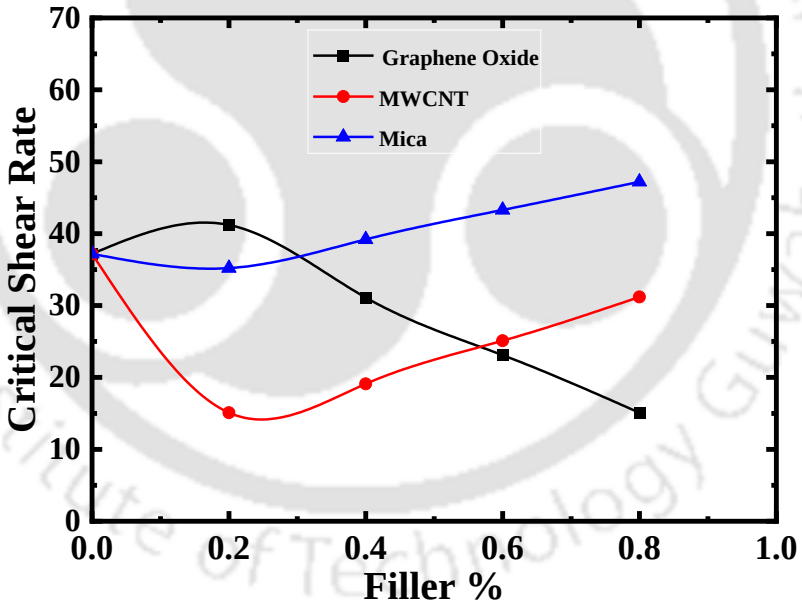

Figure 5.7 Graphical representation of the critical shear rate plotted as a function of various amounts of nanofillers dispersed in 20wt.% fumed silica suspensions

The ability of the suspension to thicken is given by the shear thickening ratio (STR) and is defined as the ratio of maximum viscosity of the suspension

(η_{max}) to the critical viscosity of the suspension (η_c). The values of critical and maximum viscosity were calculated from the above figures. **Figure** 5.8 shows the shear thickening ratio of shear thickening suspensions with different nanofillers and their influence on the weight fraction of the addition of nanofillers. It can be seen that the shear thickening ratio (STR) increases with increasing the loading of GO nanofillers. The larger the shear thickening ratio, the higher the resistance of the suspension against shear.

In contrast, a decrease in the shear thickening ratio is observed with increasing the MWCNT nanofiller concentration in the suspension. Moreover, the STR value is found to be higher for 0.2wt% addition of MWCNT than the addition of GO. Comparing the STR values of GO and MWCNT, the STR values for mica particles are much lower.

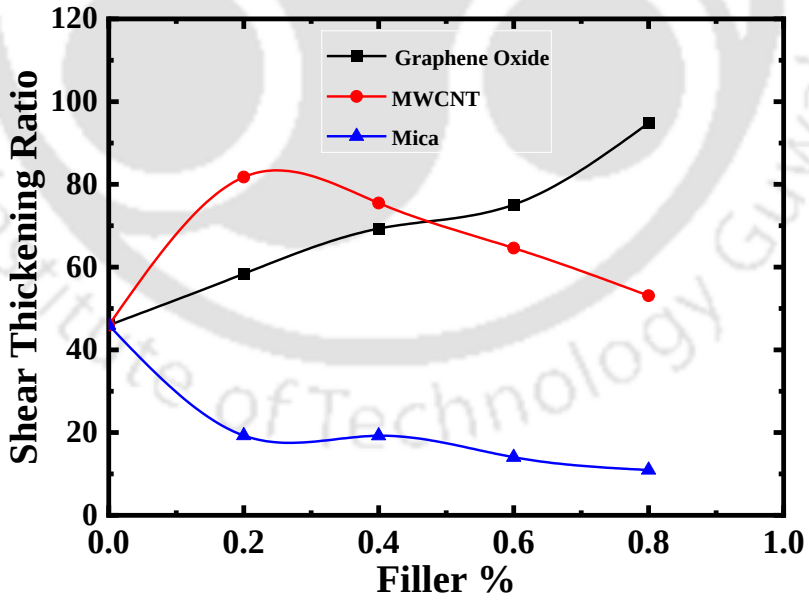

Figure 5.8 Graphical representation of shear thickening ratio plotted as a function of wt.% of nanofillers dispersed in 20wt.% fumed silica suspensions.

The shear thickening period is defined as the difference between the shear rate at maximum viscosity ($\dot{\gamma}_{max}$) and the critical shear rate ($\dot{\gamma}_c$). **Figure 5.9** shows the shear thickening period of shear thickening suspensions with different nanofillers and their influence on the weight fraction of the addition of nanofillers. It can be observed that the thickening period of GO and MWCNT increases with the addition of nanofillers. These results indicate that nanofillers disrupt the thickening mechanism thereby, completion of thickening is shifted to a higher shear rate. This can be explained by the fact that these nanofillers intervene between the fumed silica nanoparticles, thereby delaying the formation of hydroclusters. However, the thickening period for the addition of mica particles remains constant.

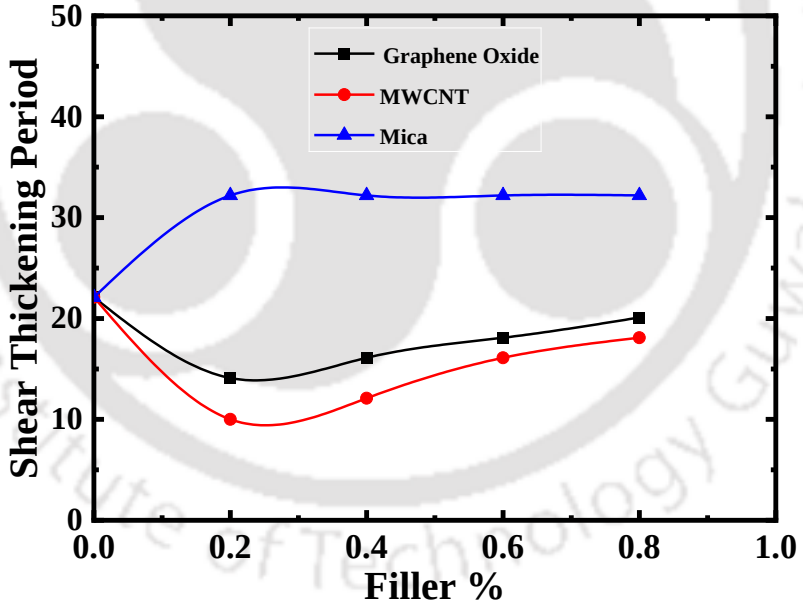

Figure 5.9 Graphical representation of shear thickening period plotted as a function of wt% of nanofillers dispersed in 20wt% fumed silica suspensions.

5.2.7 Curve Fitting

Galindo-Rosales et al. (2011) considered the three regions separately and modeled the viscosity functions for the viscosity curve using a piecewise fit. Moreover, these functions are continuous and are useful for numerical simulations. This viscosity model equation can be easily fitted in the curve for the three regions. The proposed viscosity function for the three regions is represented by Eq. (5.1), and this includes 11 parameters that are independent and determined from experimental data.

$$\eta(\dot{\gamma}) = \begin{cases} \eta_I(\dot{\gamma}) = \eta_c + \frac{\eta_0 - \eta_c}{1+[K_I(\dot{\gamma}^2/\dot{\gamma}-\dot{\gamma}_c)]^{n_I}} & for\ \dot{\gamma} \le \dot{\gamma}_c \\ \eta_{II}(\dot{\gamma}) = \eta_{max} + \frac{\eta_c - \eta_{max}}{1+[K_{II}(\dot{\gamma}-\dot{\gamma}_c/\dot{\gamma}-\dot{\gamma}_{max})\dot{\gamma}]^{n_{II}}} & for\ \dot{\gamma}_c < \dot{\gamma} \le \dot{\gamma}_{max} \\ \eta_{III}(\dot{\gamma}) = \frac{\eta_{max}}{1+[K_{III}(\dot{\gamma}-\dot{\gamma}_{max})]^{n_{III}}} & for\ \dot{\gamma}_{max} < \dot{\gamma} \end{cases} \quad (5.1)$$

Here, K_i ($i = I, II, III$) represents the transitions between the plateaus and the power law, and n_i $(i = I, II, III)$ represents the slopes of the power-law in these three regimes, respectively; Parameters η_{max} and $\dot{\gamma}_{max}$ are the maximum viscosity and the corresponding shear rate, respectively; $\dot{\gamma}_c$and η_c are the critical shear rate and corresponding critical viscosity, respectively. These parameters were obtained from the experimental measurements reported in chapter 4.2. A Levenberg-Marquardt algorithm (LMA) was used to fit the data for each curve. The parameters (K_i and n_i) were obtained by the iterative chi-square minimization technique. The fitting is said to have converged when the difference of χ^2 of two successive iterations are smaller than a given tolerance. Initial values for the parameters are chosen as close to the target to improve the accuracy of the fitting process. Curve fitting is carried out independently for the three regions of the curve

using the corresponding viscosity function of Eq. (5.1). The correlation coefficient R^2 for all the plots was observed to be greater than 0.9. The experimental data and curve fitting of suspensions with varying concentrations of nanofillers in 20wt% fumed silica suspensions dispersed in PEG 300 are shown in **Figure 5.10**(a), (b), and (c). It is evident from these plots that the experimental data accurately fits the viscosity model.

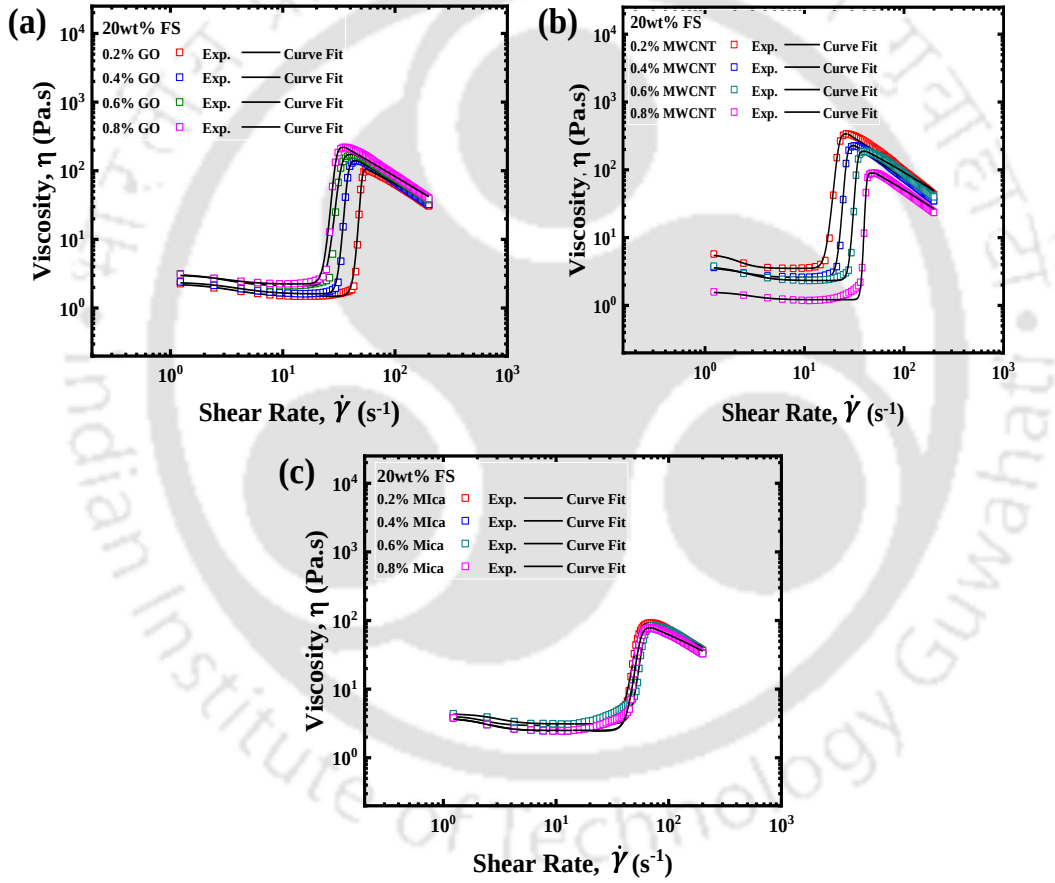

Figure 5.10 Curve fitting for the suspension viscosity as a function of shear rate for 20wt% fumed silica dispersed in PEG 300 with varying concentration of nanofillers (a) GO (b) MWCNT (c) Mica particles. Empty square boxes represent experimental data, and solid lines represent the fitted viscosity model function

5.3 Conclusions

The influence of the addition of fillers on the rheological behavior of shear thickening fluids (STF) was investigated. GO, MWCNT and mica particles were used as nanofillers, and the rheological behavior was studied. Experimental results from the prepared shear thickening fluids showed a good understanding of the addition of fillers that influence the onset of shear thickening. It was observed that the addition of Graphene oxide (GO) particles exhibited higher relative viscosities and a decrease in the onset of shear thickening. In contrast, the addition of Multi-Walled Carbon Nanotubes (MWCNT) and Mica particles showed a decrease in the shear thickening ratio and an increase in critical shear rate. Our experimental result suggests that at least 5 wt% of silica suspensions can be replaced by a minimal quantity of GO and MWCNT nanofillers to achieve similar rheological properties. The results also showed that adding mica particles to shear thickening suspensions results in poor shear thickening behavior. Finally, the experimental data fitted accurately in the viscosity function model proposed by Galindo-Rosales.

CHAPTER 6 Microstructure and Rheology of Discontinuous Shear Thickening

6.1 Introduction

In this chapter, we report visualization of microstructure in discontinuous shear thickening suspensions along with rheological measurements using a Rheo-microscopy setup. The use of rheo-microscopy is necessary to analyze the rheological measurements and microstructure simultaneously. Fumed silica-based shear thickening suspensions were prepared using a sonochemical method to investigate the shear thickening mechanism. The viscosity curves were fitted to the apparent viscosity model proposed by Galindo-Rosales et al. (2011) to describe the shear thickening regimes. In order to understand the microstructure and rheology relationship, the rheometer is coupled with a high-speed camera for the visualization of microstructures at different values of shear rates. In our experiments, the measurements of the first normal stress difference (N_1) were also carried out to understand the role of hydrodynamic and frictional forces. We have further studied the dynamic response of shear thickening suspensions to understand their viscoelastic behavior, and the correlation between shear thickening and strain thickening was checked using a modified Cox-Merz rule.

6.2 Rheo-Microscopy

Simultaneous visualization of microstructure and rheological measurements were performed with a rheo-microscopy setup. The schematic representation of the rheo-microscopy setup is shown in **Figure 6.1**(a). The main components of the experimental setup consist of a rheometer coupled with a high-speed camera (Model: Phantom VEO 640L), a 12x zoom lens, a 4x microscopic objective piece, and a white LED light source. White LED light illuminates the sample through a circular

sapphire window of 3mm thickness and is placed at the bottom of the glass Peltier system.

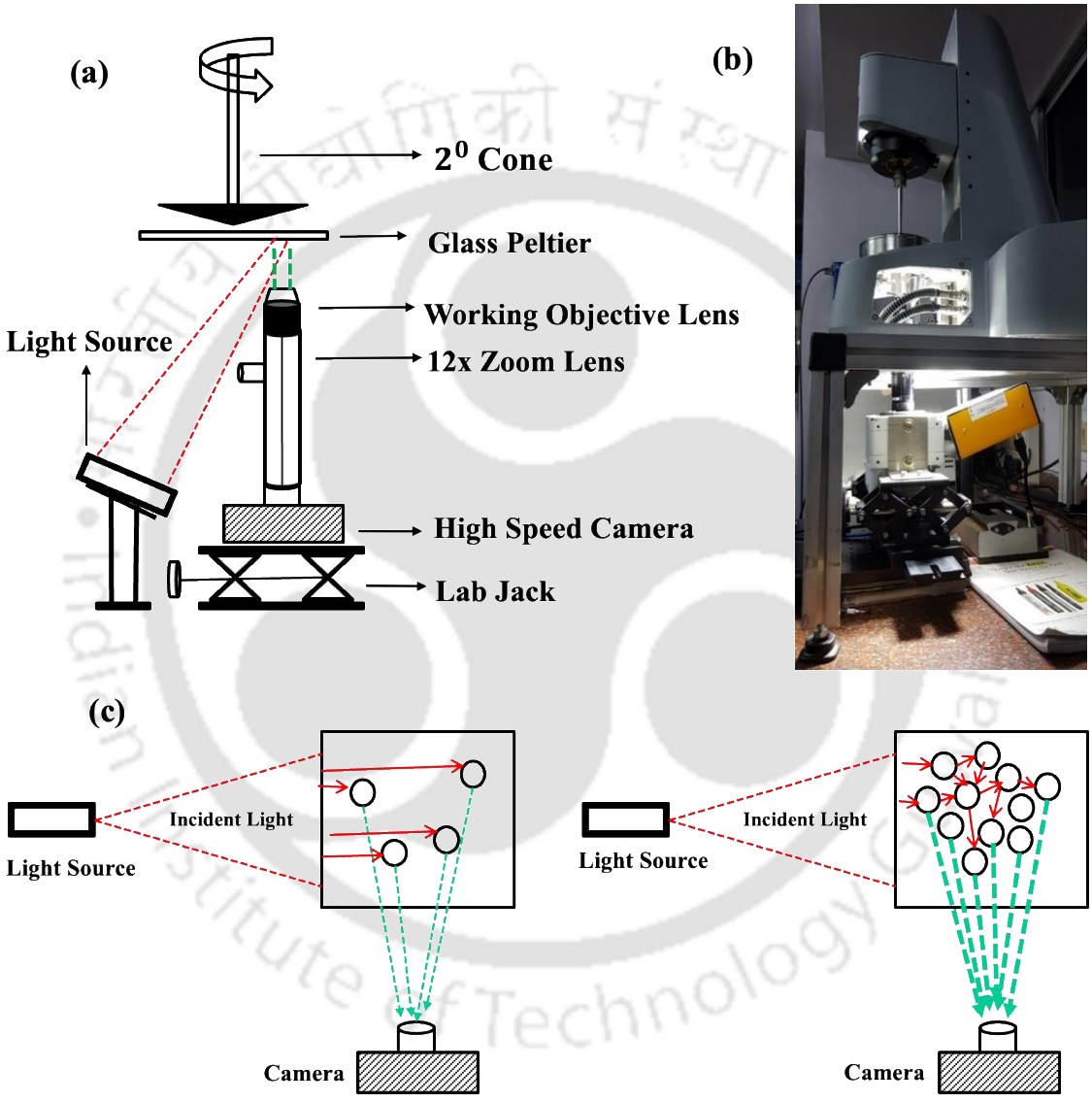

Figure 6.1 (a) Schematic of the Rheo-microscopy setup (b) pictorial view of the Rheo-microscopy experimental setup; and (c) Schematic of image capturing of clusters using tracer particles

The prepared STF samples were seeded with 0.1wt% hollow glass spheres of 10μm diameter as tracer particles to visualize the suspension. The video of tracer particle visualization was recorded at 450fps using a high-speed camera at 640x480 pixel resolution. The field of view (5 x 4 mm^2) was at a radial distance of 7mm from the center of the geometry. The single-frame images were extracted from the video at respective shear rates for the analysis of the microstructure. The pictorial view of the rheo-microscopy setup is shown in **Figure 6.1**(b). The schematic of indirect imaging of the particle clusters using the hollow tracer particles is shown in **Figure 6.1**(c). When the tracer particles are well dispersed, the intensity of reflected light collected by the lens is weak. The clustering of suspended silica particles at high shear rates also brings the hollow glass spheres closer, giving rise to an increase in the intensity of reflected light due to multiple reflections.

6.3 Results and Discussions

6.3.1 Microstructural Characterization

Figure 6.2 shows the surface morphology of the fumed silica nanoparticles and the shear thickening suspension prepared from these particles. The image is shown in **Figure 6.2**(a) was obtained by dispersing a very small amount of fumed silica particles in water. The average primary particle size of fumed silica nanoparticles was found to be 14nm, and the average length of their aggregates was found to be 200nm. **Figure 6.2**(b) shows the FESEM image of the finally prepared shear thickening suspension. It can be observed that fumed silica particles are entirely coated with PEG, but the signature of the branched structure of the particles is clearly noticeable.

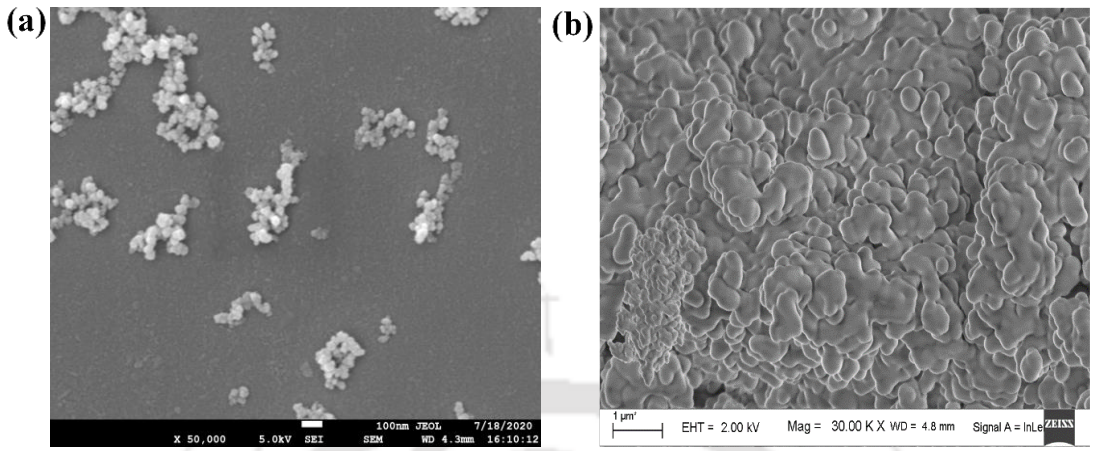

Figure 6.2 FESEM images of (a) fumed silica, 14nm primary particle size, and (b) shear thickening suspension prepared from fumed silica nanoparticles in PEG 200

6.3.2 Steady State Rheology

The steady shear rheological measurements of the prepared STF samples were performed at room temperature to determine the viscosity as a function of shear rate. **Figure 6.3**(a) shows the distinctive plot of the viscosity as a function of shear rate for 20 wt.% of fumed silica dispersed in PEG 300. As evident from the figure, the sample exhibits three distinct regions. At low shear rates (zone 1), the suspension exhibits a shear-thinning behavior that is characterized by a decrease in viscosity until the critical shear rate ($\dot{\gamma}_c$). In zone 2, the viscosity of the sample increases dramatically to a maximum viscosity value (η_{max}) exhibiting discontinuous shear thickening. Finally, zone 3 shows a second shear thinning behavior characterized by a continuous decrease in viscosity.

Shear thickening ratio (STR) and critical shear rate (CSR) are two essential parameters in shear thickening suspension. The point at which the onset of shear

thickening begins is said to be the critical shear rate ($\dot{\gamma}_c$), and the corresponding viscosity is said to be the critical viscosity (η_c). The ability of the suspension to thicken is given by the shear thickening ratio and is defined as the ratio of maximum viscosity of the suspension (η_{max}) to the critical viscosity of the suspension (η_c). The critical shear rate ($\dot{\gamma}_c$) can be determined by plotting shear stress as a function of shear rate on the log-log plot and is shown in **Figure 6.3**(b). These parameters were determined in CHAPTER 4 by varying the particle concentration, carrier fluid, and particle size distribution.

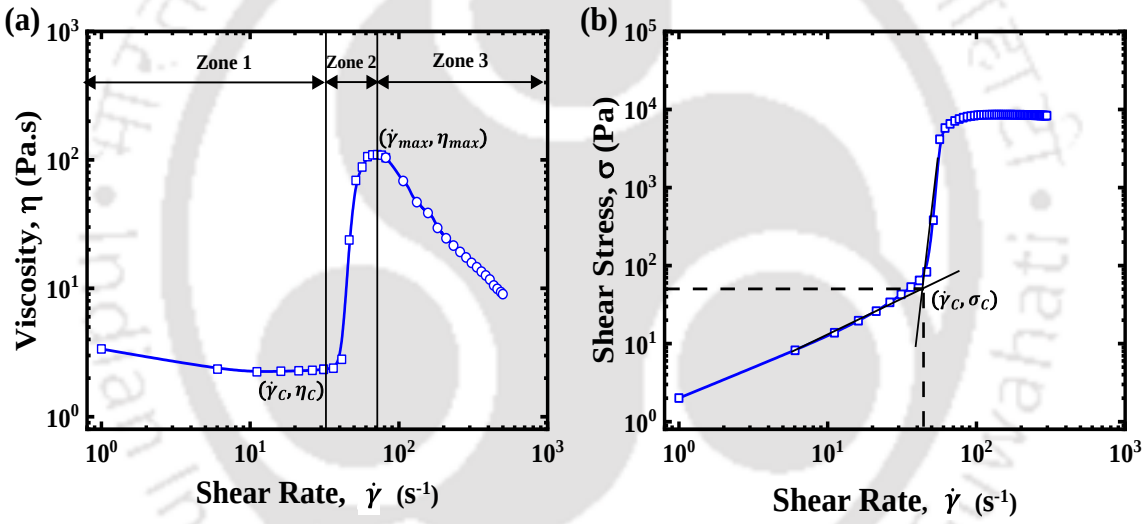

Figure 6.3 (a) Steady-state viscosity versus shear rate for 20wt% fumed silica in PEG 300 (b) Determination of the critical shear rate for the onset of shear thickening based on the point at which the slope changes

Galindo-Rosales et al. (2011) considered the three regions separately and modeled the viscosity functions for the curves shown in **Figure 6.3**(a) using a piecewise fit. These functions have been developed by following the Cross model (1965). Moreover, these functions are continuous and can be easily fitted as a smooth curve for all three regions. The proposed viscosity functions for the three

regions are represented by Eq. (6.1), and this includes 11 independent parameters that are determined from experimental data.

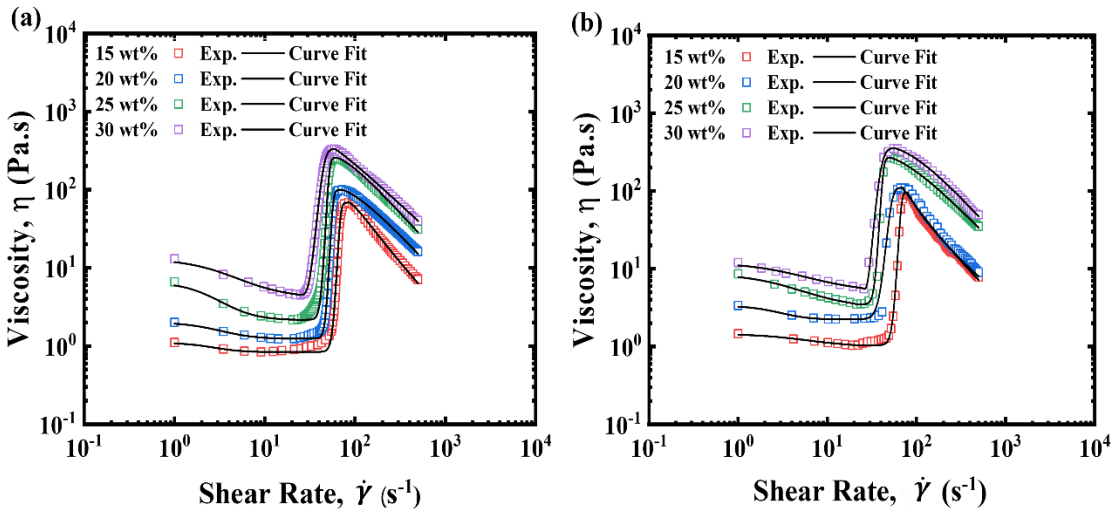

Figure 6.4 Curve fitting for the suspension viscosity as a function of shear rate for varying particle concentration (a) Fumed silica in PEG 200 (b) Fumed silica in PEG 300. Empty square boxes represent experimental data, and solid lines represent the fitted viscosity model function

$$\eta(\dot{\gamma}) = \begin{cases} \eta_I(\dot{\gamma}) = \eta_c + \frac{\eta_0 - \eta_c}{1+[K_I(\dot{\gamma}^2/\dot{\gamma} - \dot{\gamma}_c)]^{n_I}} & for\ \dot{\gamma} \le \dot{\gamma}_c \\ \eta_{II}(\dot{\gamma}) = \eta_{max} + \frac{\eta_c - \eta_{max}}{1+[K_{II}(\dot{\gamma} - \dot{\gamma}_c/\dot{\gamma} - \dot{\gamma}_{max})\dot{\gamma}]^{n_{II}}} & for\ \dot{\gamma}_c < \dot{\gamma} \le \dot{\gamma}_{max} \\ \eta_{III}(\dot{\gamma}) = \frac{\eta_{max}}{1+[K_{III}(\dot{\gamma} - \dot{\gamma}_{max})]^{n_{III}}} & for\ \dot{\gamma}_{max} < \dot{\gamma} \end{cases} \quad (6.1)$$

In the above equation, K_i ($i = I, II, III$) represents the transitions between the plateaus and the power law, and n_i ($i = I, II, III$) represents the slopes of the power-law in the three regimes, respectively. We obtained the parameter values of η_c, η_{max}, $\dot{\gamma}_c$, $\dot{\gamma}_{max}$ from the experimental measurements reported in CHAPTER 4.

A Levenberg-Marquardt algorithm (LMA) was used to fit the data for each curve (Galindo-Rosales et al., 2011). The parameters (K_i and n_i) were obtained by the iterative chi-square minimization technique. The fitting is said to have converged when the difference of χ^2 of two successive iterations is smaller than a given tolerance. Initial values for the parameters are chosen as close to the target to improve the accuracy of the fitting process. Curve fitting is carried out independently for the three regions of the curve using the corresponding viscosity function of Eq. (6.1). The correlation coefficient R^2 for all the plots was observed to be greater than 0.9. The curve fittings of experimental data for suspensions of different particle concentrations of fumed silica in PEG 200 and PEG 300 are shown in **Figure 6.4**(a) and (b). It is evident from these plots that the experimental data accurately fits the viscosity model. The numerical values of K_i and n_i obtained from the viscosity curves for fumed silica suspensions in PEG 200 and PEG 300 are presented in **Table 6.1** and **6.2**, respectively.

Table 6.1 Values of K_i and n_i obtained after curve fitting to viscosity function of Eq. (6.1) for fumed silica suspension in PEG 200

Fumed silica suspensions in PEG 200						
Weight Fractions (wt. %)	**K_I**	**K_{II}**	**K_{III}**	**n_I**	**n_{II}**	**n_{III}**
15	1.3983	0.0051	0.0158	1.108	4.99	1.22
20	2.3185	0.0087	0.0098	0.991	4.91	1.20
25	3.4889	0.0086	0.0126	0.986	4.10	1.22
30	2.1174	0.0734	0.0149	0.735	2.38	1.07

Table 6.2 Values of K_i and n_i obtained after curve fitting to viscosity function of Eq. (6.1) for fumed silica suspension in PEG 300

Fumed silica suspensions in PEG 300						
Weight Fractions (wt.%)	**K_I**	**K_{II}**	**K_{III}**	**n_I**	**n_{II}**	**n_{III}**
15	0.8061	0.0044	0.027	0.709	3.72	0.99
20	1.3713	0.0104	0.0251	1.073	3.27	1.11
25	1.67509	0.0115	0.0118	0.686	3.45	1.17
30	1.56703	0.0319	0.0104	0.643	2.06	1.23

As mentioned earlier, the shear thickening phenomenon can be classified into two types: (CST) and (DST). A smooth increase in viscosity with the shear rate is defined as a continuous shear thickening, and a sudden jump in the viscosity indicates discontinuous shear thickening. Quantitative differentiation of shear thickening is difficult since the viscosity and shear stress vary nonlinearly in the shear-thickening region. The exponent α in the power-law fit to the shear stress vs. shear rate flow curve, $\tau = \dot{\gamma}^{\alpha}$, can be used as a measure of shear thickening (Brown and Jaeger, 2014). In **Figure 6.5**, we plotted the flow curves in the shear thickening region on the log-log scale and determined α as the slope of the steepest part of the curve. The exponent α for 15, 20, 25, and 30 wt. % suspension in PEG 200 was found to be 14.21, 14.98, 15.23, and 10.99, respectively. The corresponding values of α for suspensions in PEG 300 were 11.98, 12.10, 12.66, and 9.51, respectively. A value of $\alpha \gg 2$ is typically reported as DST (Brown and Jaeger, 2014); thus, all our samples showed DST.

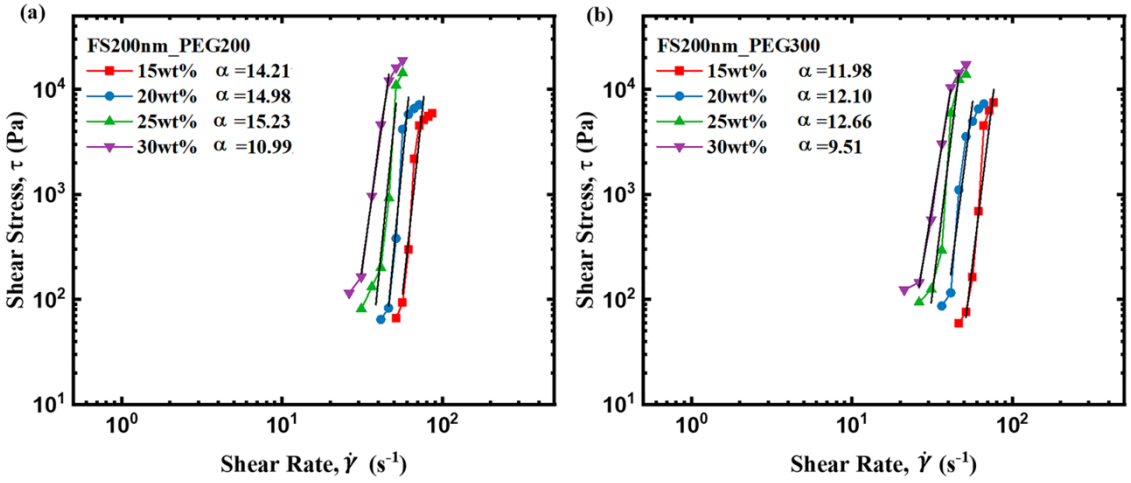

Figure 6.5. Determination of power law exponent (α) from the slope of the steepest part of the flow curve, $\tau = \dot{\gamma}^{\alpha}$. (a) Fumed silica suspensions in PEG 200 and (b) fumed silica suspensions in PEG 300.

The weight percentage of particles in our samples was low (between 15% to 30%), and considering the true density of silica particles (2.22 gm/cc), the corresponding volume concentration was calculated to lie between 8% to 18 %, which is also low for shear thickening if we try to correlate this behaviour with reported studies in the literature. It is to be noted that for fumed silica suspension, even though the true volume fraction is low, the effective volume fraction can be much higher. This is purely due to the fractal nature of the particle shape. The PEG locked in the branch corners become immobile, and the entire structure under shear moves as a single entity. There is no true measure of the effective viscosity of fumed silica particles in the sheared suspension. However, prior work in the literature has determined the effective volume fraction (φ) of many systems by finding out the value which gives the same relative viscosity (η_r) in general, suspension viscosity vs. concentration curve, such as the Krieger-Dougherty fit

given in Eq. 6.2 (Krieger and Dougherty, 1959). The estimated effective volume fraction of our samples by comparing the low shear viscosity data with the following equation was found to vary between 45% to 54 %.

$$\eta_r = (1 - \frac{\phi}{\phi_{max}})^{-2.5\phi_{max}} \qquad (6.2)$$

In the above equation, the maximum packing fraction ϕ_{max} is taken to be 0.58.

6.3.3 Microstructure

The steady shear measurements were carried out at room temperature to determine the viscosity variation of the shear thickening suspension. A transparent glass Peltier system was used as a bottom plate to visualize the microstructure. A high-speed camera in conjugation with a zoom lens placed below the glass plate enabled the imaging of microstructure at different points of shear rates. The suspension prepared using the sonochemical homogenization method was highly transparent, and this prevents the visualization of clusters if any bright light source is used. Hollow glass spheres of diameter 10μm diameter were used as tracer particles (see **Figure 6.1**c). These tracer particles allowed us indirect visualization of cluster formation during shear. When the tracer particles are well dispersed, the intensity of reflected light is weak. It is expected that due to the fractal nature of the fumed silica particles, some of the hollow tracer particles are stuck at the corners and move together with the suspended silica particles. The formation of clusters of silica particles at high shear rates also brings the hollow glass spheres closer, giving rise to an increase in the intensity of reflected light (due to multiple reflections), and it appears as a bright region in the images. The viscosity and microstructure

of the suspensions at different shear rates for 20 wt.% of fumed silica nanoparticles dispersed in PEG 300 are shown in **Figure 6.6**. As evident from the figure, the sample exhibits shear thickening, and three distinct regions can be easily identified. These single-frame images in **Figure 6.6** correspond to the points in the shear-thinning near the critical shear rate, in the shear thickening region, at maximum viscosity, and in the second shear-thinning region. The enlarged image frames can be viewed in **Figure 6.7**.

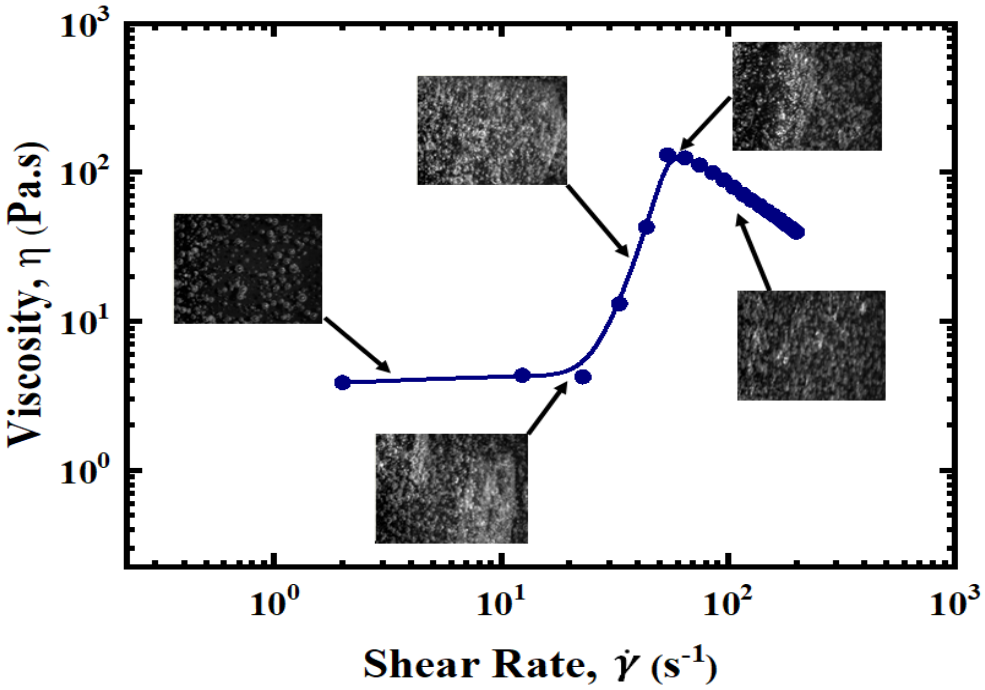

Figure 6.6 Visualization of microstructure and viscosity as a function of the applied shear rate for 20wt% fumed silica in PEG 300

The shear thickening behavior can be observed qualitatively from the images recorded at the corresponding shear rates. At very low shear rates (before the critical shear rate), the hollow glass sphere particles are randomly distributed in the sample, and most of the light is able to pass without much scatter (**Figure 6.7**(a)). This also indicates that the fumed silica particles are also uniformly

distributed, and there is absence of any visible cluster. As the shear rate increases, the suspended particles start forming large clusters. These clusters move as one chunk during the shear. The hollow glass spheres within these clusters also do not show relative motion and appear to be frozen within the clusters. The center-to-center distance between the particles of these clusters are much smaller compared to the initial separation at low shear. As illustrated previously in **Figure 6.1**(c), multiple reflections of light from hollow glass spheres makes the cluster visible as bright regions in image frames (**Figure 6.7**(b)-(d)).

The image frame in **Figure 6.6** corresponding to the onset of shear thickening shows two large clusters as white patches. As the shear rate is further increased (beyond the critical shear rate), the size of these clusters increases, and the whole region in the image becomes more bright. After the maximum viscosity is reached, the strong shear force breaks these large clusters, thereby decreasing the viscosity. This initiates the second shear thinning of the suspension. It can be clearly observed from the image frame (in the second shear-thinning region) that these clusters gradually break down and move separately with the flow field. Thus, the Rheo-microscopy studies enabled us to visualize the macroscopic behavior of cluster formation while measuring the rheological properties. The images and video are only a qualitative observation of cluster formation, and it is difficult to deduce any metric to quantify the size of clusters.

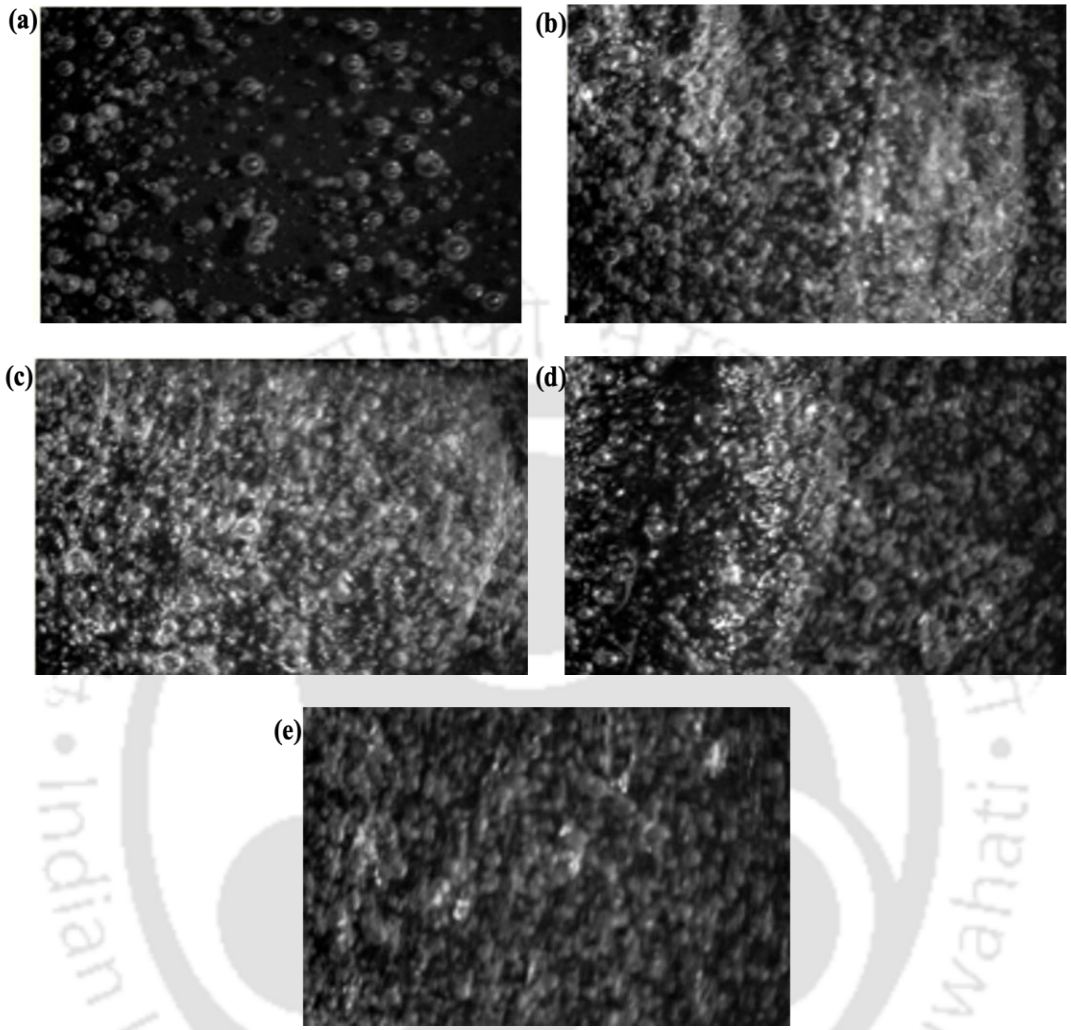

Figure 6.7 Single-frame images taken (a) before critical shear rate ($\dot{\gamma} = 2\ s^{-1}$), (b) at the critical shear rate ($\dot{\gamma} = 33.2\ s^{-1}$), (c) during the shear thickening ($\dot{\gamma} = 43.7\ s^{-1}$) ,(d) at maximum viscosity ($\dot{\gamma} = 54.1\ s^{-1}$),(e) in the second shear-thinning region ($\dot{\gamma} = 138\ s^{-1}$).

The mean light intensity at five different points of shear rates (2.0, 33.2, 43.7, 54.1, and 138.0 s^{-1}), for which the micrographs are shown in **Figure 6.7** was evaluated using ImageJ software by performing an average of over 150 image frames. The respective values of mean light intensity were found to be 27.6, 71.1, 80.9, 57.8,

and 50.6. **Figure 6.8** shows the average light intensity plotted as a function of shear rate. This indicates that clusters rapidly grow, reach the maximum value, and then decrease again. Our visualization study supports the theory of cluster formation as the primary cause for shear thickening and subsequent breaking of these clusters at higher shear rates for the second shear-thinning behaviour.

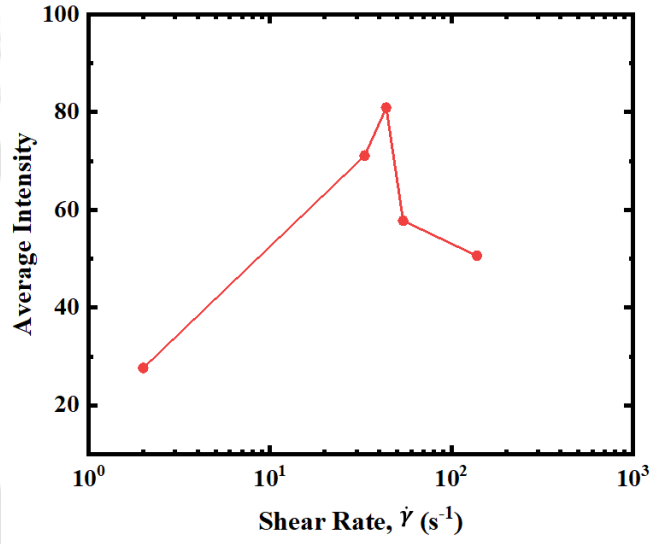

Figure 6.8. Average light intensity at different shear rates for 20 wt% suspension in PEG 300

6.3.4 First Normal Stress Difference

In addition to the microstructure visualization and viscosity measurements, we have also studied the variation in the first normal stress difference during the steady shear experiments. With the 12.5 mm radius (r) cone and plate system, the normal force (F_z) exerted by the sheared sample on the cone is measured to evaluate the first normal stress difference, $N_1 = 2F_z/\pi r^2$. The first normal stress difference (N_1) as a function of shear rate for the suspensions of various particle concentrations of fumed silica in PEG 200 and PEG 300 is shown in **Figure 6.9**.

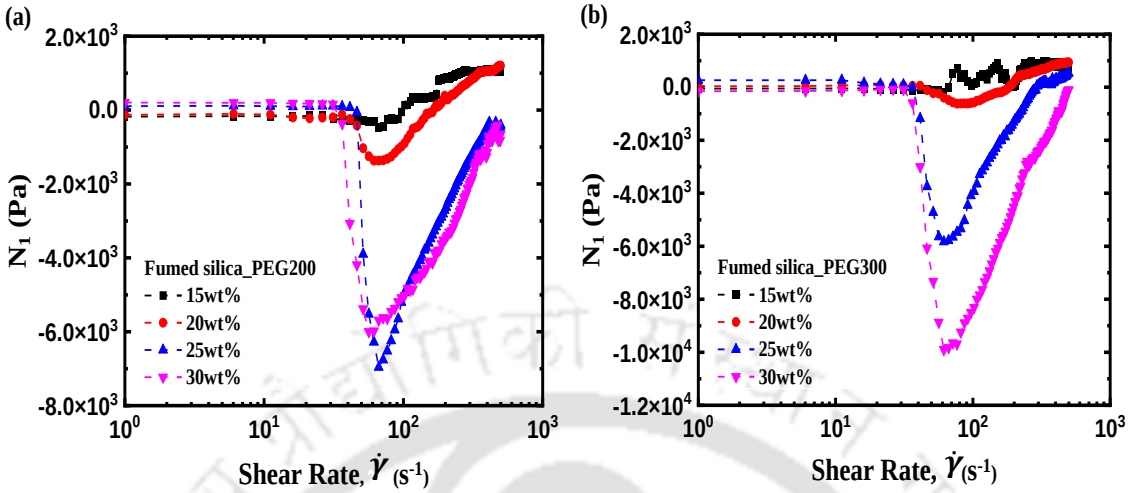

Figure 6.9 First normal stress difference (N_1) as a function of shear rate for varying particle concentration of fumed silica in (a) PEG 200 and (b) PEG 300

It can be observed from **Figure 6.9** that at low shear rates, the first normal stress difference is close to zero and independent of the shear rate. Beyond a certain critical shear rate, the N_1 shows a negative value whose magnitude rises rapidly with an increase in the shear rate. This corresponds to the shear thickening region. At lower particle concentrations (15 wt.%), the first normal stress difference showed only a slight increase in negative value in the shear thickening region, followed by irregular fluctuations but positive values at higher shear rates. The N_1 values for 20 wt.% suspension in the shear thickening region is negative with a comparatively smoother profile. At high shear rates (in the second shear-thinning region), both 15 and 20 wt. % samples showed large fluctuation and a positive value of N_1. Inertial instabilities cannot be attributed to the fluctuations since the flow Reynolds number, $Re_p \sim O(10^{-4})$, is small even at the highest shear rate. Hébraud (2009) has experimentally observed that at jamming transition, the first normal stress increases and develops fluctuations. The jamming transition occurs at both lower

shear rates and volume fractions when the colloidal particles are roughened. The fluctuations in N_1 observed in our experiments could be associated with the changes in the inter-particle contact state that is amplified in the case of fumed silica suspension. It is also likely that such inter-particle contact lead to friction and a more positive contribution to N_1. For higher concentrations of particles (25 and 30 wt.%), there is a significant increase in the negative value of the first normal stress difference in the shear thickening region. After reaching the maximum value, the magnitude of N_1 starts to decrease again with the shear rate.

However, the sign of N_1 remains negative even in the second shear-thinning region. The negative sign of N_1 in the shear thickening regime can be attributed primarily to the hydrodynamic origin of stresses. Our experimental results are in qualitative agreement with previous experimental and simulation studies where a negative N_1 is reported and linked to hydrodynamic stresses (Cwalina and Wagner, 2014; Wang et al., 2020). In a recent work, Royer et al. (2016) studied the behavior of N_1 on shear stress and observed negative N_1 for particle volume fraction, $\Phi \leq 0.52$. The negative N_1 at moderate particle concentration is attributed to the hydrodynamic lubrication forces. However, at higher particle volume fractions ($\Phi > 0.52$), the presence of frictional contact forces contributed to a transition from negative to positive N_1. Their results also showed that shear thickening is primarily driven by frictional contact forces, with hydrodynamic lubrication forces playing a supporting role at higher concentrations.

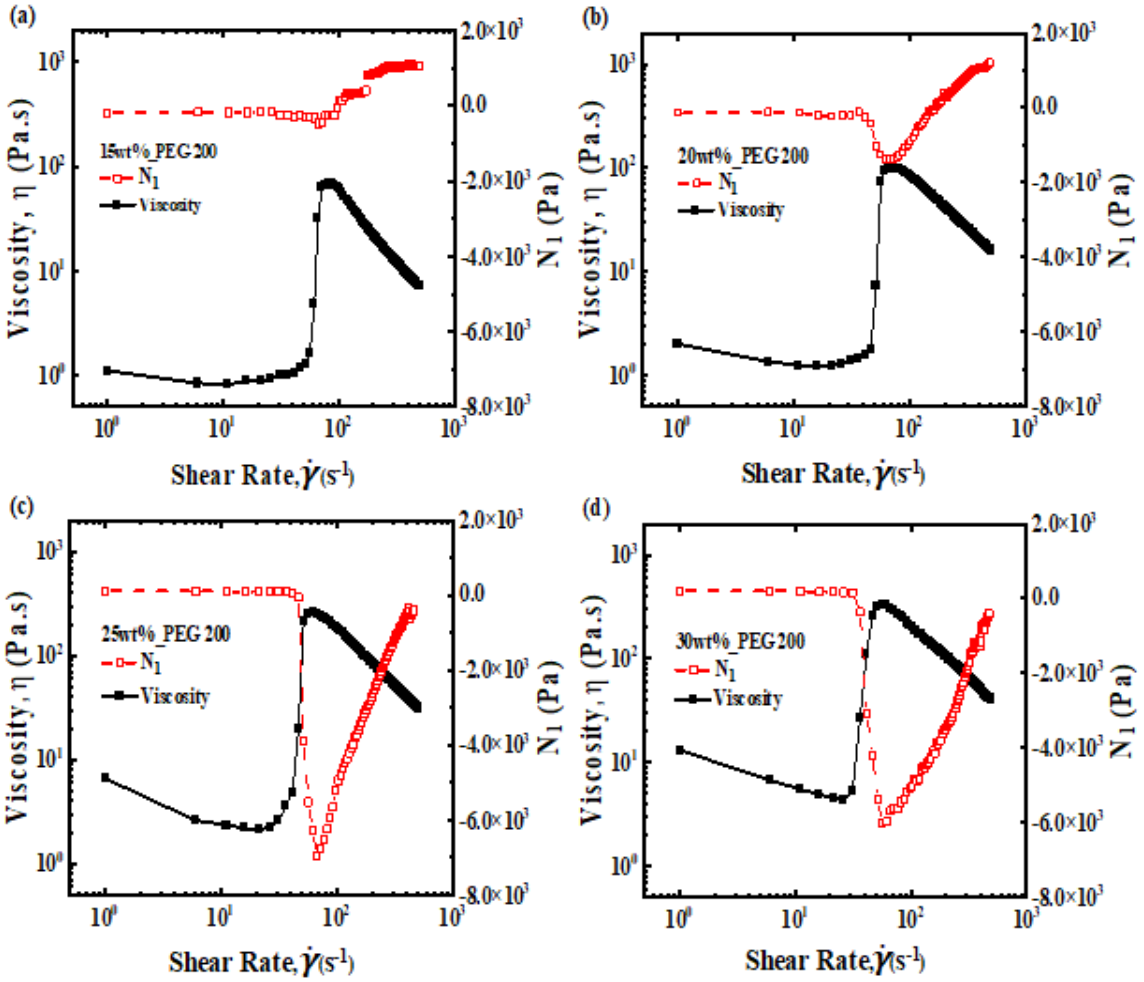

Figure 6.10 Viscosity and first normal stress difference as a function of shear rate in three regimes for fumed silica suspension in PEG-200 at (a) 15wt% (b) 20wt% (c) 25wt% (d) 30wt%. Filled circles are the steady-state viscosity measurements. Open circles are the first normal stress difference measured as a function of shear rate

Recently, Cao et al. (2021) studied shear jamming in a granular suspension and reported the transition from discontinuous shear thickening to shear jamming, accompanied by a transition from negative to positive N_1 at higher particle concentration. Both Royer et al. (2016) and Cao et al. (2021) observed negative N_1 at lower packing fractions where shear thickening is continuous, but positive N_1 was

reported at higher packing fractions (when the shear thickening is more discontinuous). The positive N_1 observed in discontinuous shear thickening can be attributed to the dominance of frictional contacts over hydrodynamic interactions. Simulation studies based on purely hydrodynamic lubrication forces resulted in a negative N_1 at lower particle concentration. Similarly, studies considering frictional contact forces and short-range lubrication forces between the particles showed a positive N1 at higher particle concentrations (Singh et al., 2018; Seto and Giusteri, 2018). In **Figure 6.9**(a), we notice that the peak value of N_1 of 30 wt.% is lower compared to the 25 wt.% samples in PEG 200. On the other hand, the peak N_1 of 30 wt.% is higher compared to 25 wt.% samples in PEG 300 (**Figure 6.9**(b)). At higher wt.%, the inter-particle distances are smaller, and the low molecular weight (low viscosity) carrier fluid is unable to prevent close contact of particles at high shear rates. A positive contribution of frictional contact forces may be responsible for the lower peak value of N_1. The molecular weight and viscosity of PEG 300, being higher, delays the frictional contact even for 30 wt% samples (Please see **Figure 6.9**(b)). However, the hydrodynamic contribution of N_1 for both samples was much more than the frictional contribution during the shear thickening and second shear-thinning regime.

To understand the synergy between the viscosity and N_1 data, we have shown their variation with the shear rate in the same plot. **Figure 6.10** and **Figure 6.11** show the viscosity and first normal stress difference data as a function of shear rate for suspensions in PEG 200 and PEG 300, respectively. As the shear rate increases, the suspension exhibits a discontinuous shear thickening behavior which is characterized by a sudden increase in the viscosity of the sample to a maximum

viscosity value (η_{max}) and a negative first normal stress difference (N_1). The critical shear rate at which viscosity shows a steep rise coincides with the rise in negative N_1. The decrease in N_1 after reaching the peak value indicates a more positive contribution of normal stress. The breakage of the force chain in the clusters can also leads to a decrease in the normal force on the plate causing the decrease in N_1.

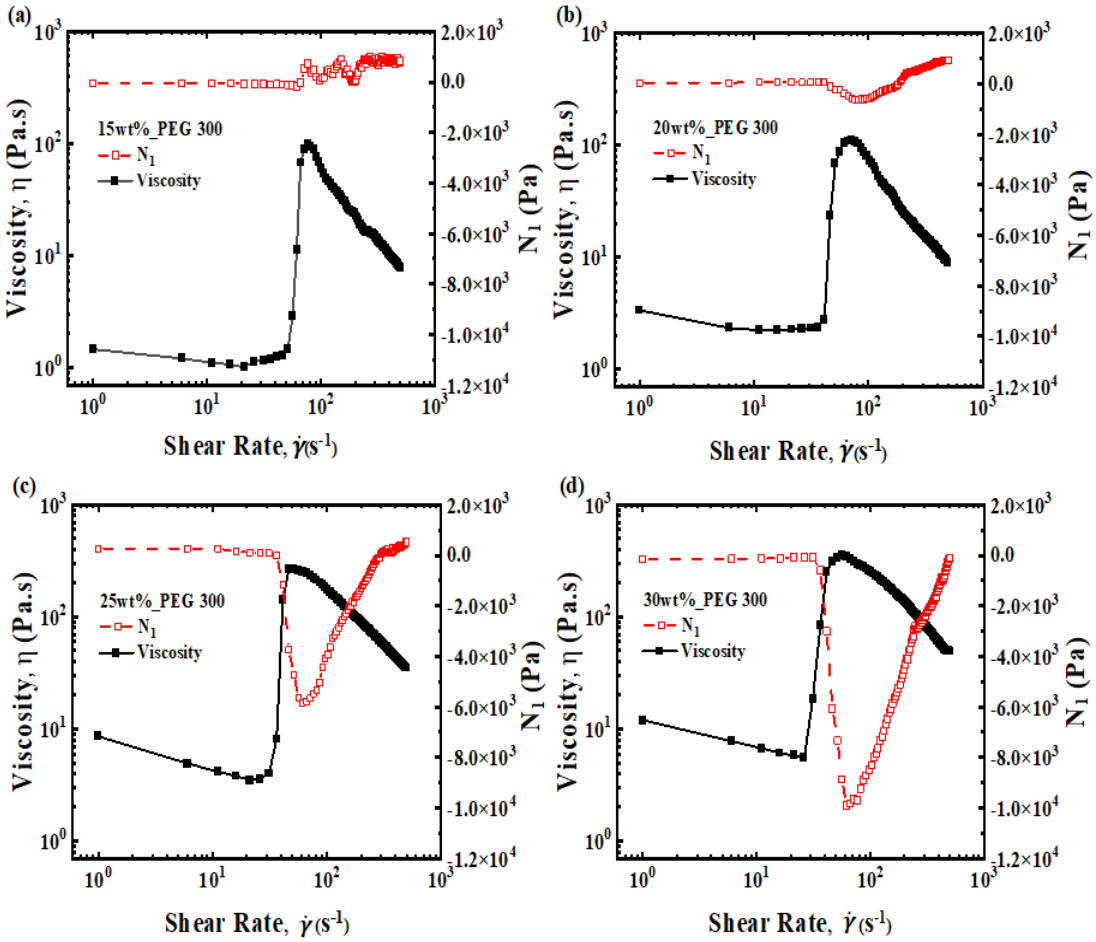

Figure 6.11 Viscosity and first normal stress difference as a function of shear rate in three regimes for fumed silica suspension in PEG-300 at (a) 15wt% (b) 20wt% (c) 25wt% (d) 30wt%. Filled circles are the steady-state viscosity measurements. Open circles are the first normal stress difference measured as a function of shear rate

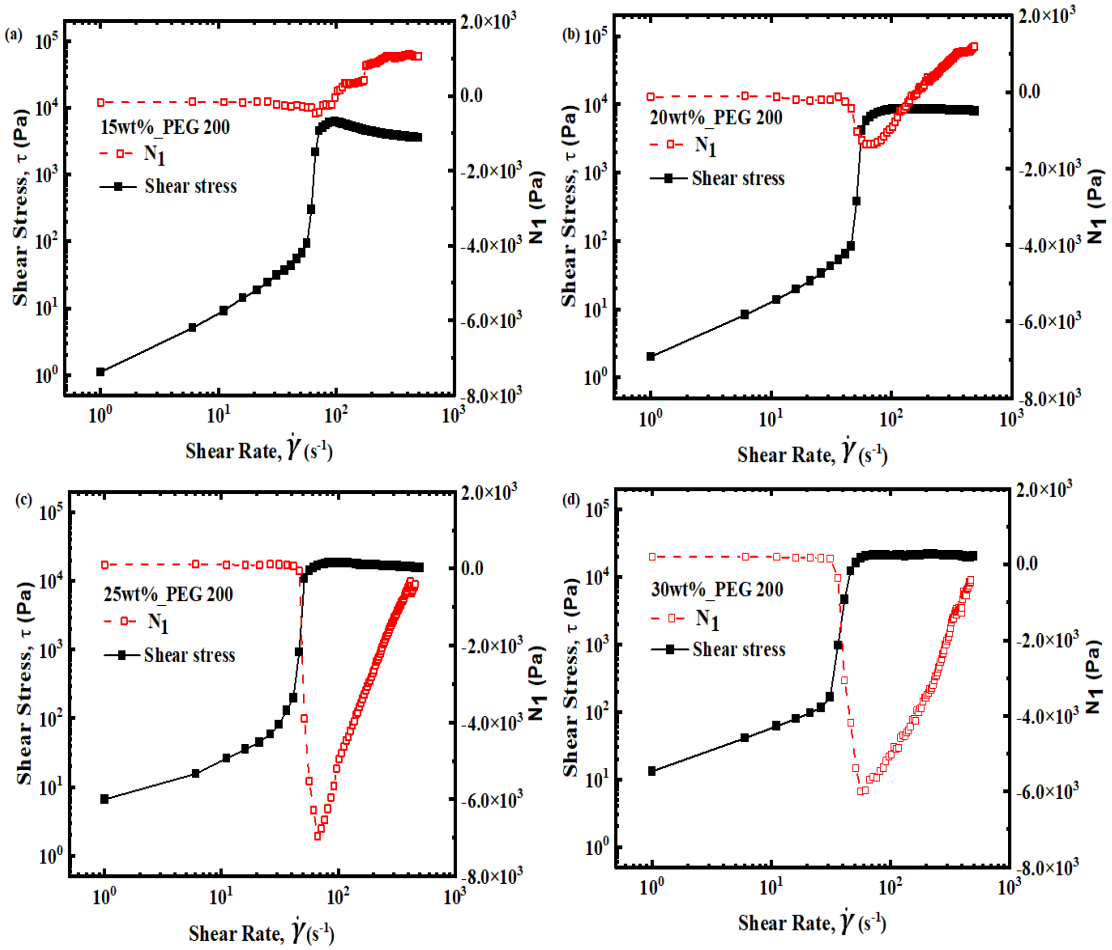

Figure 6.12 Shear stress and first normal stress difference as a function of shear rate for fumed silica suspension in PEG-200 at (a) 15wt% (b) 20wt% (c) 25wt% (d) 30wt%

Figure 6.12 and **Figure 6.13** show the shear stress and normal stress difference (N_1) plotted on the same axis as a function of shear rate for suspension in PEG 200 and PEG 300, respectively. The critical stress values of all samples varied between 90 and 160 Pa. It can also be observed that in the second shear-thinning region, the shear stress reaches a plateau indicating rapid breakage of

clusters. Brown and Jaeger (2012) have studied the variation of maximum shear stress (τ_{max}) on the ratio of surface tension of the solvent to particle radius (γ/a) for a wide variety of suspensions and observed a linear scaling. However, they observed a large variation in the values of τ_{max} within a band by about an order of magnitude. The factors they attributed to this variation were particle shape, particle roughness, and particle interaction. It is interesting to note that our values of maximum shear stress and their variation is well within the band specified by Brown and Jaeger (2012) for colloidal silica suspension of spherical particles. The difference in τ_{max} for spherical colloidal silica and fumed silica suspension further indicates that the geometric factor of the particles also play an essential role in the generation of stress during shear thickening.

The experimental data are replotted on a linear scale in each of the shear thickening and second shear-thinning regions to further analyze the scaling of the first normal stress difference N_1 with the shear rate. It is evident from **Figure 6.14** that the value of the first normal stress difference in the shear thickening region (for both the suspensions) varies almost linearly with the shear rate. A linear variation of N_1 is an indication that hydrodynamic forces dominate over any other nonhydrodynamic contact forces, such as friction. On the other hand, during second shear-thinning, the first normal stress difference (N_1) decreases in a non-linear way before reaching to a small value at high shear rates. As observed earlier, the microstructure (after reaching the maximum viscosity) showed the breakage of large clusters into smaller ones, and the non-linear variation in N_1 could be due to frictional contacts among these hydroclusters. In highly concentrated suspensions of noncolloidal particles, dilation and stresses are strongly coupled in DST (Lootens

et al., 2005; Fall et al., 2009). Dilation in colloidal suspension at moderate concentration has not been reported. Therefore, we do not expect dilatancy in our system. The second shear-thinning and associated decrease in N_1 are predominantly due to the breakage of force chains and hydroclusters. The shear-thinning after shear thickening is commonly observed with other shear-thickening suspensions and are consistent with the studies by Chatté et al. (2017).

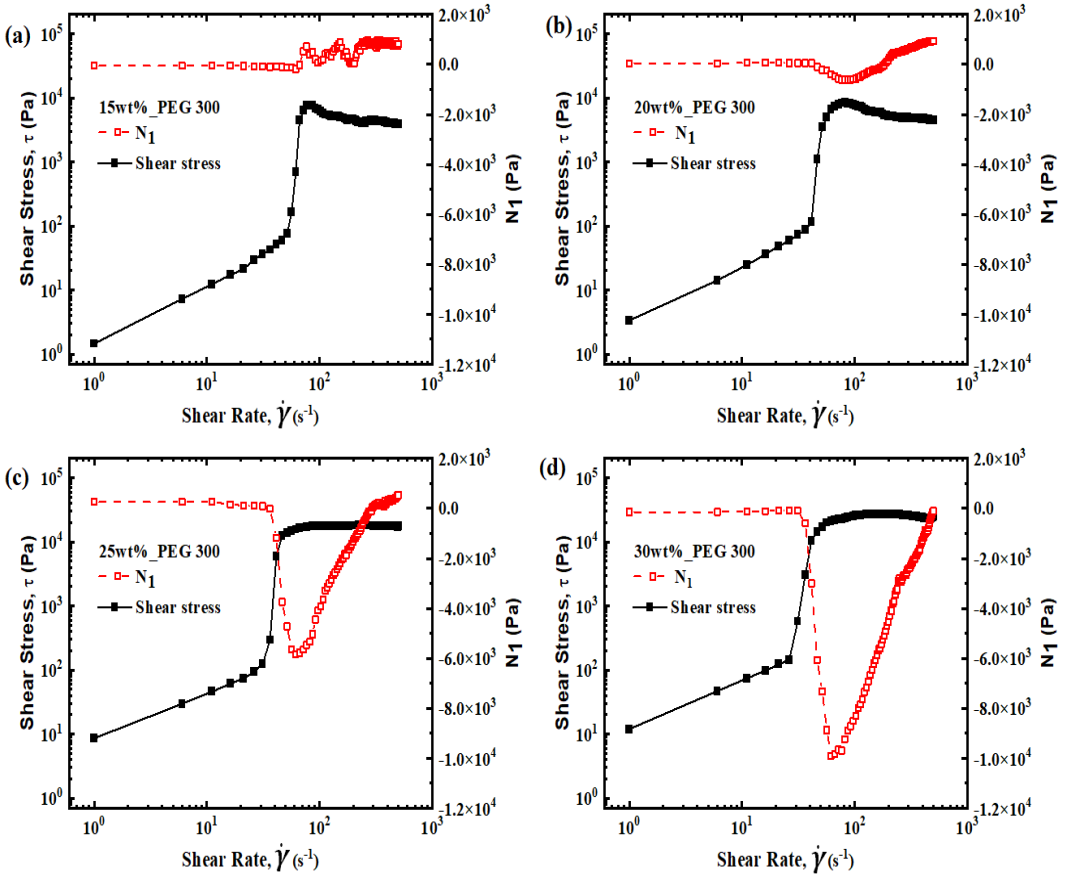

Figure 6.13 Shear stress and first normal stress difference as a function of shear rate for fumed silica suspension in PEG-300 at (a) 15wt% (b) 20wt% (c) 25wt% (d) 30wt%

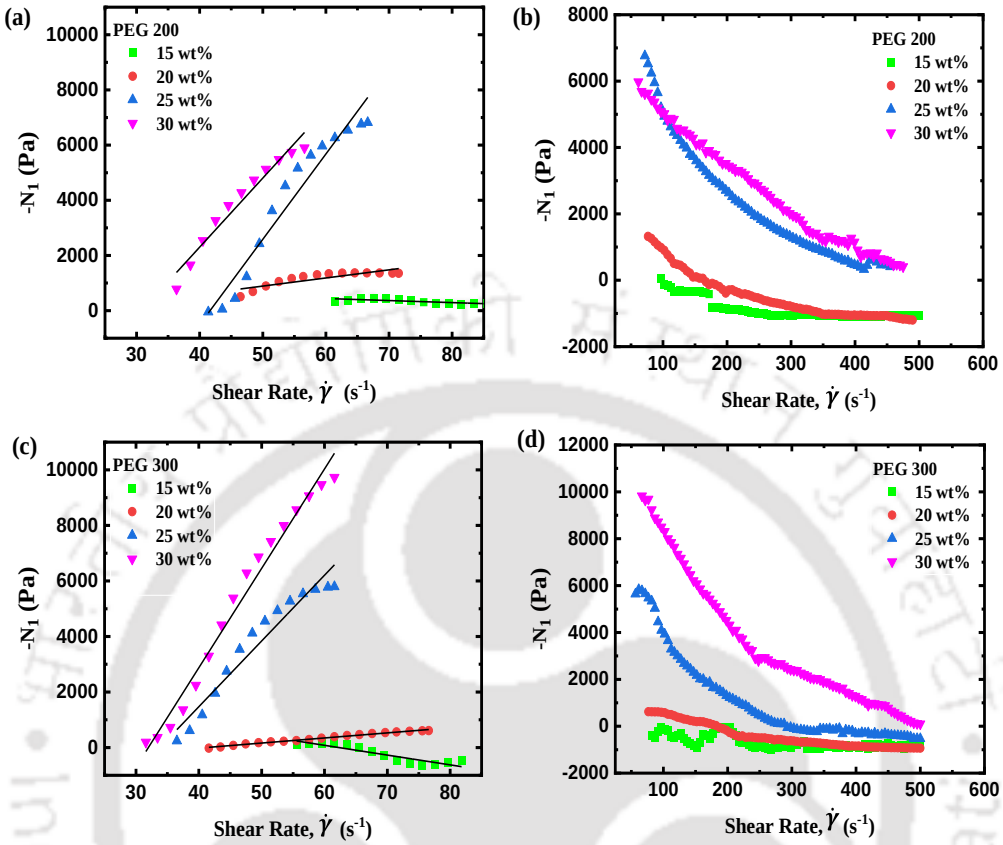

Figure 6.14 First normal stress difference as a function of shear rate plotted on linear axes in (a) Shear thickening regime in PEG 200 (b) Second shear-thinning regime in PEG 200 (c) Shear thickening regime in PEG 300 (d) Second shear-thinning regime in PEG 300. Solid lines are linear regression fit to the experimental data in the shear thickening region.

The rheological properties of the suspensions are often characterized by the first normal stress difference coefficient, which in dimensionless form is defined as $\Upsilon_1 = -N_1/(\eta_f \dot{\gamma})$, where η_f is the solvent viscosity. The first normal stress difference coefficient (Υ_1) values as a function of shear rate for different particle concentrations are shown in **Figure 6.15**. Both PEG 200 and PEG 300 suspensions

showed a positive value of Υ_1 in the shear thickening region at moderate particle concentration (25 and 30 wt.%). However, at lower particle concentrations (15 and 20 wt%), the first normal stress difference coefficient (Υ_1) remains constant in the shear thickening region. These findings are in qualitative agreement with the experimental studies by Cwalina and Wagner (2014), who observed a positive Υ_1 at a high Peclet number (Pe) in the shear thickened state.

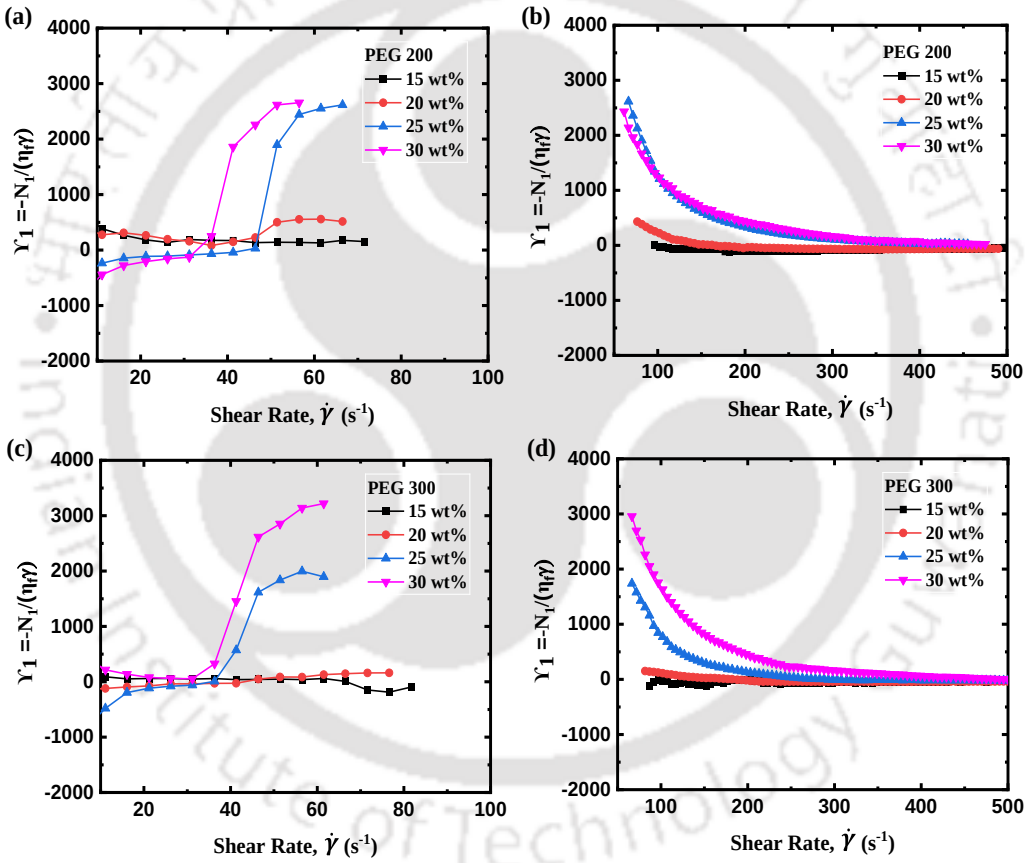

Figure 6.15 First normal stress difference coefficient as a function of shear rate in (a) Shear thickening regime in PEG 200 (b) the Second shear-thinning regime in PEG 200 (c) Shear thickening regime in PEG 300 (d) Second shear-thinning regime in PEG 300

It is worth mentioning here that simulations with modified hydrodynamic interactions (resulting from surface roughness) without considering any frictional contact force have also shown a discontinuous shear thickening at a high particle volume fraction ($\Phi = 0.52$) with a negative first normal stress difference (N_1) at high Peclet number (Wang et al., 2020). Our observations of discontinuous shear thickening in fumed silica suspension with negative N_1 are at relatively lower concentration of particles. The fractal nature of fumed silica particles can significantly modify the hydrodynamic interactions. Moreover, the effective phase volume fraction can be considered much higher since a significant amount of liquid is occluded within the loosely packed silica aggregates (Raghavan and Khan, 1997). Therefore, we observe discontinuous shear thickening with negative N_1 in a system where hydrodynamic forces appears to dominate over frictional contacts. The fractal nature of the particles further ensures that the force chains are quickly formed at the critical shear rate, and the gap-spanning clusters are mainly responsible for the generation of large normal stresses. The negative value (almost linear in shear rate) in the shear thickening region also indicates that the normal stresses in the flow direction are weak compared to that in the gradient direction. Therefore, we speculate that the frictional forces are masked by the hydrodynamic forces in our system. We cannot rule out the dominant role of frictional forces in some other system.

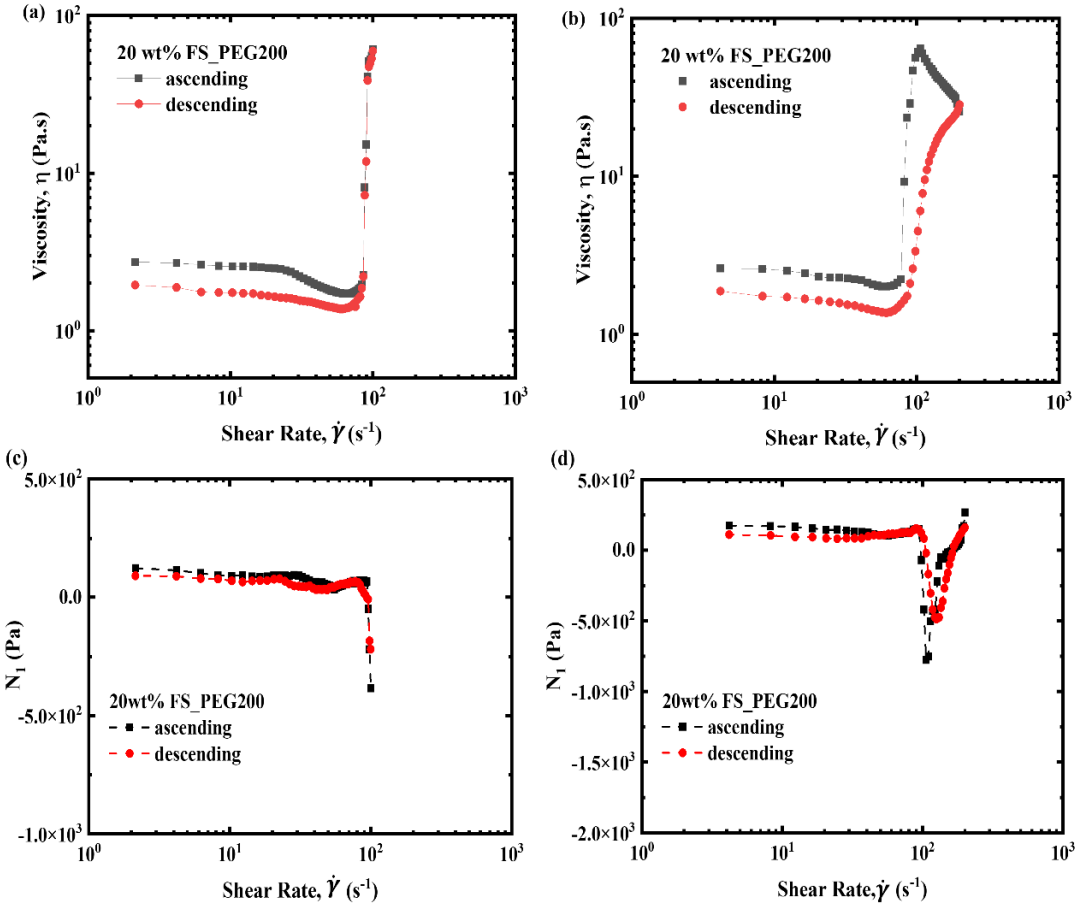

Figure 6.16 Viscosity first normal stress difference variation plotted against shear rate for ascending and descending shear ramp with 20 wt.% suspension in PEG 200. (a) Viscosity data up to the shear thickening region, (b) viscosity data up to the second shear thinning region, (c) first normal stress difference data up to the shear thickening region, and (d) first normal stress difference data up to the second shear thinning region.

The reversible/irreversible nature and hysteretic behavior of rheological curves were checked by conducting two sets of experiments on 20 wt.% sample in PEG 200. In the first experiment, the steady shear ramp extended only up to the shear thickening region, while for the second, it extended in the second shear-thinning region. **Figure 6.16**(a) shows the viscosity variation up to the shear-

thickening region during ascending and descending shear rate measurements. The corresponding behavior of N_1 is shown in **Figure 6.16**(c). These curves show reversibility with hysteresis, which is more pronounced in viscosity variations. On the other hand, the analysis of the viscosity curve in **Figure 6.16**(b) clearly shows the irreversibility. The reason for irreversibility can be attributed to the fractal nature of irregular-shaped fumed silica particles. Once the clusters are broken during the shear thinning, a reduction in the shear rate does not produce the same microstructure. The corresponding behavior of N_1, as shown in **Figure 6.16**(d), is still reversible with noticeable hysteresis. Further investigation is required to understand the nature of interactions and microstructure in the second shear-thinning region.

6.3.5 Oscillatory Shear Rheology

The oscillatory shear rheology was studied to understand the viscoelastic behavior of the suspension. In the oscillatory test, both the strain amplitude sweeps at a constant angular frequency and the angular frequency sweeps at constant strain amplitudes were performed on the 20 wt.% suspensions prepared in PEG 200 and PEG 300. The strain amplitude sweeps were carried out by varying the strain from 1% to 1000% at a constant frequency of 10, 50, and 100 rad/s, and their viscoelastic behavior is shown in **Figure 6.17**. In both the suspensions, the storage modulus (G') and loss modulus (G'') showed three distinct regions similar to that of steady shear measurements. At lower strains, both moduli decrease with an increase in strain amplitude. After the critical strain, both (G') and (G'') exhibit a sudden jump to higher values with an increase in strain amplitude. It can also be observed

that critical strain amplitude decreases with an increase in the frequency for both suspensions. These results are consistent with the earlier experimental studies on fumed silica suspensions in polypropylene glycol (PPG) (Raghavan and Khan, 1997; Galindo-Rosales et al., 2009).

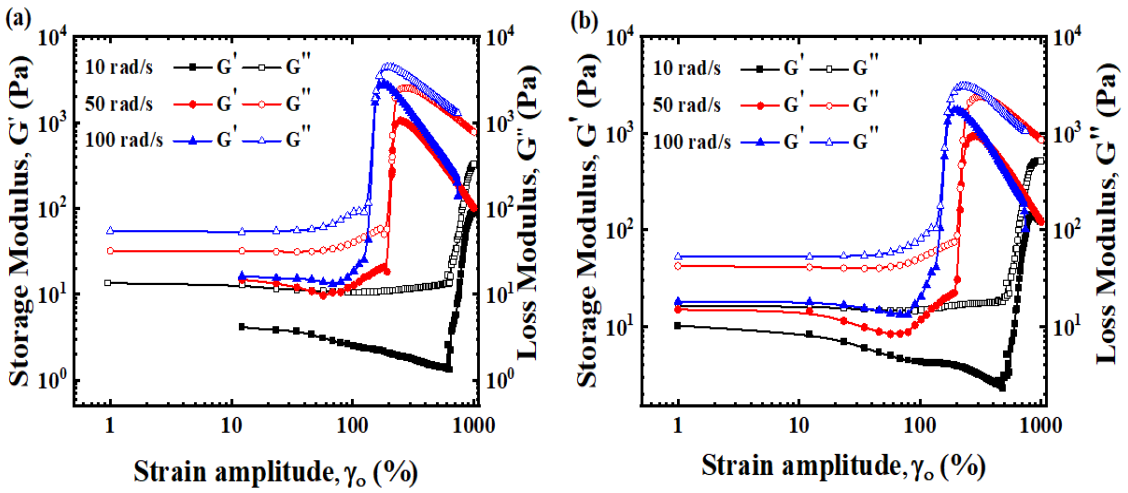

Figure 6.17 Storage modulus and Loss modulus as a function of strain amplitude at frequency 10, 50, and 100 rad/s for 20 wt% fumed silica suspensions in (a) PEG 200 (b) PEG 300

Similarly, the angular frequency sweep measurements were performed by varying the frequency in the range of 0.1 to 100 rad/s at a constant strain amplitude of 100%, 500%, and 1000%. **Figure 6.18** shows the frequency-dependent storage and loss moduli at constant strain amplitude for 20 wt.% fumed silica suspensions in PEG 200 and PEG 300. From the figure, it can be observed that $G'' > G'$ over the entire range of frequency, which signifies that the suspension of fumed silica is non-flocculated. At very low strain amplitude (10%), the suspension does not show any characteristics of strain-hardening. Fall et al. (2009) have shown that at very low shear, other than contact interactions, the existence of yield stress can only be

ascribed to the formation of a jammed contact network. Our samples are at much lower concentrations and do not exhibit yield stress. However, at higher strains (500% and 1000%), similar to steady shear measurements, loss modulus $G''$and storage modulus G' for both the systems show a sudden transition to higher values. This sudden jump in the storage and loss modulus can be attributed to the formation of hydroclusters. Additionally, an increase in complex viscosity η^* can also be observed at higher strain amplitudes.

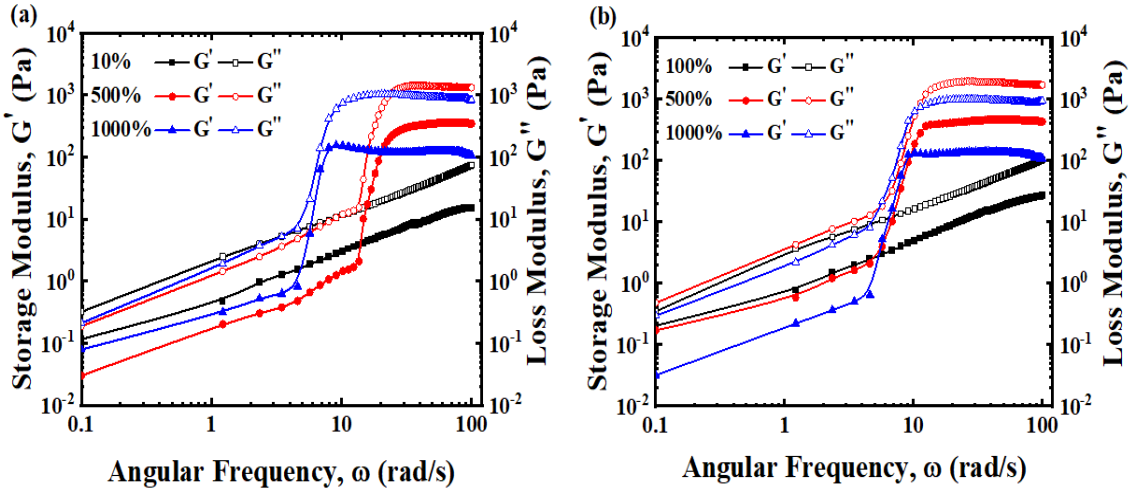

Figure 6.18 Storage modulus and Loss modulus as a function of angular frequency at a constant strain amplitude of 100%, 500%, and 1000% for 20 wt% fumed silica suspensions in (a) PEG 200 (b) PEG 300

Figure 6.19 shows the complex viscosity (η^*) as a function of angular frequency for 20wt.% fumed silica suspensions in PEG 200 and PEG 300. A consistent decrease in complex viscosity is observed at lower strain amplitudes (up to 100%) but at higher strain amplitude $(\gamma_0 > 500\%)$ the trend was similar to the steady shear viscosity. It can also be noted that the critical frequency increases with a decrease in the strain amplitude (γ_0). The oscillatory shear measurements

reveal that fumed silica suspensions in polyethylene glycol exhibit strain-thickening behavior that is similar to the shear thickening phenomenon observed in the steady shear measurements. Raghavan and Khan called this sudden increase in complex viscosity observed at the critical frequency as "Strain thickening" (Raghavan and Khan, 1997). They attributed the strain-thickening behavior to the formation of hydrogen bonding between surface hydroxyl groups and polymer chains of the carrier fluid, leading to the formation of hydroclusters.

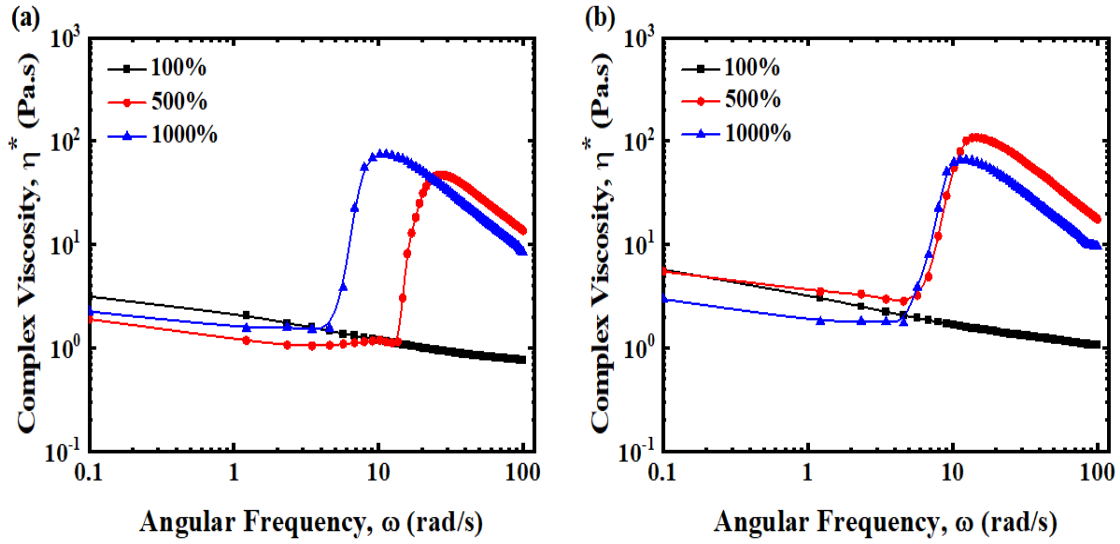

Figure 6.19 Complex viscosity η* as a function of angular frequency at a constant strain amplitude of 100%, 500%, and 100% for 20 wt% fumed silica suspensions in (a) PEG 200 (b) PEG 300

6.3.6 Validation of Modified Cox-Merz Rule

Doraiswamy et al. (1991) first proposed the modified Cox-Merz rule to correlate steady shear viscosities with complex viscosities. The modified Cox-Merz rule has been shown to be working well for complex systems with high nonlinearities. The modified Cox-Merz rule compares the non-linear behavior of suspension under

oscillatory shear with the steady shear rheology and allows us to correlate strain thickening and shear thickening. Mathematically, the modified Cox-Merz rule can be represented as:

$$\eta^*(\gamma_0\omega) = \eta(\dot{\gamma}), \qquad (6.3)$$

where, $\gamma_0\omega = \dot{\gamma}^{dyn}$ is the maximum dynamic shear rate.

Raghavan and Khan (1997) first implemented the modified Cox-Merz rule for fumed silica suspensions in PPG and observed an excellent overlap between complex viscosity and steady shear viscosity when the strain amplitude is high ($\gamma_0 > 500\%$). In **Figure 6.20**(a) and (b), we have plotted complex viscosity as a function of dynamic shear rate ($\gamma_0 = 500\%, 1000\%$) along with the steady-shear viscosity as a function of shear rate to validate the modified Cox-Merz rule. Also shown in **Figure 6.20** (c) and (d) are viscosity variations with dynamic shear stress. The average dynamic shear stress $\bar{\tau}_d$was calculated using the formula given in Lee and Wagner (2003).

It can be observed that the dynamic shear viscosity curves show qualitative agreement with the steady-state viscosity curves. It is also important to note that the critical dynamic shear stress is very close to the critical shear stress, but the peak viscosity for shear thickening is slightly higher than the strain thickening. We can interpret from these results that the modified Cox-Merz rule appears to be valid for the fumed silica suspensions in polyethylene glycol. The synergy between the complex viscosity and steady shear viscosity gives further indication of the clustering mechanism in shear thickening.

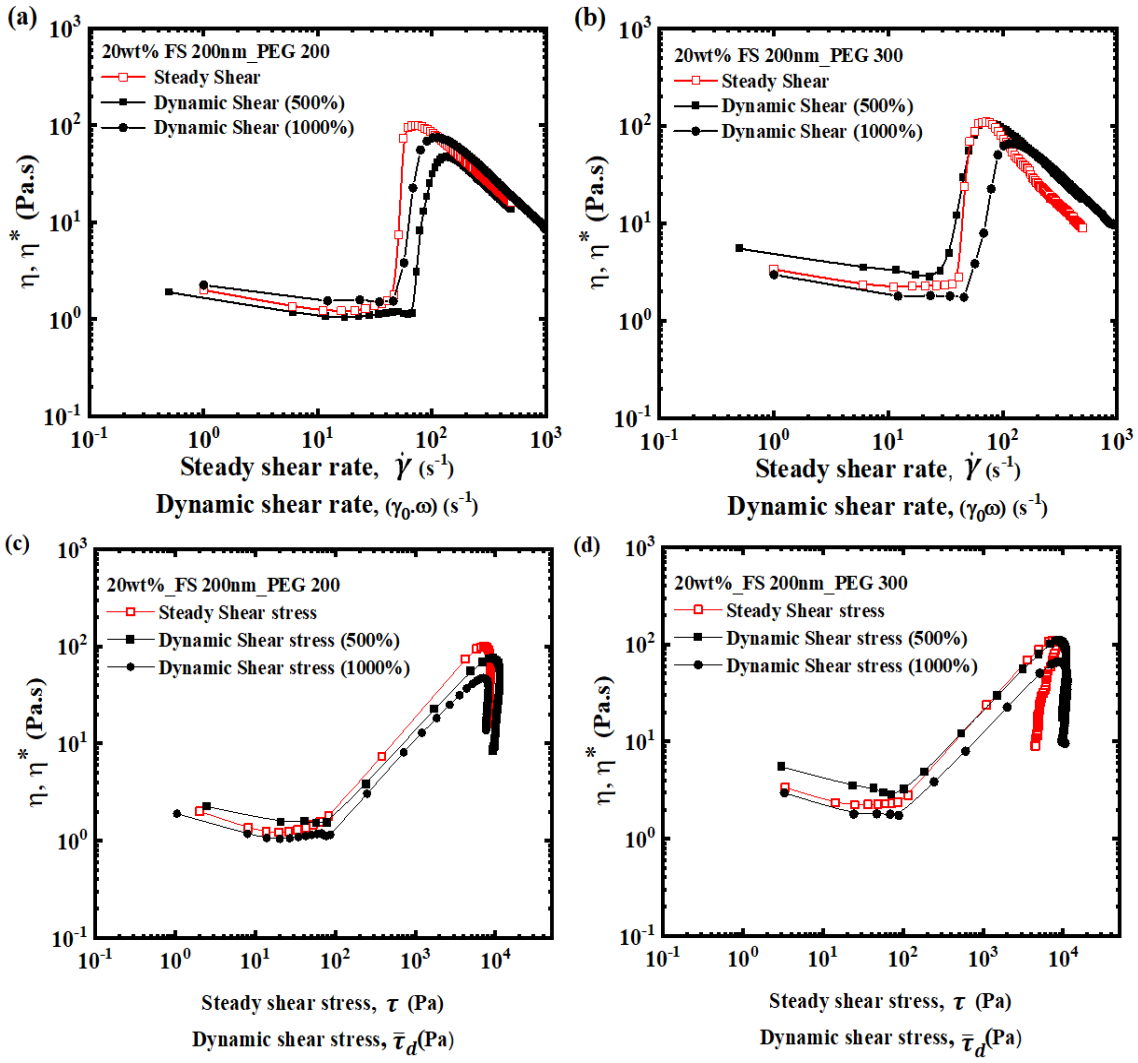

Figure 6.20 Correlation of steady and dynamic shear rate experiment data for 20 wt.% fumed silica suspensions in (a) and (c) PEG 200 and (b) and (d) PEG 300 using modified Cox-Merz rule

6.4 Conclusions

The simultaneous visualization of microstructure and rheological measurements were performed to understand the origin of shear thickening behavior. The steady shear experiments with fumed silica suspension in polyethylene glycol exhibited three distinct regions, characterized by first shear thinning, shear

thickening, and second shear thinning. The suspension showed discontinuous shear thickening. By visualizing the reflected light from the tracer particles embedded in the suspension, we could relate the microstructure with the rheology. In addition to the study of viscosity variations, the mechanism of shear thickening was also analyzed quantitatively by the measurements of first normal stress difference (N_1) . Beyond the onset of shear thickening, we observe a negative first normal stress difference (N_1) whose magnitude first increases and then decreases with the shear rate. The increasing negative N_1 is consistent with hydrocluster theory that attributes shear thickening to the formation of flow-induced clusters. These clusters are temporary in nature and, at a higher shear rate (after the maximum viscosity is reached), break into smaller ones, thereby again decreasing the viscosity. In the discontinuous shear thickening region, a nearly linear variation of the first normal stress difference with shear rate indicates its hydrodynamic origin. The nonlinear decrease in the first normal stress difference with the shear rate in the second shear-thinning region is primarily due to the breaking of large clusters into smaller ones with a possibility of frictional contacts within these hydroclusters. We believe that the shape of the particles plays an important role. In highly concentrated suspensions of rough spherical particles less viscous fluids, the frictional forces at high stresses would be dominant over hydrodynamic forces in the shear thickening region and large enough to produce discontinuous shear thickening. On the other hand, irregular-shaped particles or particles with high surface asperities can lead to large stresses even at moderate concentration due to complex hydrodynamics frustrating the relative particle motion. In such cases, discontinuous shear thickening can be obtained even if the frictional contact forces are masked by the

strong hydrodynamic lubrication forces. Oscillatory shear measurements were conducted to understand strain thickening behavior. It was observed that at high amplitudes, both storage modulus $G''$and loss modulus G' displayed a sudden jump to higher values at a critical strain resulting in strain thickening. It was observed that the rheological response of the samples at high amplitude oscillatory shear is similar to that under steady shear.

CHAPTER 7 Summary and Future Scope

7.1 Summary

This work aimed to provide insight into the fundamental behavior of shear thickening suspensions and to visualize the microstructure in discontinuous shear thickening suspensions. The effects of different parameters on the rheology of shear thickening suspensions will be helpful in the application of shear thickening suspensions for the fabrication of impact mitigation materials. The research discussed in this thesis highlights the importance of the preparation of shear thickening suspensions by the sonochemical homogenization method over the mechanical agitation method. Our experimental results highlight the use of Rheo-microscopy to observe the microstructure of shear thickening suspensions.

Achieving shear thickening at lower weight fractions is highly desired in many practical applications, which is possible by proper procedure followed for preparing the suspension that enables the removal of air bubbles and any water contamination. Chapter 3 shows that the suspension prepared by the mechanical agitation method did not produce the desired shear thickening behaviour compared to the sonochemical method. It was observed that the presence of even tiny bubbles is detrimental to the preparation of shear thickening suspension and lead to continuous shear thickening and poor shear thickening behaviour. We have prepared the shear thickening suspensions with fumed silica particles dispersed in PEG by the sonication method.

In Chapter 4, experiments were carried out to study the influence of various parameters on the rheological behavior of shear thickening suspensions. Experimental results from the prepared shear thickening fluids resulted in a good

understanding of the parameters that influence the rheology. The onset of shear thickening can be influenced by particle loading, carrier fluid, and particle size. The experiments have also demonstrated that high shear thickening ratio can be achieved with a lower molecular weight carrier fluid, whereas lower critical shear rates are observed by increasing the particle concentration. On the other hand, by increasing the smaller particles in a bimodal suspension comprised of two different sized particles, we observed a decrease in the maximum suspension viscosity and a shift in the onset of shear thickening to higher values of critical shear rates. These results showed that polydisperse suspension might result in poor shear thickening behavior.

The influence of addition of fillers on the rheological behavior of shear thickening fluids were studied in chapter 5. The experiments were carried out by adding three different nanofillers to shear thickening suspensions to understand the influence on the onset of shear thickening. It was found that the addition of Graphene Oxide particles exhibited higher relative viscosities and a decrease in the onset of shear thickening. Adding these fillers provided tensile strength to the shear thickening fluids and allows more efficient load transfer throughout the material. However, the addition of Multiwalled carbon nanotubes and mica particles showed a decrease in the shear thickening ratio and an increase in critical shear rate. Finally, we concluded that the classification of additive effects is not possible as some disrupt the thickening mechanism while some improve the behaviour. In order to understand the effect of fillers, it is required to carry out more investigations using various types of fillers in STFs as the rheological behavior of shear thickening fluids with the addition of fillers is dependent on various factors.

Finally, using these suspensions, simultaneous visualization of microstructure and rheological measurements was performed to understand the origin of shear thickening behavior in chapter 6. By visualizing the reflected light from the tracer particles embedded in the suspension we could relate the microstructure with the rheology. In addition to the viscosity characterization, the mechanism of shear thickening was also analyzed quantitatively by the measurements of first normal stress difference (N_1). Beyond the onset of shear thickening, we observe a negative N_1 whose magnitude first increases and then decreases with the shear rate. These results are consistent with hydrocluster theory, which attributes shear thickening to the formation of flow-induced clusters. In addition, oscillatory shear measurements were also conducted to understand strain thickening behavior. It was observed that at high amplitudes, both storage modulus $G''$and loss modulus G' displayed a sudden jump to higher values at a critical strain resulting in strain thickening. The modified Cox-Merz rule was validated to relate shear thickening and strain thickening, which suggests that the shear thickening or strain thickening behavior is consistent with the hydrocluster theory.

We were also able to relate microstructure with rheology and observed that the formation of hydroclusters give rise to shear thickening behaviour. The findings from the experimental measurements are in good agreement with previous studies, and results from these studies can be used to prepare the shear thickening fluids of desired properties. Most of the objectives outlined in chapter 1 has been achieved, and the knowledge gained can be used to design better shear thickening fluid.

7.2 Future Scope

There are several opportunities for extending this research work. Further investigation could include

1. Studying the effect of modifying the silica surface on the rheology of STFs.
2. Studying the effect of stability of these suspensions over a long duration of time, with suspensions stored in a normal environment.
3. Determining particle displacements, velocities, and particle-particle interactions.
4. Study the nonlinear rheological properties of fumed silica suspension using large amplitude oscillatory shear (LAOS).

References

Barnes HA (1989) Shear-thickening ("dilatancy") in suspensions of nonaggregating solid particles dispersed in Newtonian liquids. J Rheol 33:329–366

Boersma WH, Laven J, Stein HN (1990) Shear thickening (dilatancy) in concentrated dispersions. AIChE J 36:321-332

Brady JF, Bossis G (1985) The rheology of concentrated suspensions of spheres in simple shear flow by numerical simulations. J Fluid Mech 155:105-129

Besseling R, Weeks ER, Schofield AB, Poon WCK (2007) Three-dimensional imaging of colloidal glasses under steady shear. Phys Rev Lett 99:028301

Besseling R, Isa L, Weeks ER, Poon WCK (2009) Quantitative imaging of colloidal flows. Adv. Colloid Interface Sci. 146 (1), 1–17

Brown E, Jaeger HM (2009) Dynamic jamming point for shear thickening suspensions. Phy Rev Lett 103:086001:1-4

Brown E, Forman NA, Orellana CS, Zhang H, Maynor BW, Betts DE, DeSimone JM, Jaeger HM (2010) Generality of shear thickening in dense suspensions. Nat Mater. 9(3):220-4

Brown E, Jaeger HM (2012) The role of dilation and confining stresses in shear thickening of dense suspensions. J Rheol 56:875-923

Brown E, Jaeger HM (2014) Shear thickening in concentrated suspensions: phenomenology, mechanisms, and relations to jamming. Reports Prog. Phys 77 (046602) 1-23

Cao S, Wang Y, Pang H, Zhang J, Wu Y, Xuan S, Gong X (2021) Shear jamming onset in dense granular suspensions. Journal of Rheology 65, 419-426

Chatté G, Comtet J, Niguès A, Bocquet L, Siria A, Ducouret G, Lequeux N, Fran çoisand Lenoir, Ovarlez G, Colin A (2017) Shear thinning in non-brownian suspensions. Soft Matter, 14:879–893.

Chen J, Spear SK, Huddleston JG, Rogers RD (2005) Polyethylene glycol and solutions of polyethylene glycol as green reaction media. Green Chem. 7, 64–82.

Chen Y, Xu W, Zeng G, Liu W (2015) Shear-thickening behavior of precipitated calcium carbonate particles suspensions in glycerine. Applied Rheology 25, 1–8.

Cheng X, McCoy JH, Israelachvili JN, Cohen I (2011) Imaging the microscopic structure of shear thinning and thickening colloidal suspensions. Science 333:1276–1279

Cohen I, Mason TG, Weitz DA (2004) Shear-induced configurations of confined colloidal suspensions. Phys. Rev. Lett. 93 (4), 046001

Comtet J, Chatt´e G, Nigu`es A, Bocquet L, Siria A, Colin A (2017) Pairwise frictional profile between particles determines discontinuous shear thickening transition in non-colloidal suspensions. Nat Commun 8:15633:1-7

Collins EA, Hoffmann D, Soni PL (1979) Rheology of PVC dispersions: i. Effect of particle size and particle size distribution. J Colloid Interface Sci 71:21–9

Couturier É, Boyer F, Pouliquen O, Guazzelli É (2011) Suspensions in a tilted trough: second normal stress difference. J. Fluid Mech 686:26–39

Cross MM (1965) Rheology of non-newtonian fluids: a new flow equation for pseudoplastic systems. J. Colloid Sci. 20 417–437

Cwalina CD, Wagner NJ (2014) Material properties of the shear thickened state in concentrated near hard-sphere colloidal dispersions. J. Rheol. 58(4), 949–967

Derks D, Wisman H, Van Blaaderen A, Imhof A (2004) Confocal microscopy of colloidal dispersions in shear flow using a counter-rotating cone plate shear cell. J. Phys Condens Mater 16: S3917–27

D'Haene P, Mewis J (1994) Rheological characterization of bimodal colloidal dispersions. Rheol Acta 33:165–74

Dhar S, Chattopadhyay S, Majumdar S (2020) Signature of jamming under steady shear in dense particulate suspensions. J Phys Condens Matter 32:124002:1-6

Ding J, Tracey P, Li W, Peng G, Whitten P, Wallace G (2013) Review on shear thickening fluids and applications. Text. Light Ind. Sci. Tech. 2, 161–173.

Doraiswamy D, Mujumdar AN, Tsao I, Beris AN, Danforth SC, Metzner AB (1991) The Cox–Merz rule extended: A rheological model for concentrated suspensions and other materials with a yield stress. J. Rheol. 35, 647

Egres RG, Nettesheim F, Wagner NJ (2006) Rheo-sans investigation of acicular-precipitated calcium carbonate colloidal suspensions through the shear thickening transition. J. Rheol. 50, 685–709

Fall A, Bertand F, Hautemayou D, Meziere C, Moucheront P, Lemaitre A, Ovarlez G (2015) Macroscopic discontinuous shear thickening versus local shear jamming in cornstarch. Phy Rev Lett 114:098301:1-5

Fall A, Bertrand F, Overlex G, Bonn D (2009) Yield stress and shear banding in granular suspensions. Phys Rev Lett 103, 178301:1-4

Fischer C, Braun SA, Bourban PE, Michaud V, Plummer CJG, Manson JAE (2006) Dynamic properties of sandwich structures with integrated shear-thickening fluids. Smart Mater Struct 15:1467–75

Foss DR, Brady JF (2000) Structure, diffusion and rheology of Brownian suspensions by Stokesian dynamics simulation. J. Fluid Mech. 407, 167–200

Galindo-Rosales FJ, Rubio-Hernández FJ, Velázquez-Navarro JF (2009) Shear-thickening behavior of Aerosil® R816 nanoparticles suspensions in polar organic liquids. Rheol Acta 48(6):699–708

Galindo-Rosales FJ, Rubio-Hernández FJ, Sevilla A (2011) An apparent viscosity function for shear thickening fluids. J. Nonnewton.Fluid Mech. 166 321–5

Gates Jr LE (1968) Evaluation and development of fluid armor systems. Report no: AFML-TR-68-362

Ge J, Tan Z, Li W, Zhang H (2017) The rheological properties of shear thickening fluid reinforced with SiC nanowires. Results in Physics 7, 3369-3372

Greenwood R, Luckham PF, Gregory T (1997) The effect of diameter ratio and volume ratio on the viscosity of bimodal suspensions of polymer lattices. J Colloid Interface Sci 191: 11-21

Gurnon A, Wagner N (2015) Microstructure and rheology relationships for shear thickening colloidal dispersions. Journal of Fluid Mechanics, 769, 242-276 (2015)

Gürgen S, Kushan MC (2016) Rheological properties of shear thickening fluids. J Polytechnic 19:409–14

Gürgen S, Kushan MC, Li W (2016) The effect of carbide particle additives on rheology of shear thickening fluids. Korea-Aust. Rheol. J. 28, 121–128

Guy BM, Ness C, Hermes M, Sawiak LJ, Sun J, Poon WCK (2020) Testing the wyart–cates model for non-brownian shear thickening using bidisperse suspensions. Soft Matter, 16:229–237

Hasanzadeh M, Mottaghitalab V. Tuning of the rheological properties of concentrated silica suspensions using carbon nanotubes. Rheol Acta2016;55:759–66

Hébraud P (2009) Normal and tangential stress fluctuations during jamming. Rheol Acta 48, 845–853

Hoffman RL (1972) Discontinuous and dilatant viscosity behavior in concentrated suspensions. I. Observation of a flow instability. J Rheol 16:155–73

Hoffman RL (1974) Discontinuous and dilatant viscosity behavior in concentrated suspensions II. Theory and experimental tests. J. Colloid Interface Sci. 46:491–506

Huang W, Wu Y, Qiu L, Dong C, Ding J, Li D (2015) Tuning rheological performance of silica concentrated shear thickening fluid by using graphene oxide. Adv Condens Matter Phys 2015:1–5

Kalman D, Schein J, Houghton J, Laufer CH, Wetzel ED, Wagner NJ (2007) Polymer dispersion based shear thickening fluid-fabrics for protective applications. Proc SAMPE Baltimore USA 1:35–38

Kalman DP, Merrill RL, Wagner NJ, Wetzel ED (2009) Effect of particle hardness on the penetration behavior of fabrics intercalated with dry particles and concentrated particle–fluid suspensions. Appl. Mater. Interfaces 1 (11), 2602–2612

Krieger IM, Dougherty TJ (1959) A Mechanism for Non-Newtonian Flow in Suspensions of Rigid Spheres. Trans. Soc. Rheol. 3, 137-152

Laha A, Majumdar A, (2016) Shear thickening fluids using silica-halloysite nanotubes to improve the impact resistance of p-aramid fabrics. Applied Clay Science 132, 468–474.

Laun HM, Bung R, Schmidt F (1991) Rheology of extremely shear thickening polymer dispersions. J. Rheol. 35 999–1034

Lee YS, Wagner NJ (2003) Dynamic properties of shear thickening colloidal suspensions. Rheol Acta 42:199–208

Lee YS, Wagner NJ (2006) Rheological properties and small-angle neutron scattering of a shear thickening, nanoparticle dispersion at high shear rates. Ind Eng Chem Res 45:7015–24

Lee BW, Kim IJ, Kim CG (2009) The influence of the particle size of silica on the ballistic performance of fabrics impregnated with silica colloidal suspension. J Compos Mater 43:2679–98

Lee Y, Luo Y, Brown SC, Wagner NJ (2020) Experimental test of a frictional contact model for shear thickening in concentrated colloidal suspensions. J. Rheol 64, 267-282

Lin NYC, Guy BM, Hermes M, Ness C, Sun J, Poon WCK, Cohen I (2015) Hydrodynamic and contact contributions to continuous shear thickening in colloidal suspensions. Phys. Rev. Lett., 115:228304

Lootens D, Van Damme H, Hémar Y, Hébraud P (2005) Dilatant flow of concentrated suspensions of rough particles. Phys Rev Lett 95(26):268302

Maharjan R, O'Reilly E, Postiglione T, Klimenko N, Brown E (2021) Relation between dilation and stress fluctuations in discontinuous shear thickening suspensions. Phys. Rev. E. 103, 012603

Majumdar S, Krishnaswamy R, Sood AK (2011) Discontinuous shear thickening in confined dilute carbon nanotube suspensions. Proceedings of the National Academy of Sciences, 108 (22):8996-9001

Maranzano BJ, Wagner NJ (2001) The effects of particle size on reversible shear thickening of concentrated colloidal dispersions. J Chem Phys 114:10514–27

Maranzano BJ, Wagner NJ (2002) Flow-small angle neutron scattering measurements of colloidal dispersion microstructure evolution through the shear thickening transition. J Chem Phys 117:10291–302

Mari R, Seto R, Morris JF, Denn MM (2014) Shear thickening, frictionless and frictional rheologies in non-Brownian suspensions. J Rheol 58:1693–724

Metzner AB, Whitlock M (1958) Flow behavior of concentrated (dilatant) suspensions. Trans. Soc. Rheol. 2, 239–254

Montgomery TS, Macknight W (2005) Introduction to polymer viscoelasticity. Third edition, Wiley Inter Science

Moriana AD, Tian T, Sencadas V, Li W (2016) Comparison of rheological behaviors with fumed silica-based shear thickening fluids. Korea-Australia Rheol J 28:197–205

Qin Xu, Majumdar S, Brown E, Jaeger HM (2014) Shear thickening of highly viscous granular suspension. Eur Phy Lett 107:68004:1-6

Qin J, Zhang G, Shi X (2017) Study of a shear thickening fluid: the suspensions of monodisperse polystyrene microspheres in polyethylene glycol. J Dispers Sci Technol 38:935–42

Phung TN, Brady JF, Bossis G (1996) Stokesian dynamics simulation of Brownian suspensions. J. Fluid Mech. 313, 181–207

Raghavan S.R, Khan S.A (1997) Shear-Thickening Response of Fumed Silica Suspensions under Steady and Oscillatory Shear. J Coll Int Sci 185: 57-67

Raghavan SR, Walls HJ, Khan SA (2000) Rheology of silica dispersions in organic Liquids: New Evidence for solvation forces dictated by hydrogen bonding. Langmuir 16:7920-7930

Raghavan SR, Riley MW, Fedkiw PS, Khan SA (1998) Composite polymer electrolytes based on poly(ethylene glycol) and hydrophobic fumed silica: dynamic rheology and microstructure. Chem Mater 10(1):244–251

Royer JR, Blair DL, Hudson SD (2016) Rheological Signature of Frictional Interactions in Shear Thickening Suspensions. Phy Rev Lett 116:188301:1-5

Sha X, Yu K, Cao H, Qian K (2013) Shear thickening behavior of nanoparticle suspensions with carbon nanofillers. J. Nanopart. Res. 15, 1816.

Seto R, Giusteri G (2018) Normal stress differences in dense suspensions. Journal of Fluid Mechanics, 857, 200-215

Seto R, Mari R, Morris JF, Denn MM (2013) Discontinuous shear thickening of frictional hard-sphere suspensions. Phy Rev Lett 111:218301:1-5

Singh A, Nott PR (2003) Experimental measurements of the normal stresses in sheared Stokesian suspensions. J. Fluid Mech. 490, 293–320

Singh A, Mari R, Denn MM, Morris JF (2018) A constitutive model for simple shear of dense frictional suspensions. J. Rheol. 62 (2), 457–468

Singh M, Sanjeev KV, Biswas I, Mehta R (2019) Rheology of fumed silica and polyethylene glycol shear thickening suspension with nano-clay as an additive. Defence Science Journal 69(4), 402-408

Swarna, Pattanayek SK, Ghosh AK (2018) Dynamic shear rheology of colloidal suspensions of surface-modified silica nanoparticles in PEG. J. Nanopart Res 20, 53

Wagner N, Wetzel E (2006) Advanced body armor utilizing shear thickening fluids. US Patent 20060234577A1

Wagner NJ, Brady JF (2009) Shear thickening in colloidal dispersions. Phys Today 62:27–32

Wang M, Jamali S, Brady JF (2020) A hydrodynamic model for discontinuous shear-thickening in dense suspensions. J. Rheol 64, 379-394 (2020)

Warren J, Offenberger S, Toghiani H, Pittman CU, Lacy TE, Kundu S (2015) Effect of temperature on the shear-thickening behavior of fumed silica suspensions. ACS Appl Mater Interfaces 7:18650-18661

Wei M, Lv Y, Sun L (2020) Rheological properties of multi-walled carbon nanotubes/silica shear thickening fluid suspensions. Colloid Polym Sci 298, 243–250

Wyart M and Cates ME (2014) Discontinuous shear thickening without inertia in dense non-brownian suspensions. Phys. Rev. Lett., 112:098302

Yu-lei Xu, Xing-long Gong, Chao Peng, Ying-qiang Sun, Wan-quan Jiang, Zhong Zhang (2010) Shear Thickening Fluids Based on Additives with Different Concentrations and Molecular Chain Lengths. Chin. J. Chem. Phys. 23 342

Zhang X, Li W, Gong X (2010) Thixotropy of MR shear-thickening fluids. Smart Mater Struct 19:125012:1–6

Research Outcomes

Publications

1. T. Ajeeth Prabhu, and Anugrah Singh, "Effect of carrier fluid and particle size distribution on the rheology of shear thickening suspensions," Rheol Acta 60, 107–118 (2021)

2. T. Ajeeth Prabhu, and Anugrah Singh, "Rheology and microstructure of discontinuous shear thickening suspensions," Journal of Rheology 66, 731-747 (2022)

3. T. Ajeeth Prabhu, and Anugrah Singh, "Effect of nanofillers on the shear thickening behavior of fumed silica suspensions," (Manuscript in Preparation)

4. T. Ajeeth Prabhu, and Anugrah Singh, "Flow visualization studies in Lid Driven cavity for concentrated suspensions," (Manuscript in Preparation)

Conferences

1. T. Ajeeth Prabhu, Anugrah Singh, "Microstructure and Rheology of Shear Thinning and Shear Thickening Suspensions" in International Conference CompFlu-2018, Dec 6-9 2018, IIT Roorkee

2. T. Ajeeth Prabhu, Anugrah Singh, "Studies on Effect of Polydispersity on Rheology of Shear Thickening Fluids" in International Conference CompFlu-2017, Dec 18-20 2017, IIT Madras

3. T. Ajeeth Prabhu, Anugrah Singh, "Synthesis and Studies of Shear Thickening Fluids" in national Conference Reflux-2017, March 24-26, 2017, IIT Guwahati